Synthesis and characterization of quantum dot coated silicon dioxide surfaces and their application for optical sensing of surface charges in dusty low temperature plasmas

Master's thesis for the award of the academic degree
Master of Science
in Applied Chemistry
at the Faculty of Applied Natural Sciences
at TH Köln – University of Applied Sciences

Handed in by: Kai-Kilian Albert
Registration number: 11159660
Adress: [redacted]

Supervisor: Prof. Dr. Dirk Burdinski
Second reviewer: Dr. Mikhail Pustylnik (DLR)

Bergheim, 19.08.2024

Statutory declaration

I herewith declare that I have composed the present thesis myself and without use of any other than the cited sources and aids. Sentences or parts of sentences quoted are marked as such; other references regarding the statement and scope are indicated by full details of the publications concerned.

The thesis in the same or similar form has not been submitted to any examination body and has not been published.

Bergheim, 19.08.2024 Signature (K. Albert)

Abstract

In the experimental part of the following thesis to acquire the academical grade Master of Science (M.Sc.), two different procedures were developed which enable to coat pre-functionalized CdSe/ZnS-core/shell quantum dots onto silicon dioxide single crystal wafers as well as onto pre-functionalized silicon dioxide microspheres in a size range of 4 to 11 µm through amide formation between the surfaces of the quantum dots and corresponding the SiO_2 surfaces.

To enable the coating of the single crystals, they first had to be hydrophilized through Peroxymonosulfuric acid (H_2SO_5) which was formed in-situ through mixing sulfuric acid and hydrogen peroxide in a ratio of 1:2.

After hydrophilization, the free hydroxy groups on the surface were used to form a layer of (3-aminopropyl)triethoxysilane (APTES) via organosiloxane formation to generate free primary amino groups, which were then used to form amides between the single crystal surface and the quantum dots. In the case of microparticles, the existing amino groups on the surface reduced the need of further derivatization before the main reaction, but an activation agent for carboxylic groups, namely 1-ethyl-3-(3-dimethylaminopropyl)carbodiimide (EDC) was applied to ensure a fast amide formation through the decomposition of the activated O-isoacylurea intermediate formed between EDC and the carboxylic acid groups of the quantum dot surfaces. The optimized amide formation was observable through e.g. UV-VIS spectroscopy and other techniques.

After the successful development of both procedures, the coatings were tested in a low temperature RF argon discharge plasma at the facilities of TU Eindhoven. After the tests, the data showed that further optimization of the procedures will be needed in terms of degradation protection in plasma environments and coating homogeneity/quantitative coating of both substrates.

Keywords: cadmium selenide, core-shell-QD, quantum confined stark effect, silicon dioxide, microspheres, optical sensor, dusty plasma, photoluminescence, fluorescence, artificial atoms, quantum confinement

Zusammenfassung

Im experimentellen Teil der folgenden Arbeit zur Erlangung des akademischen Grades Master of Science (M.Sc.) wurden zwei verschiedene Verfahren entwickelt, die es ermöglichen, vorfunktionalisierte CdSe/ZnS-core/shell-Quantendots auf Siliziumdioxid-Einkristallwafer sowie auf vorfunktionalisierte Siliziumdioxid-Mikrosphären in einem Größenbereich von 4 bis 11 µm durch Amidbildung zwischen den Oberflächen der Quantendots und den entsprechenden SiO_2-Oberflächen zu beschichten. Um die Beschichtung der Einkristalle zu ermöglichen, mussten diese zunächst durch Peroxomonoschwefelsäure (H_2SO_5) hydrophilisiert werden, die in-situ durch Mischen von Schwefelsäure und Wasserstoffperoxid im Verhältnis 1:2 hergestellt wurde. Nach der Hydrophilisierung wurden die freien Hydroxygruppen mit (3-Aminopropyl)triethoxysilan (APTES) zur Reaktion gebracht, um primäre Aminogruppen auf der Oberfläche zu erzeugen, die infolgedessen die Amidbildung zwischen QD-Oberfläche und Einkristalloberfläche ermöglichten. Im Falle der Mikropartikel reduzierten die vorhandenen Aminogruppen auf der Oberfläche die Notwendigkeit einer weiteren Derivatisierung vor der Hauptreaktion. Allerdings wurde ein Aktivierungsreagenz für Carboxylgruppen, genauer 1-Ethyl-3-(3-dimethylaminopropyl)carbodiimid (EDC), eingesetzt, um eine schnelle Amidbildung durch die Zersetzung des aktivierten O-Isoacylharnstoff-Zwischenprodukts zu gewährleisten, das zwischen EDC und den Carbonsäuregruppen der Quantendot-Oberflächen gebildet wurde.

Nach der erfolgreichen Entwicklung beider Verfahren wurden die Beschichtungen in einem Niedertemperatur-Argon-Entladungsplasma in den Einrichtungen der TU Eindhoven getestet. Nach den Experimenten sowie der folgenden Datenanalyse wurde entschieden, die jeweiligen Prozeduren bezüglich Degradationsschutz und quantitativer Beschichtung in den kommenden Monaten DLR-intern weiterzuentwickeln.

Schlüsselwörter: Cadmiumselenid, core/shell-QD, QCSE, Siliziumdioxid, Mikrosphären, optischer Sensor, staubiges Niedertemperaturplasma, Photolumineszenz, Fluoreszenz, Einkristallwafer

Acknowledgement

In this section I want to express my gratitude to everyone who enabled me to successfully conduct all experiments and measurements and to successfully document the conducted research in this work as well as for guiding me throughout this process of this work.

I want to thank Dr. Mikhail Pustylnik for his high engagement and aid throughout the whole experimental work, and for the emotional and professional support in any situation of need, as well as for his scientific expertise and his theoretical background which enabled me to conduct experimental research regarding new optical sensors for dusty plasma diagnostics.

I want to thank Dr. Hubertus Thomas for the optimal and seamless inclusion in his working group and for his positive attitude as well as the interesting conversations along the way.

I want to thank Marlo Kunzner, PhD candidate at our institute, for his daily aid in the institute and beyond, and for being a real friend and investing his time throughout the process of this thesis and for correction reading throughout the writing process.

I want to thank Dr. Matthias Kolbe for the assistance with scanning electron microscopy and for the special and remarkably interesting conversations along the way. As you taught me a lot in a short time. I wish you the absolute best for your upcoming and well-deserved retirement and I look up to your great scientific success throughout your career.

I also want to thank Dr. Klemens Kelm for the generous help with the measurements on the transmission electron microscope, for the aid with image interpretation and for the interesting scientific discussions.

For the assistance and generous as well as informing conversations along the way while acquiring fluorescence microscopy images, I want to express my gratitude to Dr. Yannick Lichterfeld.

Finally, I want to express my gratitude to Sim Bouwmans and Guido Classen for the great and productive atmosphere in Eindhoven and for their experimental expertise which enabled us to gain knowledge and understanding for the properties of the coated samples in realistic plasma environments as well as for their positive energy and drive while carrying out the tests.

Contents

Table of figures

1 Introduction

In the research group of Dr. Hubertus Thomas at the Institute for Material Physics in Space at the German Aerospace Centre, a statistical model was developed predicting the possibility of measurement of microparticle charges using the Quantum confined Stark effect (QCSE) in quantum dots attached to their surface.[9]

Now, the microparticle charges are measured predominantly by dynamical methods which have several disadvantages in terms of reliability and spatiotemporal resolution.[9,20] The results of the work could further influence the development of optical charge measurements and could improve the understanding of charging dynamics on solid surfaces in plasma environments.

The understanding of dust particle charge dynamics is important for the further development of different industrial applications, especially for XUV lithography.[9,20]

In 2023, the noble prize for chemistry was awarded to researchers that initially discovered and synthesized quantum dots, which underlines the high relevance of QDs and QD-based materials for scientific research and the development of novel technologies with optically active materials, as planned in this work.[28]

1.1 Cadmium selenide and CdSe nanocrystals

In general, nanomaterials are defined as particles and materials in a size range below 100 nm.[1] Semiconductor nanocrystals are important materials for scientific research and industrial applications and can be synthesized from e.g. cadmium and selenium, corresponding salts or organometallic precursors like alkylcadmium.[3,4]

Cadmium selenide is a so-called II-VI-semiconductor material formed out of the transition metal cadmium (12th group) and the chalcogenide selenium (16th group).[5]

The applicability of CdSe-based materials was limited through the high toxicity of the material combined with low oxidation stabilities. The drawbacks were reduced with further developments in terms of the mentioned core/shell-structures in the last years.[5,15].

The formation of an ionic structure of cadmium and selenium ions can lead to the formation of two different crystal structures that depend on the orientation of the tetrahedra.[6] The tetrahedra can align to form cubic zincblende or hexagonal wurtzite structures. Cubic CdSe QDs are known to exhibit higher quantum yield than hexagonal CdSe QDs.[6,15]

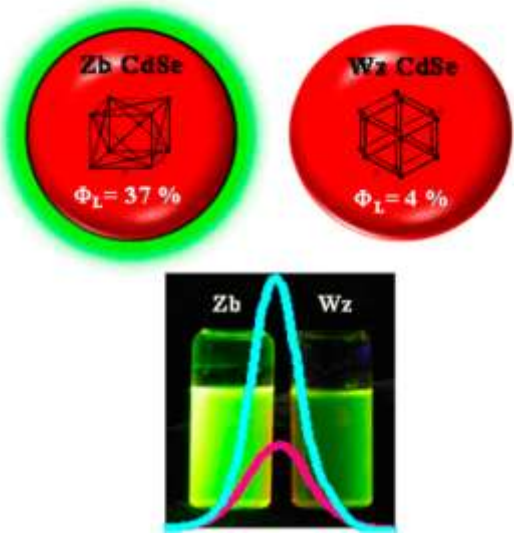

Figure 1. Comparison of quantum efficiency of cubic zinc blende and hexagonal wurtzite crystal structures of CdSe-QD.[6]

Zinc sulphide is an inorganic semiconductor with the formula ZnS which is also known to crystallize in the cubic zinc blende structure (for which it is the standard for its nomenclature) with optional orientation of atoms described by hexagonal wurtzite structure.[5] It is used as non-fluorescent barrier shell for the fluorescent core of core/shell-QD.[7]

Besides the barrier function, literature suggested that a bigger outer shell leads to a reduction of interferences through non-radiative recombination, e.g. Auger recombinations.[7] Through the possible oxidation to sulphates when exposed to water and oxygen,

the coated powders should be stored dry and protected from other environmental influences after successful synthesis.[7]

ZnS can be considered as an effective optical barrier material for the fluorescent CdSe core, because the bandgap energy of ZnS is higher (3,73 eV for ZnS and 1,67 eV for CdSe). The excitation of ZnS crystals is therefore suppressed through the high energy difference of valence and conduction band.[16] The used CdSe/ZnS-core/shell quantum dots can be synthesized by various methods from the corresponding metal and chalcogenide salts or from the pure elements and are already broadly available for direct purchase. An exemplary synthetic strategy to produce the mentioned QD is the so-called TOP-SILAR method is shown in the following figure, as no data of the manufacturing process was available from the supplier.[4] A precursor in form of CdSe crystals (the photoluminescent core) is being solved in trioctylphosphine (TOP) which leads to the formation of trioctylphosphine selenide on the surface of the core as the activated species of the CdSe cores.[4]

After activation of CdSe cores, SILAR, which is an abbreviation for **successive ionic layer adsorption and reaction,** is applied to form multilayered ZnS shell structures around the activated core through subsequent adsorption and reaction of elemental zinc and sulphur in a solvent, including the ionization and formation to the ZnS salt with Zn^{2+} and S^{2-}.[4] For the growth of monodisperse core/shell-QD with equiaxial fluorescence, the reaction conditions need to be controlled precisely to prevent the formation of non-spherical geometries.[3,4,20]

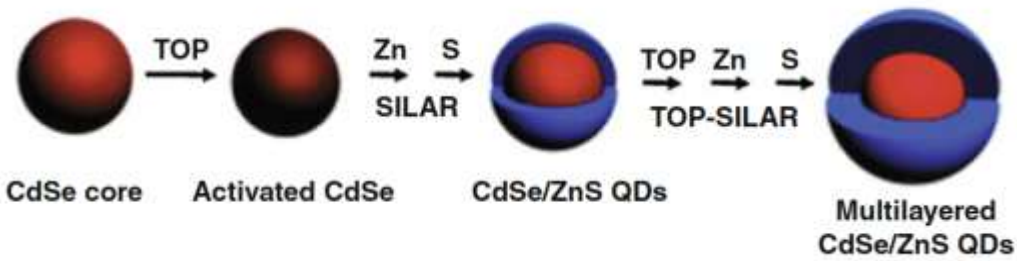

Figure 2. Synthesis procedure and simplified growth mechanism of core/shell-CdSe/ZnS-QD through the TOP-SILAR-method.[4]

1.2 Charging of surfaces in dusty low temperature plasmas

Dusty or complex low temperature plasmas represent the plasma state of soft matter and consist of weakly ionized gas and solid particles of different sizes.[14] The charging of particle surfaces is facilitated through ions and electrons of the plasma.[9,14]

The charge of particles immersed into low temperature plasmas (the surface charge of the so-called dust) can be considered as one of the most influential parameters of particles in a plasma to observe and discuss the behaviour of particles in plasma environments.

In laboratory conditions, the surfaces predominantly acquire negative charges due to the smaller size and limited variability of the system (in comparison to e.g. extraterrestrial plasmas) as well as missing UV-influences which would facilitate the dissipation of surface electrons, leading to the adsorption of cations in extraterrestrial environments.[14]

An example for the various applications of dusty or complex low temperature plasmas is the monodisperse synthesis of various nanoparticles for industrial and academic applications like catalysis and optical sensoring.[9]

For these and other relevant applications like XUV lithography, charging dynamics need to be measurable with high spatiotemporal resolution.

In the conducted experiments, the quantum confined Stark effect (QCSE) of surface-coated CdSe/ZnS-core/shell-QD should be used as a size-dependent surface charge sensor for the dust particles of the plasma that surround the synthesized QD-coated microparticles.

The charging and de-charging effects were not observable with high spatiotemporal resolution which would have allowed to further characterize the charging of surfaces, for which optical methods such as QCSE-based sensors were proposed to be feasible and effective.[9]

1.3 Charge sensing in plasmas using QDs

Quantum dots (QDs) are important within optically active nanomaterials due to their size-dependent and narrow fluorescence emission peaks whose wavelength directly is dependent on the particle size in a range between 0,1 – 5 nm with new developments in the size range up to 100 nm, depending on the used material.[1,16,26]

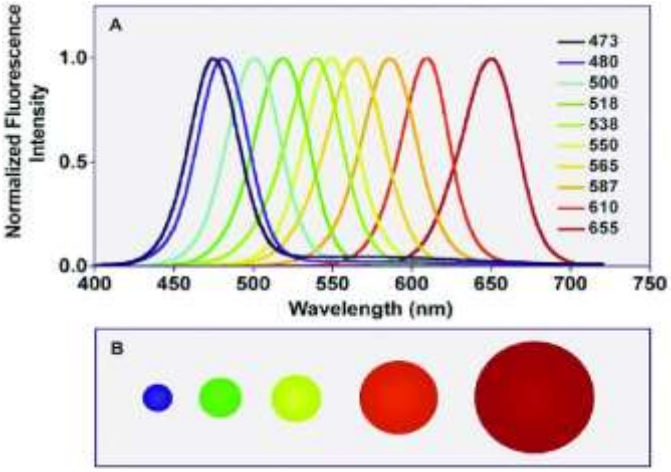

Figure 3. Emission wavelengths of CdSe quantum dots with increasing particle sizes from left to right.[1]

Through the size-dependent property profiles, semiconductor nanocrystals like cadmium selenide in the mentioned size range differ inherently from the corresponding bulk material in terms of discrete energy levels due to the quantum confinement of electron-hole pairs.[1,16] In bulk semiconductors, the band gap width is determined by their bulk properties.[16] Semiconductors support excitons, quasiparticles that can be understood as electron-hole pairs.[16] The reduction of the size of a semiconductor crystal below the Bohr exciton diameter a_B (which is 5,6 nm for CdSe QDs [27]) leads to the reduced statistical possibility of electron movements and to the onset of the band gap width dependence on the semiconductor size.[16,27]

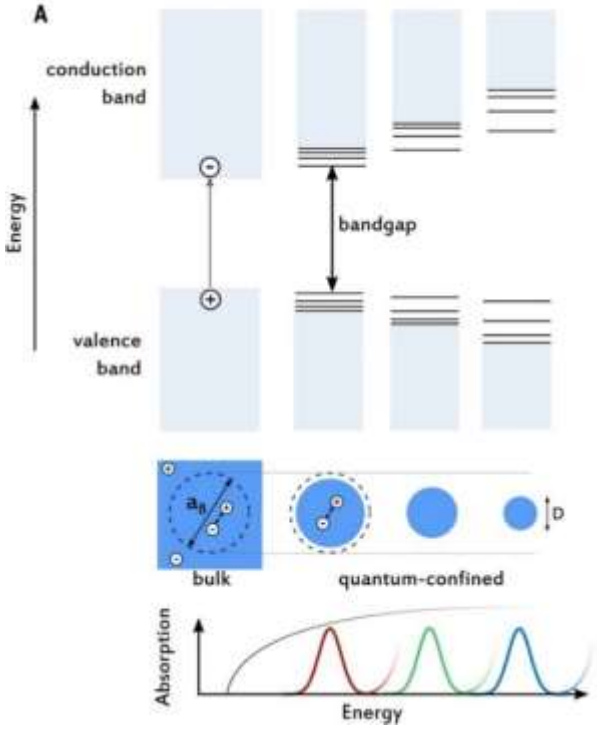

Figure 4. Influence of the material or particle size on intrinsic properties like the band gap and visual explanation of quantum confinement through the reduction of particle sizes of semi-conductive matter below the Bohr exciton diameter a_B.[16]

In the typical size area of semiconductor nanocrystals (1-100 nm) the extent of the band gap width reduces on the increase of nanocrystal size. Due to this variation in the bandgap width, smaller QDs exhibit higher excitation energy (corresponding to shorter wavelengths of e.g. lasers used for photoexcitation).[2,16] The excited state is formed after the absorption of a photon, which transfers a valence electron into the conduction zone, which forms the mentioned exciton.[2,16]

An excited QD would spontaneously relax into the ground state by emitting a photon whose energy is equal to the energy of the band gap, finally leading to the recombination of the electron-pair.[2,16] Regarding the size area, most QDs are commercially available as pre-functionalized dispersions or unfunctionalized powders in the mentioned size range, predominantly in sizes from 0,5 – 5 nm depending on the Bohr exciton radius of the corresponding material and the desired emission wavelength of the nanocrystal.

To really gain **sufficient** understanding of the mentioned general differences between bulk and nanoscale of semiconductor materials like CdSe, the difference between free and confined electrons needed to be briefly explained through quantum mechanical principles. When considering a free electron in a non-confined space, the energy of the system can be determined through the determination of the kinetic energy. A quantum-confined system can be understood as an exciton confined in a box whose dimensions are equal to the dimensions of a nanocrystal.[21]. The Hamiltonian of a confined system can be expressed as [21,22]

$$H = E_{kin} + E_{confinement} = E_{kin} + V(x) \quad (1)$$

Where E_{kin} is the kinetic energy of a particle and $V(x)$ is the box potential. The solution of the Schrödinger equation for quantum-confined system yields differences in energy levels scaling as L^{-2}, where L is the nanocrystal size.[21]

If the dimension L rises, the spacing between the energy levels decreases. With $L = \infty$, the spacing disappears and continuous bulk phenomena can be observed again.[21,22]

Without the existence of an electric field in the observed system, the electrons of the QDs can only acquire energy levels in discrete and characteristic values.[8] If excited without the presence of a strong electric field, the QDs emit fluorescence of characteristic wavelengths which depend on the size of the QD. The statistical model for surface charge determination is based on a red shift of the QD fluorescence peaks which is facilitated through local charge fluctuations in presence of an external electric field. If possible to calibrate and quantify the extent of red shift in dependence of particle sizes, this new optical method could increase the spatiotemporal resolution of the measurement

and thus, the understanding of charging dynamics in low temperature plasmas.[9] The mentioned red shift can be calculated through the following equation, in which the diameter of the QD material is included with a_{QD}^4. This indicates that the extent of the red shift increases with increasing nanocrystal diameter.[9]

$$\Delta\lambda = 0.03\,\frac{\lambda^2}{hc}\,(m_v + m_h)\,a_{QD}^4\left(\frac{2\pi eE}{h}\right)^2 \ldots\ldots\ldots\ldots\ldots\ldots \quad (2)$$

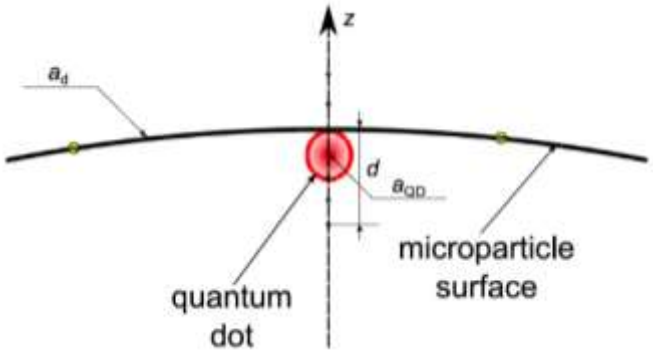

Figure 5. Simplified model for the calculation of the Stark shift induced by QCSE, with the QD (red) located at d = a_{QD}.[9]

The strength of the applied electrical field is included with E, e denotes the elementary charge of the electron. The masses of valence electron and electron hole are included with m_v and m_h, respectively. The mentioned theoretical background of the QCSE was applied to develop a microsensor concept, which exploited optical phenomena of QD fluorescence and their red shift in dependency of the electrical field strength.[9] In literature, an additional protective layer in form of a silicon dioxide coating was synthesized around the surface-coated QD, leading to a core/QD/protection layer structure.[9] In the conducted experiments, the protective layer was substituted using core/shell-QD in which the ZnS shell acted as a protective layer regarding oxidative and thermal degradation, as well as enhancing the quantum efficiency of the material while reducing non-radiative recombinations.[9]

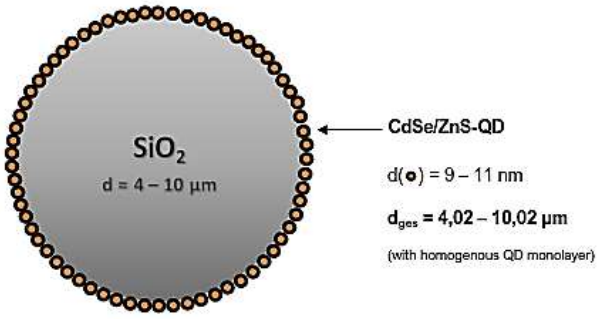

Figure 6. Schematic description of the QD-coated microparticle as charge sensor for the optical determination of surface charges in dusty low temperature plasmas, with the SiO_2 core and the coated core/shell QD on the microparticle surface.

The synthesized, coated particles should be acquiring a diameter which increases by around 0,02 µm with a homogenous QD layer coated onto the surfaces. As the target was to yield dry and storage-stable powders after synthesis, the procedure had to be adjusted according to the stability needs of the used reagents and, more important, towards the stability of the coating itself.

The other potential sensor concept consisted of a homogenous QD coating on a silicon dioxide single crystal wafer. Here, the same optical effects of the used QD for the development of the sensor model for a flat surface were exploited.

1.4 Chemistry of QD bonding on surfaces

The chemical bonding of QDs and the underlying technologies and processes that were developed enabled the production of valuable materials for technical and research applications as summarized below.

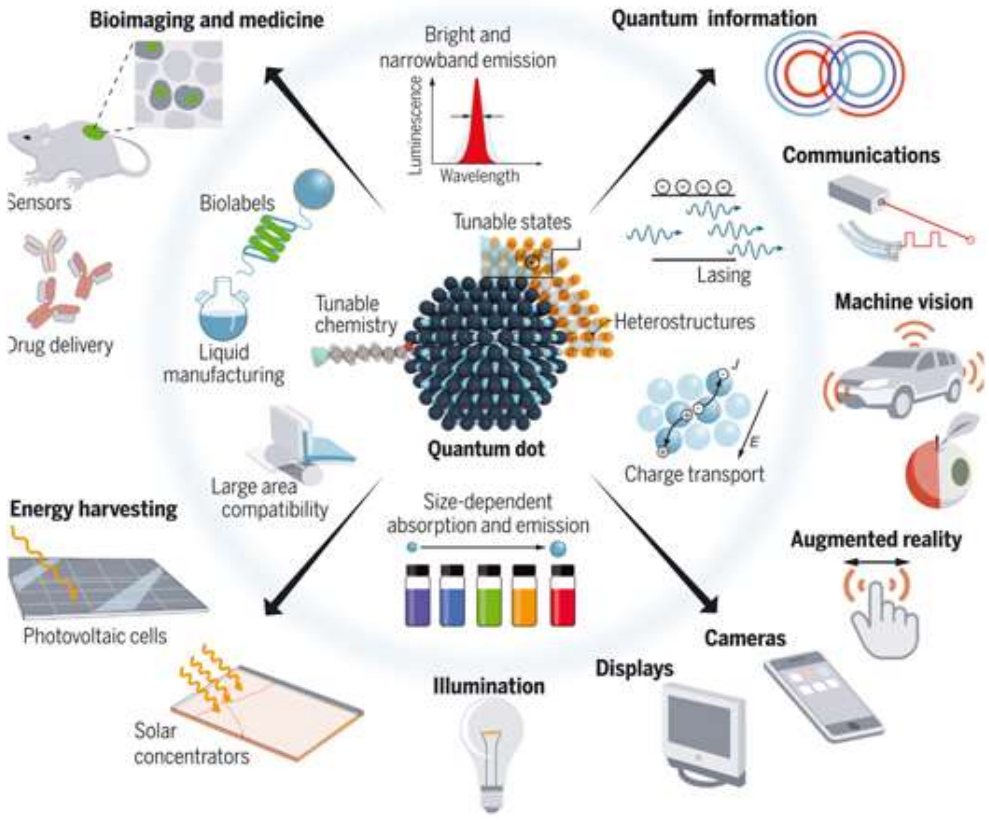

Figure 7. Overview of properties, synthesis and applications of QDs and QD-coated surfaces.[35]

Efforts were made in e.g. the development of novel methods regarding photoluminescent markers in cells, immobilization and detection of biomarkers themselves as well as QD-coated surfaces for various optoelectronic applications.[35,36] The different bonding

technologies for the applications shown in fig. 7 include covalent bonding (through reactive surface groups), often done with silane coupling agents to coat glass or silicon surfaces, physical adsorption through e.g. electrostatic interactions or Van der Waals forces, bioconjugation techniques like avidin/biotin systems for bonding QDs to biomolecules and self-assembly methods e.g. the Langmuir-Blodgett method for thin film formation.[35,36,37]

In this work, covalent bonding between surface-coated amines and carboxylic acid groups was chosen for the coating of QDs onto silica microparticles and silica single crystal wafers, with additional silane chemistry to pre-functionalize the silicon dioxide single crystal wafers with primary amino groups.

1.5 Problem formulation

In the experimental part of the work, the task was to develop reproducible procedures for the coating of different silicon dioxide surfaces, namely a pre-functionalized microsphere as well as a non-pre-functionalized silicon dioxide single crystal wafer with QDs. The target for both coating procedures was to deposit a homogeneous monolayer of quantum dots onto the substrates. This was especially important to satisfy the requirements of the statistical model.[9] The coated microspheres had to be tested regarding storage stability. For the understanding and analysis of the acquired properties, the samples had to be investigated and characterized by means of fluorescence-spectroscopy, TEM-EDX and other diagnostic methods. For fluorescence-spectroscopy, the CdSe/ZnS quantum dots and their dependencies had to be further characterized in terms of linearity, concentration range of fluorescence emission of the bare quantum dots and detection limits. The acquired results of pre-studies and synthesis had to be compared with literature data and needed to be further analysed in terms of validity and reproducibility. The coatings were further characterized and tested in realistic plasma conditions in a low temperature argon RF discharge plasma. The acquired results were summarized in the results and had to be discussed in the concluding chapters of the work.

2 Materials and methods

2.1 QDs, microparticles and silica wafers

The used **CdSe/ZnS-core/shell QD** with emission wavelengths of 540, 600 and 645 nm were acquired from Sigma Aldrich and delivered as aqueous suspensions. They were pre-functionalized with COOH groups through a coating with the copolymer poly(methyl vinyl ether-alt-maleic anhydride). The colloidal solution was stabilized with octadecylamine and had to be stored below 5°C.

The following QD that are summarized in the table below were used for the coatings.

Table 1. Overview of the properties of the used QD materials.

Name	Manufacturer	Nr.	λ_{em} [nm]	Colour of emission	*quantum yield*
QD_1	Sigma Aldrich	900221	540 ± 10	green	≥ 50%
QD_2		919179	600 ± 10	orange	≥ 50%
QD_3		900226	645 ± 10	red	≥ 50%

For the extraction of surfactant groups on the QD surfaces, HPLC-grade toluol (99,7%, Carl Roth) was used. As solvent, ethanol (HPLC grade, 99%, Carl Roth) was used in combination with distilled water. HCl (37%, Sigma Aldrich) was acquired and used in a diluted solution of 1 mol/L for pH adjustment throughout the synthesis runs. For the activation of the carboxylic acid groups on the QD surfaces, an activation reagent, namely **1-ethyl-3-(3-dimethylaminopropyl)carbodiimide** (abbreviated as EDC in the following chapters), was acquired from VWR chemicals and used in all synthesis runs**.** For pH control of the reaction solutions, a digital pH-meter was used **(PeakTech 5310A)**. The activation reaction and the coating procedure were conducted in beakers (Schott Boro 3.3 and Schott Corning PP). For the workup of the coated particles, a centrifuge (Eppendorf 5702, rpm_{max} = 4400) and a desiccator (HAJOKA 300) in combination with a membrane vacuum pump (Pfeiffer MVP020) were used to wash and dry the powder dispersions after synthesis. For the synthesis itself, a heating plate with magnetic stirrer (VELP AREX-6 Digital Pro) was used in combination with single-use pipettes, Teflon tweezers and transfer pipettes (Brand Transferpette, different volumes from 10 to 1000 µL).

The used **silica microparticles** in a size range of 3,92 – 10,95 µm were delivered as aqueous suspensions and acquired from microparticles GmbH. They were pre-functionalized with primary amino groups. As there was no specific information about the type of molecule used on the microparticles for functionalization, it was expected that the amines resided from a coating with ethylene diamine as shown on the supplier website.

The following table summarizes the manufacturer data regarding the particle sizes and the comparable SEM measurement to estimate the accuracy of the monodisperse size distribution of the used microparticles.

Table 2. Comparison of manufacturer data and SEM data towards sizes and size distribution of the used silica microparticles.

Manufacturer data		**SEM data**		Difference to manufacturer data
d / µm	**St.dev. / µm**	**d / µm**	**St.dev. / µm**	
3,92	± 0,14	3,90	± 0,14	0,5 %
10,58	± 0,35	10,40	± 0,26	0,8 %
10,95	± 0,54	No data, new samples of supplier shortly before end of thesis		

The **single crystal wafers** were acquired from Merck and were not pre-functionalized. The used SiO_2 wafers had a size of 10x10x0,5 mm. For the pre-functionalization of the wafers, 3-(aminopropyl)triethoxysilane was acquired from Carl Roth. As solvent, ethanol (HPLC grade, 99%, Carl Roth) was used in combination with distilled water as well as aqueous acetic acid (technical grade, 80%, VWR) for APTES-functionalization.

2.2 Chemical procedures

For the **coating of microparticles**, pre-functionalized variants of QDs and microparticles were chosen. The QD surface was coated with the mentioned copolymer, in which the maleic anhydride groups within the polymer chains formed free carboxylic acid groups through hydrolysis. The general idea was to induce the formation of covalent amide bonds between free carboxylic acid groups on the QD surfaces and primary amino groups on the microparticle surface.

The used QDs were combined with different microparticle sizes. In addition, samples with two different QD types on it were synthesized. An exemplary setup of a synthesis row with the mentioned reagents is summarized in the following table.

Table 1. Exemplary overview of synthetic combinations for QD-coated microparticles.

No.	QD_1	QD_2	QD_3	SiO_2 (4 µm)	SiO_2 (10 µm)
1	**x**			**x**	
2	**x**				**x**
3		**x**		**x**	
4		**x**			**x**
5			**x**	**x**	
6			**x**		**x**
7	**x**	**x**		**x**	
8	**x**	**x**			**x**
9	**x**		**x**	**x**	
10	**x**		**x**		**x**
11		**x**	**x**	**x**	
12		**x**	**x**		**x**

The QDs were used in excess to facilitate a homogenous coating. The used QD dispersions had a mass concentration of 1 mg/mL, the concentration of the microparticle suspensions were 5 mg/mL

To underline the composition of the layer structure of the used QD, an overview was summarized in the following figure.

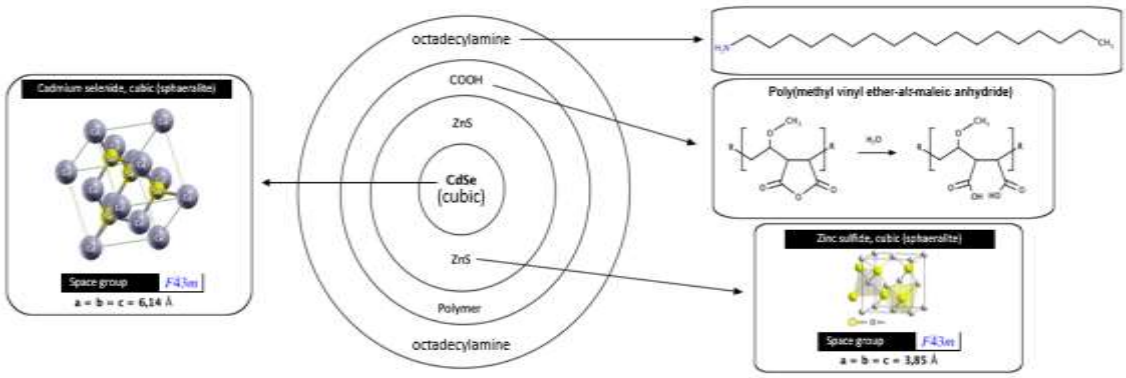

Figure 8. Composition of the layer structure of the used core/shell-QD with a CdSe core, a ZnS shell, a copolymer coating for COOH-functionalization and the used surfactant octadecylamine. Besides of the unit cell of CdSe[17] and ZnS[18], the figure is self-produced.

After deprotecting and hydrolysing the QD surfaces, the free COOH groups could be activated through the formation of an O-isoacylurea-intermediate from reaction of COOH with e.g. 1-ethyl-3-(3-aminopropyl)carbodiimide (EDC).

The formed intermediate is highly reactive towards primary amines and should therefore induce sufficient amide formation in a short time.

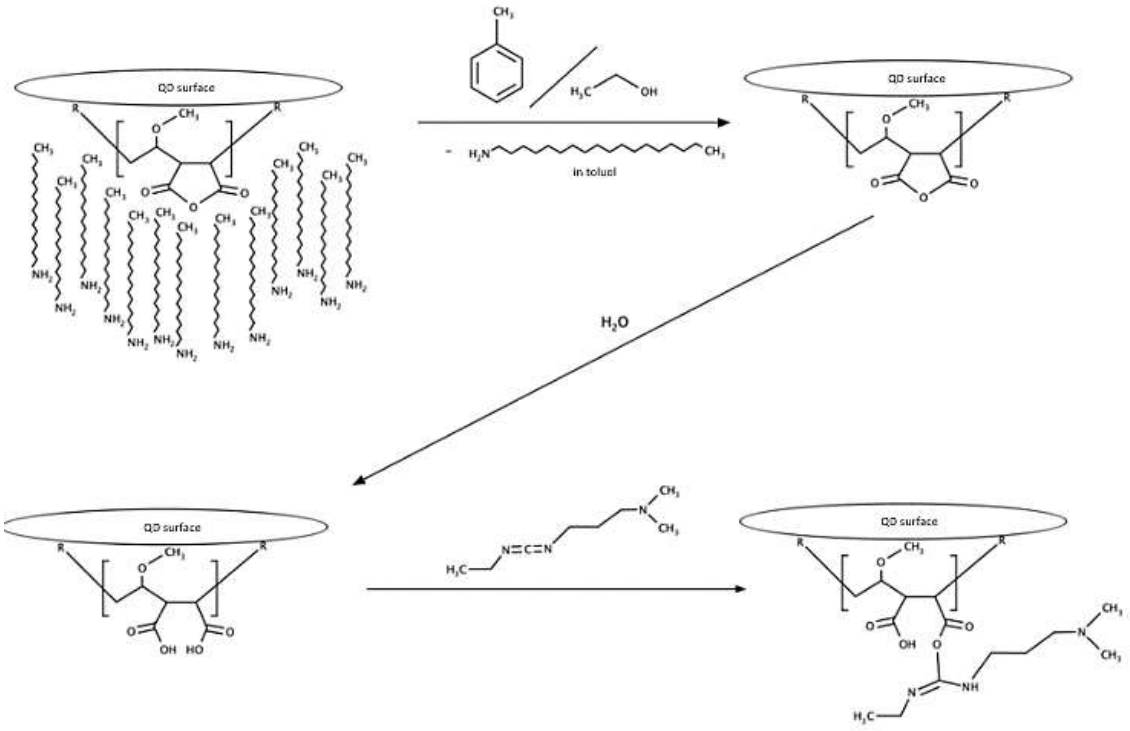

Figure 9. Principle of preparation of the used QD by extractive deprotection from the surfactants in an apolar solvent, hydrolysis to gain free carboxylic acid groups and activation reaction with EDC.

In the following, an exemplary calculation of needed QD amounts for the coating of microparticles was summarized. The basic data used for the mentioned calculations was listed below. It should be mentioned that the QD diameters had to be estimated based on literature data, which caused some uncertainty in the calculated values. As the largest sample size for the measurements of TU Eindhoven was 25 mg, the exemplary calculations are based on this amount.

$$r_{QD} = 2 \times 10^{-9}\, m$$

$$M_{QD} = 173 \frac{kg}{mol}$$

$$r_{SiO_2\,(10\,\mu m)} = 5 \times 10^{-6}\, m$$

$$\rho_{SiO_2} = 1850 \frac{kg}{m^3}$$

$$m_{SiO_2\,(10\,\mu m)} = 2{,}5 \times 10^{-5}\, kg$$

With the aid of the mentioned data, the needed QD quantity to coat 25 mg of silicon dioxide microparticles with a diameter of ten µm was calculated.

$$N_{QD\ @\ SiO_2\ (10\ \mu m)} = \frac{4\times\left(r_{SiO_2\ (10\ \mu m)}\right)^2}{\left(r_{QD}\right)^2} = \frac{4\times\left(5\times10^{-6}\ m\right)^2}{(2\times10^{-9}\ m)^2} = 2{,}5\times10^7 \quad (3)$$

With that result the **mass of QD on one single microparticle** was estimated with the use of the QD molar mass and the Avogadro constant N_A.

$$m_{QD\ @\ SiO_2\ (10\ \mu m)} = \frac{M_{QD}\times N_{QD\ @\ SiO_2\ (10\ \mu m)}}{N_A} = \frac{173\frac{kg}{mol}\times(2{,}5\times10^7)}{6{,}023\times10^{23}\frac{1}{mol}} = 7{,}2\times10^{-15}\ kg \quad (4)$$

With the mass of needed QD to coat one single silicon dioxide particle with the size of 10 µm, the total mass of QD that are necessary were estimated after calculating the quantity of SiO_2 microparticles in 25 mg of powder.

$$N_{SiO_2\ (10\ \mu m)} = \frac{3\times m_{\ SiO_2\ (10\ \mu m)}}{4\pi\times\rho_{SiO_2}\times r_{SiO_2\ (10\ \mu m)}} = \frac{3\times(2{,}5\times10^{-5}\ kg)}{4\pi\times1850\frac{kg}{m^3}\times(5\times10^{-6}\ m)} = 2{,}6\times10^7 \quad (5)$$

$$m_{QD}\ =\ N_{SiO_2\ (10\ \mu m)}\times m_{QD\ @\ SiO_2\ (10\ \mu m)} = (2{,}6\times10^7)\times(7{,}2\times10^{-15}\ kg) \quad (6)$$

$$\boldsymbol{=1{,}9\times10^{-7}\ kg = 0{,}19\ mg}$$

This implicated that 190 µg or 190 µL of a 1 mg/mL-dispersion had to be sufficient to coat the whole amount of powder in a homogenic way.

Herein, the density of amino groups at the microparticle surfaces exceeded 30 µg/g NH_2, which had to be considered while determining or estimating the different QD amounts needed for the coatings. The different particle sizes and therefore different surface areas also had to be included in the calculations of needed QD amounts. As the QD as well as the silicon dioxide microparticles were pre-functionalized, there was no further need for pre-functionalization in that case. For the microparticle synthesis, two different variants of a comparable method were developed.

After the process stated in literature [24] (coating through solution addition and slight shaking) was not working properly with the used reagents, the process was initially further developed and adjusted in terms of reaction conditions (new temperature of 40°C for activation energy, magnet stirrer for homogeneity of the solution) to enable the coating reactions with the used reagents and their different properties. The QD amount was transferred to a prepared mixture of ethanol and water which should at first enable the hydrolysis of the maleic anhydride groups included in the surface polymer of the QD. After hydrolysis, the pH was adjusted to pH = 8-9 to enable carboxylate formation as suggested by literature. Afterwards, the prepared microparticle solution (pH 3-4) was added very slowly and dropwise to the QD solution that was stirred at 120 rpm throughout the microparticle addition with a constant reaction temperature of 40°C. After the addition

was finished, the mixture was stirred for another 1-2 h to enable complete reaction between amines and carboxylates.

The **final and optimized procedure** consisted of the preparation of the QD-solution with further extraction of octadecylamine surfactants with toluol as extraction solvent and subsequent centrifugation at 4400 rpm for two minutes. Following up, the carboxylic acid groups on the QD surfaces were hydrolysed through immersion of the surfactant-free QD in a prepared solution of aqueous ethanol (which was previously adjusted to a slightly acidic pH of 5-6 through 0,1 M HCl) and through addition of EDC to the QD solution. After activation through EDC, the QD solution was prepared as described above and stirred at 40°C throughout the reaction within a range of 100-150 rpm. The increase in rotation speed was necessary to prevent coagulation at the beaker bottom and the magnetic stirrer. The microparticles were added directly through a pipette (Brand Trasferpette) while the mixture was homogenized through the magnetic stirrer. The dilution and concentration of the QD solutions and microparticles in the synthesis rows were adjusted based on theoretical calculations and information from literature.[24] The opaque dispersions were stirred for two to five hours, compromising on a reaction duration of at least 4 hours at 40°C.

After successful synthesis, the unbound QDs were separated from the coated powder through centrifugation (4000 rpm, 2 min) and rinsing with water and isopropanol, respectively. The wet and cleaned powders were dried in a desiccator with aid of a vacuum pump. After drying, the storage stability of the powders was investigated through subsequent measurements of UV-VIS spectra of samples that were stored with and without light and temperature influences (20°C to 2°C in the fridge).

The following figures should underline the whole process from QD preparation to post-processing of the coated samples. Initially, the deprotection (1) and hydrolysis (2) of the QD surfaces was facilitated as shown below.

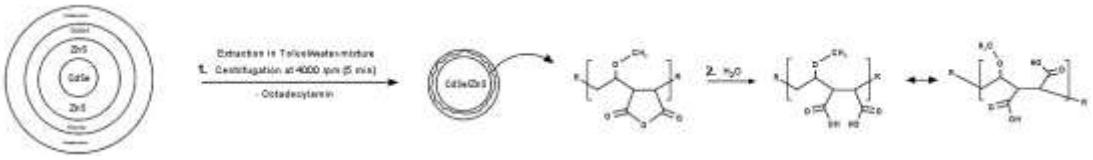

Figure 10. Synthesis concept for QD-coated SiO_2-microparticles (1-2). At the beginning, octadecylamine had to be removed through extraction in toluol and subsequent centrifugation (1). After surfactant removal, the maleic anhydride monomers within the polymer had to be hydrolysed to form free carboxylic acid groups (2).

With the addition of the microparticles to the activated QD surfaces (3), the formation of amide bonds with the subsequent elimination of a urea byproduct residing from EDC is facilitated, which was easily separable from the coated powders (4).

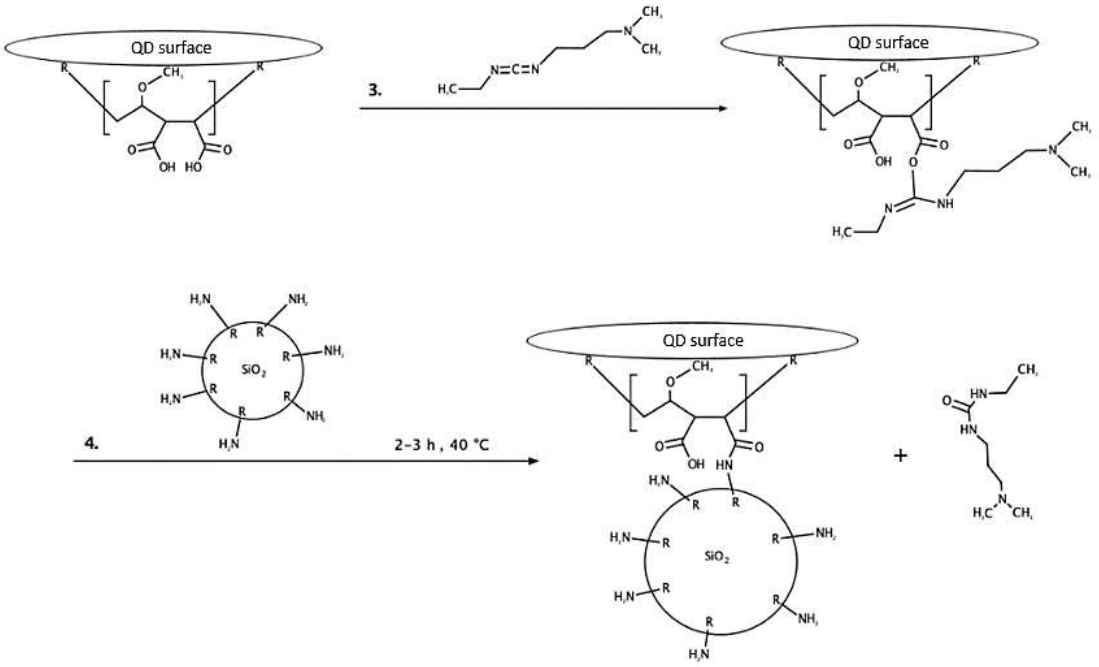

Figure 11. Synthesis scheme (follow-up steps) of the QD coating procedure onto silicon dioxide microparticles. After hydrolysis, the free COOH groups at the QD surface should form an activated intermediate with EDC (3) which is known to be highly reactive towards primary amines. In the last step, amide bonds are formed with subsequent elimination of the shown urea byproduct (4).

An optional, further reaction was the formation of imides in presence of elevated temperature and acid traces with subsequent elimination of water, where the nitrogen would reside from the microparticles while the carbonyl groups were part of the polymer on the QD surface.

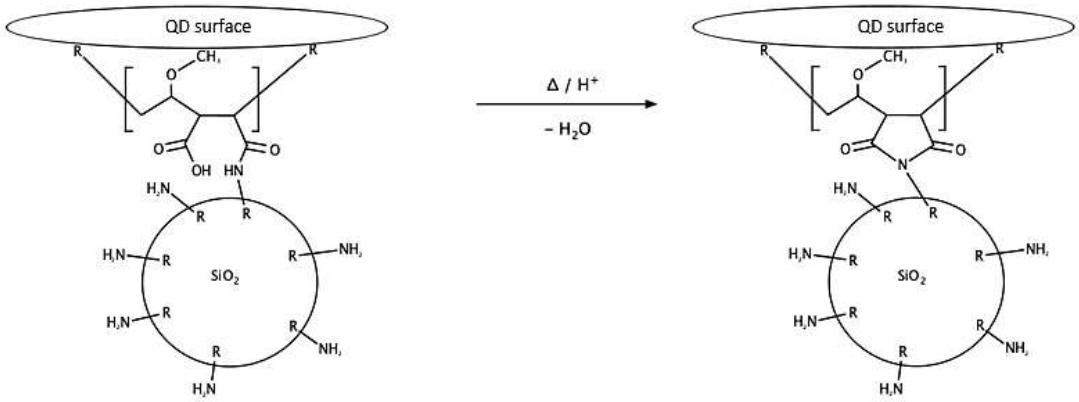

Figure 12. Optional reaction after amide formation: after dehydration, the amides between QD and silica and the free carboxylic groups of the QD surface can form imides through the influence of higher temperature and in presence of acids.

Here the influences of microparticle and QD sizes as well as dependencies from reaction parameters like temperature, solvent and pH have been investigated. Special attention was paid to the influence of an activation reagent for carboxylic acid groups regarding amide formation.

For the coating of the **single crystal wafers**, different synthesis runs were done with one or more QD specimen on the same substrate. All the synthesis runs followed the same procedure described below.

Initially, the wafers needed to be cleaned and hydrophilized in a solution of peroxymonosulfuric acid (H_2SO_5) which was prepared in-situ through mixing of concentrated sulfuric acid and hydrogen peroxide (1:2). The substrates were left in the solution for clean-up and hydrophilization for 30-60 minutes. The reduced formation of bubbles from the substrate indicated that the hydrophilization of the surfaces was completed. The substrates were rinsed with distilled water and dried under nitrogen. After drying, the substrates were transferred to a prepared solution of APTES (< 2% v/v in aqueous acetic acid) and coated with a monolayer of amine-terminated siloxane molecules for covalent immobilization of the QD through amide bonds. The APTES coating reaction was conducted at 90-100°C for one hour.

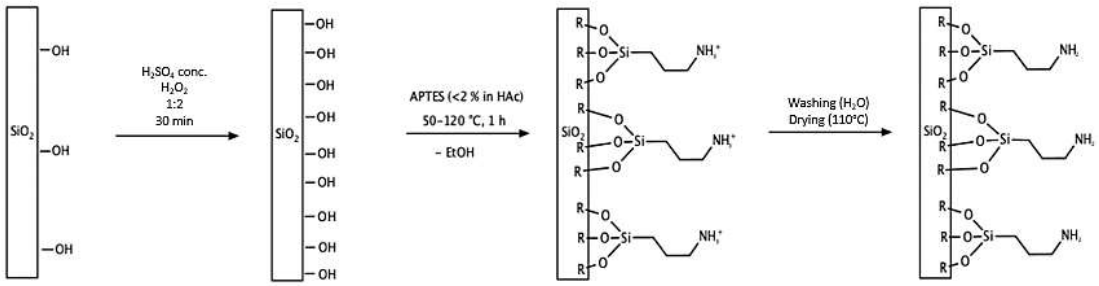

Figure 13. Preparation and pre-functionalization of silicon dioxide single crystal wafers through cleaning and hydrophilization with H_2SO_5 and surface functionalization with APTES to form free primary amino groups on the surface.

After surface functionalization, the QD solution (prepared and activated as described above) was heated up to 40°C and kept at this temperature for the coating reaction. The APTES-coated substrates were cleaned with aqueous acetic acid and distilled water and transferred to the QD solution. The substrates were left in the QD solution for 20-24 hours and dried and cleaned with nitrogen and water after successful QD coating.

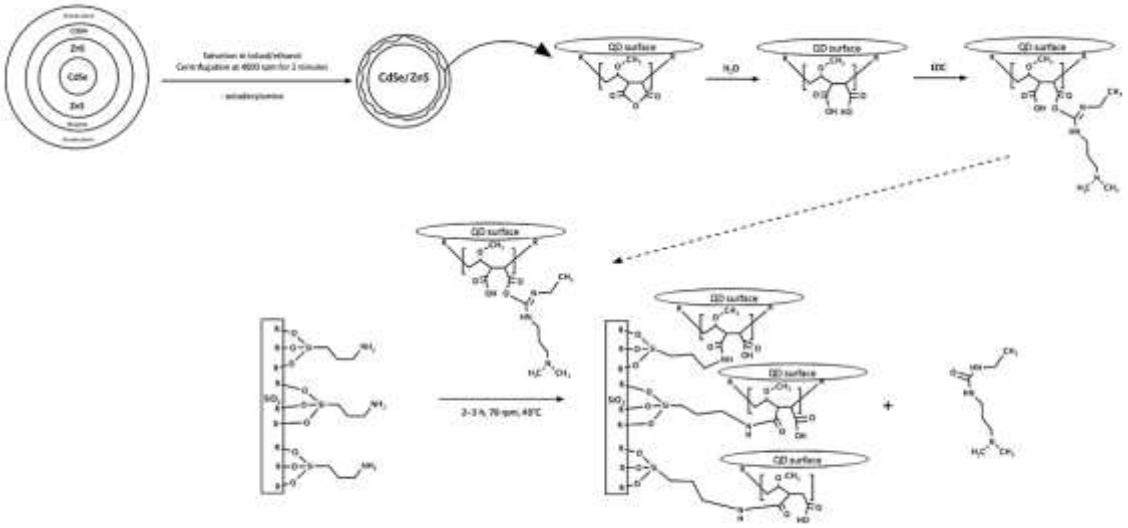

Figure 14. Preparation of the COOH-functionalized QD with the described procedure through deprotection, hydrolysis and EDC activation and amide formation between the activated QD and the prepared APTES-groups on the surface of the single crystal wafers.

Additional heat curing (70 -100 °C) was done after drying and cleaning the sample to further stabilize the layer. The coated single crystals were stored at room temperature in a dry environment.

2.3 Diagnostic methods

The main diagnostic method used in this thesis was **fluorescence spectroscopy**. From a physical point of view, fluorescence can be understood as a spontaneous re-emission of photons (statistically, in all directions) after excitation through a light source with shorter wavelength than the emitted fluorescence wavelength.[12] The following Jablonski diagram summarizes the process behind excitation and fluorescence within an optically active nanocrystal.[12]

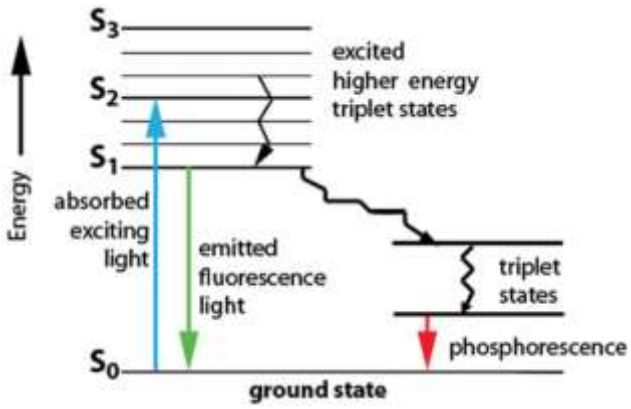

Figure 15. Simplified Jablonski diagram of the process of excitation and formation of excited states, especially singlet states are relevant for fluorescence. The absorbed energy of the excitation is re-emitted as fluorescence in a material-characteristic wavelength when the electron goes back to ground state, with some energy loss in terms of vibrations and heat.[12]

When electron-hole pairs within semiconductor nanocrystals are excited, highly energetic singlet states are formed that are spin-pared with the ground state. As the return of spin-paired electrons in the ground state is physically allowed, the lifetime of fluorescence emissions is in the range of nanoseconds.[19]

In the experiments, the observed wavelength range was defined between 400 and 800 nm with excitation through a 405 nm laser. The following fluorescence-spectroscopy setup was used throughout the time of this work.

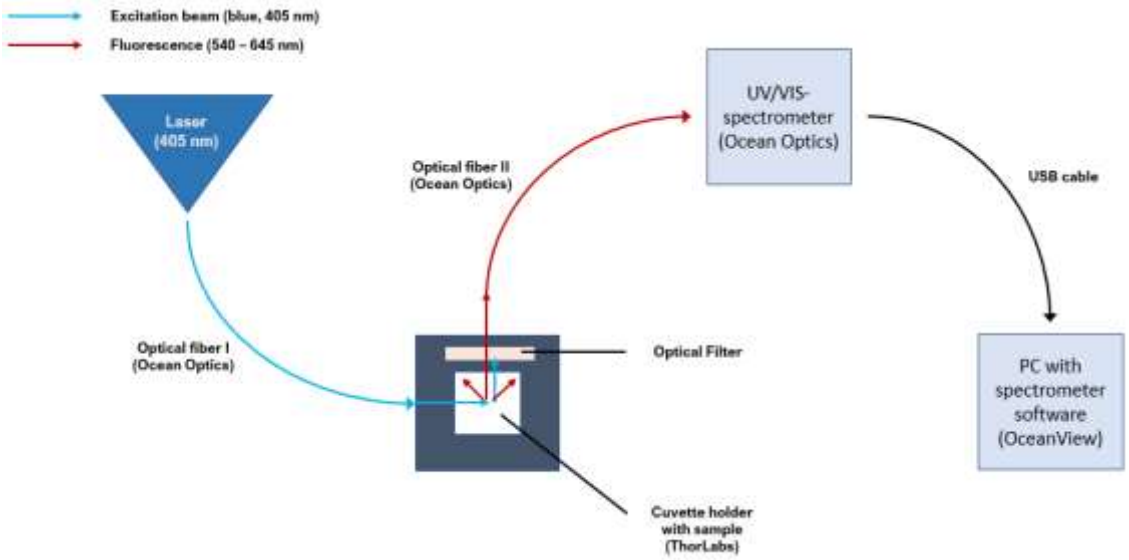

Figure 16. Schematic description of the used measurement setup for fluorescence detection in the UV/VIS range with an excitation laser (ThorLabs, 405 nm, blue) and a UV/VIS-spectrometer (Ocean Insight USB2000) which were connected through optical fibres (OceanOptics). The spectrometer data was transferred through USB connection for analysis in the OceanView software of OceanOptics.

The used laser emitted a monochromatic excitation beam with a wavelength of 405 nm which was transferred to the measuring chamber through an optical fibre. In the measuring camber (CVH100 (Thorlabs)) the monochromatic light beam hit the cuvette with the sample (powder or dispersion), leading to fluorescence emission in all directions (red lines). The fluorescence signals after excitation were transferred to the spectrometer through another optical fibre. The spectroscopic information was transferred to the PC through an USB cable. The mentioned setup was used to determine the linearity of the fluorescence signals, to determine qualitative synthesis results as well as storage stabilities of the coated powders and coated single crystal wafers.

The fluorescent properties of reagents, intermediates and products were characterized through fluorescence-spectroscopy in terms of peak intensity and full width at half maximum (FWHM). Before measuring the samples, background and blind spectra of the

system were acquired, including empty measuring cell, empty cuvette, and cuvette with all used solvents to distinguish the QD peaks from the background. The chosen integration times had to be adjusted to the intensity of the measured signal, with the pristine QD solutions that needed low integration times (2-3 ms) and high dilution and the powders that were measured with sufficiently longer integration time of 50-200 ms in dependence of the fluorescence intensity. Data evaluation was done with the OceanView software of OceanOptics. It was possible to analyse all microparticle samples with fluorescence-spectroscopy. For the single crystal wafers, fluorescence microscopy was used in combination with fluorescence-spectroscopy for the analysis of qualitative results.

Scanning electron microscopy is based on the interactions of electrons with solid matter in terms of elastic backscattering (BSE detector), secondary electron emission (SE detector) and X-rays. As the backscattering intensity is dependent on the atomic number, heavier elements appear brighter in the image.[30] Secondary electrons are lower in energy in comparison to BSE and are ejected from the surface atoms of the sample.[30] The detection of secondary electrons is commonly used for high-resolution imaging of surface topography and facilitated by Everhart-Thornley-detectors (scintillator-photomultiplier system), an additionally through In-Lens-detectors of electrons near the beam's axis for higher resolution images at lower electron beam energies.[30] The principal structure of a SEM is demonstrated in the figure below and consists of an electron gun as source, an anode for acceleration and the optical aperture in form of magnetic lenses.[30,31] The detection of the three main interactions is facilitated by the corresponding detectors.[30]

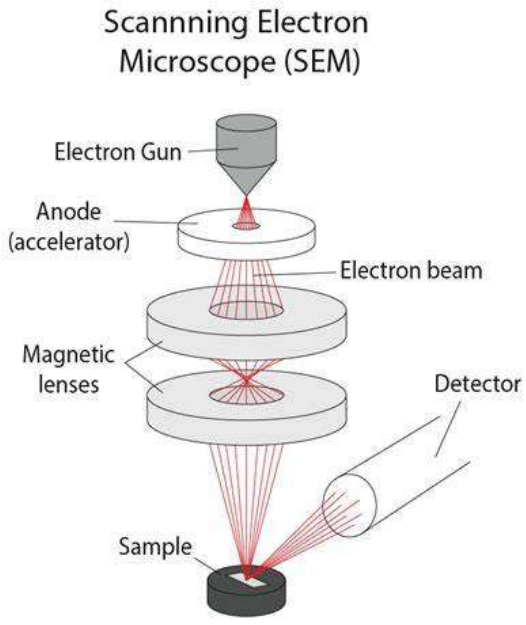

Figure 17. General principle of scanning electron microscopy with electron source, acceleration, refocusing and detection.[31]

In **transmission electron microscopy**, the principal structure is comparable with SEM, with differences in higher electron beam energy (up to 300 kV), therefore higher resolution, and utilization of transmission instead of scattering and secondary emission.[32] The sample preparation is more complicated compared to SEM as extremely thin samples are needed to reduce backscattering for optimal transmission and imaging. The electrons are scattered, diffracted and absorbed through the internal structure of the sample.[32] The transmitted electrons are collected through i.e. fluorescent screens or complementary metal-oxide semiconductor (CCD) cameras.[32] Herein, bright-field imaging utilizes the directly transmitted electrons to form high-contrast images with high electron density appearing darker. Dark-field imaging uses diffracted electrons to highlight specific crystallographic features like defects or specific crystal planes.[32] Energy-dispersive X-ray spectroscopy (EDX) can be applied in combination with TEM through detection of X-rays that acquire characteristic energies in dependence of the included elements of the sample, enabling the determination of the atomic composition of images.[32]

Fluorescence microscopy is a form of light microscopy in which the sample is additionally excited through a laser beam to induce fluorescence. However, the principal setup is more complex due to the need of excitation and emission filters. It includes a light source, the excitation filter followed by a dichroic mirror and an objective lens, with an emission filter in front of the detector, camera or ocular.

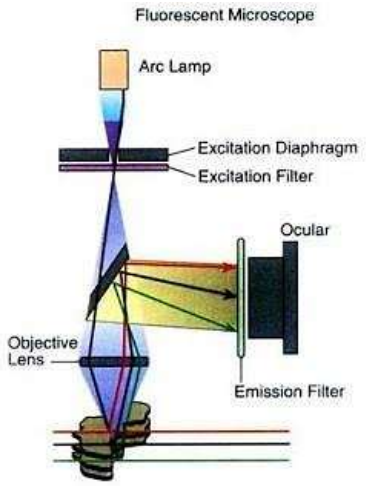

Figure 18. General principle of fluorescence microscopy.[33]

The light source emits excitation light which is transformed to a monochromatic light beam in the excitation filter. The beam gets refocused in the dichroic mirror and objective lens onto the sample and induces fluorescence.[34] The fluorescence emission gets transferred to the camera, ocular or detector, enabling sample observation or image generation.[34]

2.4 Tests in plasma environments

The plasma experiments with the QD-coated microparticles and single crystals were conducted at TU Eindhoven in the working group of Prof. Job Beckers.

The measuring setup consisted of a stainless-steel chamber for plasma formation, evacuated with a turbomolecular pump. Plasma ignition was facilitated through applying radiofrequency power to an included electrode. UV/VIS-spectrometer backed by and ICCD camera (Andor) was used to observe the fluorescence spectrum. A CMOS camera (Photron) was used to visualize the levitating microparticles. and a fluorescence spectrometer were used for imaging of particle levitation and fluorescence analysis.

For excitation, a pulsed 405 nm laser was used. The particles were stored in a shaker, immersed into the plasma through shaking and levitated through the plasma within the chamber. When hit by the laser beam, the particles were observable in the ICCD-camera as well as in the fluorescence spectrum. Before, the optical aperture had to be adjusted to the height of the levitating particles in the chamber. The QD-coated single crystals had to be placed into a sample holder, mounted on a stainless-steel holder, and experienced less plasma exposure as no levitation was necessary. The following figure schematically describes the measuring system as well as the effect of plasma onto the fluorescence peaks that are red shifted under the influence of external electrical fields.

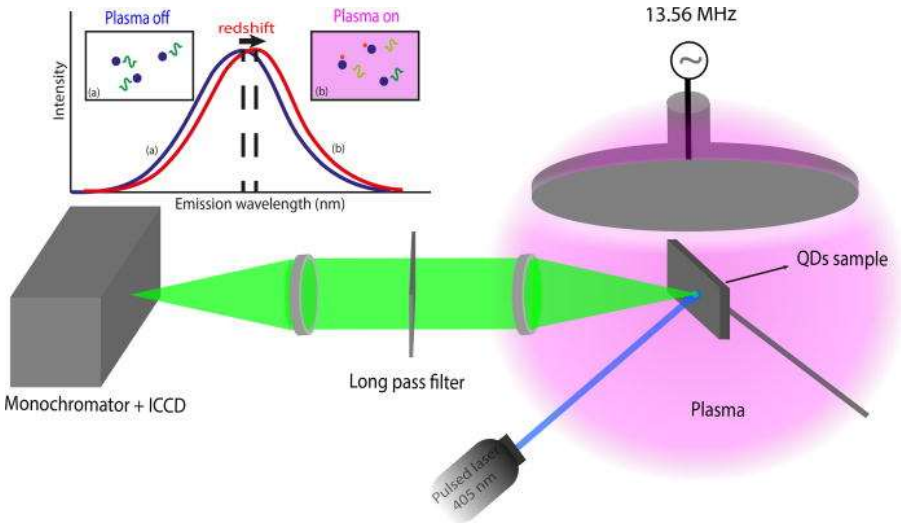

Figure 19. General concept of the measurement of the red shift within the fluorescence peaks of QD-coated single crystal wafers under the influence of a strong, external electrical field through the QCSE. In the used setup, the monochromator and ICCD were used without a long pass filter, the excitation source was chosen similarly as 405 nm pulsed laser, and the electrical field strength was also chosen as 13,56 MHz corresponding to previous data which is shown.[25]

For the single crystals, a sample holder was constructed which enabled to place two single crystals within the measurement setup, the excitation and analysis techniques were similar to the microparticle procedure.

3 Results

3.1 Conduction of synthesis and fluorescence spectroscopy

3.1.1 Coating of microparticles

The procedures that were described before led to different results, as the procedure had to be adjusted to the properties of the acquired QD and microparticles. The general feasibility of the coating reaction onto microparticles and single crystal wafers was confirmed after properly adjusting the procedures to the needs of the used reagents.

Before the synthesis, the properties of the pristine QDs had to be determined. Therefore, a fluorescence linearity analysis with subsequent dilution in the measured cuvettes was performed for all three QDs.

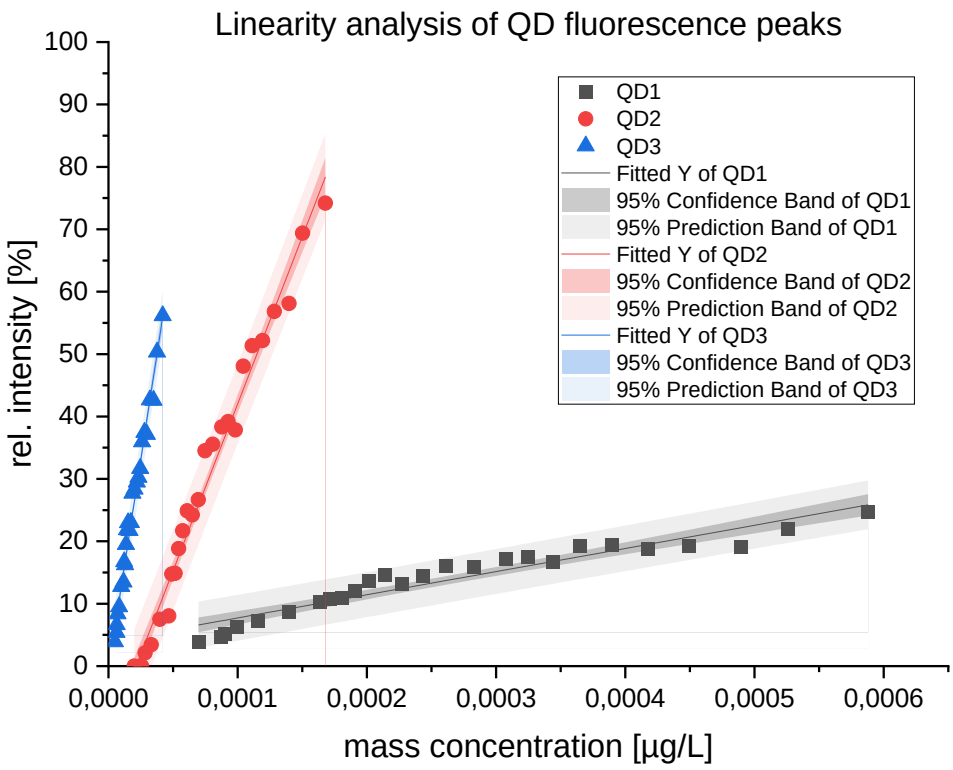

Figure 20. Determination of linearity of QD fluorescence peaks in dependence of QD mass concentration in aqueous solution with confidence- and prediction bands of expected variances of the values.

A linear increase was observed for all three used QDs, with the strongest signal and highest slope for the biggest QD (QD_3) and the lowest limit of detection. The intensity in in contrast to the QD concentration significantly lowered with reducing the QD core size. A straightforward comparison of intensities at different wavelengths was not possible, as

the spectral dependence of the sensitivity of the used spectrometer had to be considered too. The best linear fit was acquired for QD_3 as well, which could be explained by the higher quantum yield and therefore fluorescence intensity in dependence to the concentration.

Besides linearity, detection limits of the used QDs were estimated with a similar dilution strategy in one cuvette.

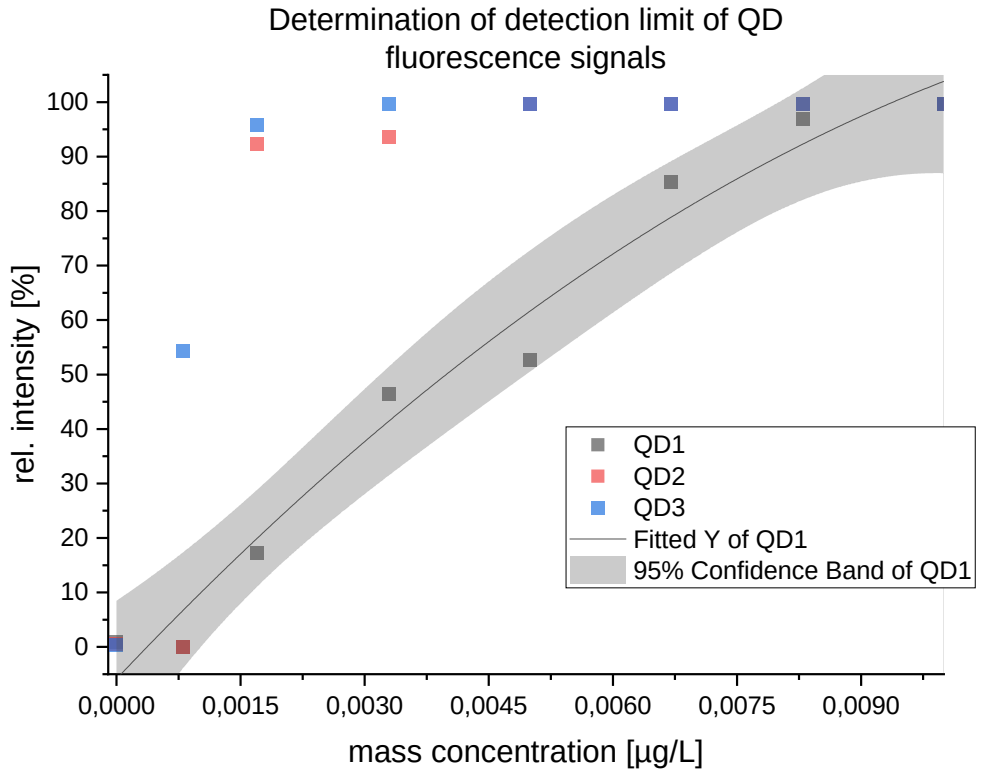

Figure 21. Determination of detection limits of the diluted, aqueous solutions of the used QD, measured at a constant integration time of 20 ms. The highest fluorescence intensity in dependence of the concentration is found for QD3 which is also detectable below 1 ng/L.

The detection limit or saturation threshold was determined to be 0,7 ng/L for QD1, 0,3 ng/L for QD3 and 0,08 ng/L for QD_3. The saturation of QD_2 and QD_3 was already observed at a mass concentration above 1,5 ng/L, using an integration time of 20 ms. The significant difference the data shows a quick saturation of the fluorescence signals after a linear increase in terms of intensity which supports the previously acquired results.

At the beginning, a literature-inspired procedure was evaluated which was then further optimized and developed throughout the time of the thesis.

The initial idea to separately prepare two activated solutions of QD and microparticles that react through simple addition did not work out in terms of amide formation, as observed in fluorescence spectroscopy.

As this was not feasible for the used materials, the procedure had to be further adjusted. The lack of success could be explained by considering the formation of two inactive species (carboxylates and ammonium ions) through acid-base chemistry.

This probably led to salt formation, which is known to be less stable than covalently bonded compounds as there would only be electrostatic interaction between QD and microparticle surface. Therefore, the coating could easily be altered or removed while working in aqueous solution. As there were no peaks observable in the fluorescence-spectra for these reactions, neither in solution after reaction, nor in the dried powder, a modified procedure was established.

The experiments stated in literature were based on elemental cadmium and included the synthesis of own QDs used for the coatings.[24] The QDs were synthesized and functionalized within the work described in literature.[24] In this work, pre-functionalized QDs were acquired, which hindered the accurate reproduction of the reaction conditions in literature. The first optimization approach with constant stirring and additional heating in combination with longer reaction times led to the first observation of fluorescence peaks in the dried powders as a qualitative proof for the coating reaction. As the intensity still was too low compared to pristine QD data (no separate peak observable with reasonable integration time), the procedure had to be further optimized in terms of reagent activation, where the activation of carboxylic acid groups on the QD surface was chosen using EDC. The last optimization finally led to positive results for both the particle coating as well as the coating of the single crystal wafer.

After the method development and validation through fluorescence spectroscopy (before actual characterization), comparable spectra were acquired which show the altering of the peak shape when coated onto a microparticle in comparison to blank values of the system, including the empty cuvette, solvents and the pristine QD.

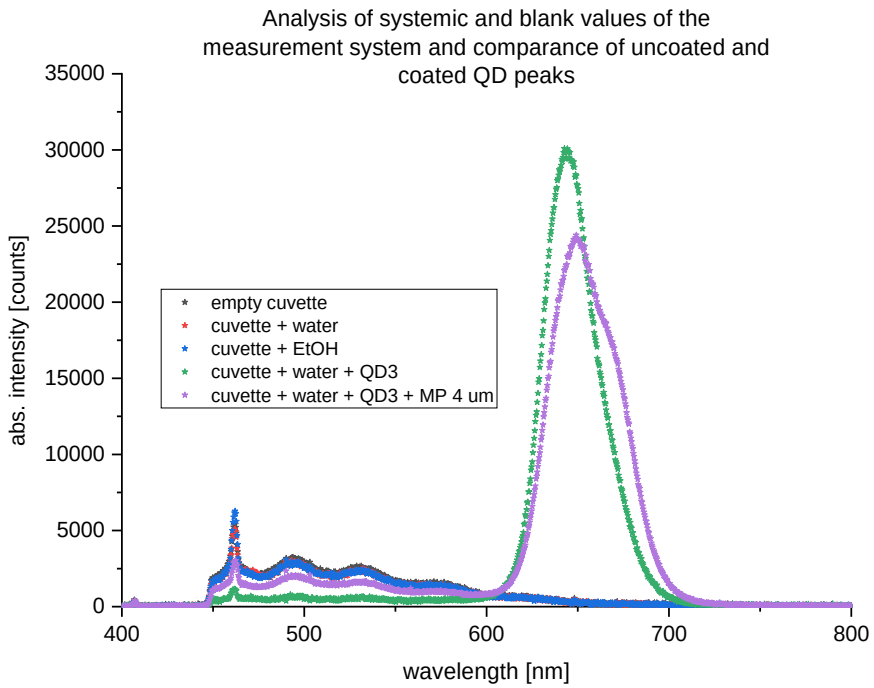

Figure 22. Fluorescence-spectroscopy data of the blank values of the measuring system in comparison to the fluorescence peaks of pristine and coated QD on a microparticle. Slightly visible are the excitation frequency of the used laser (405 nm) as well as systemic and solvent impurities in the range of 400-600 nm. All the shown data was acquired at 200 ms of integration time with a dilution of the pristine QD-solution to 1 ng/L.

It was observed that the peak gets broader and less intense after the coating reaction, and that ethanol as solvent caused impurities in the spectral range of 450-550 nm in combination with the cuvette, with a main peak located at 461 nm. There also was a red shift of the peak centre observable after the coating reaction (645 to 650 nm) which could be attributed to the altered local environment of the QD cores to a microparticle.

The lowered intensity could be explained through the consideration of the shares of non-fluorescent and fluorescent parts of the particles where the non-fluorescent part had a share of 99% of the total volume. Another explanation was the inhomogeneity of the coating and coating reaction which was observed at the beginning of EDC usage and was reduced throughout the optimization of the procedure.

As the monodisperse microparticles tended to agglomerate and stick to each other, the drying process and the adherence of homogenous reaction conditions were hindered to some extent. This issue was further reduced through increasing the stirring speed from 100 to 150 rpm. There were some uncertainties to consider while interpreting the acquired spectra, especially at the beginning of the deployment of the first optimization. It was exceptionally complicated to differ between covalently bonded QD and QD that were electrostatically attached to the microparticle surfaces (or to coated QDs) with fluorescence-spectroscopy. After the optimization with the removal of surfactants from the QD

through extraction with toluol and activation of the carboxylic groups with EDC, reliable fluorescence spectra were acquired from a reproducible procedure for the chosen reagents which was confirmed by fluorescence-spectra as well as TEM and SEM.

One of the main observations in the fluorescence spectra was the proportionality of peak intensity in dependency of the surface area of the used microparticles. This correlated with the higher surface area of the bigger microparticles. It was also possible to show irregularities when the used amounts of QD in dependence of the surface area were altered to higher values, as it was done with the combination of QD_1 with the smaller microparticle, where the used amount of QD was significantly higher on purpose.

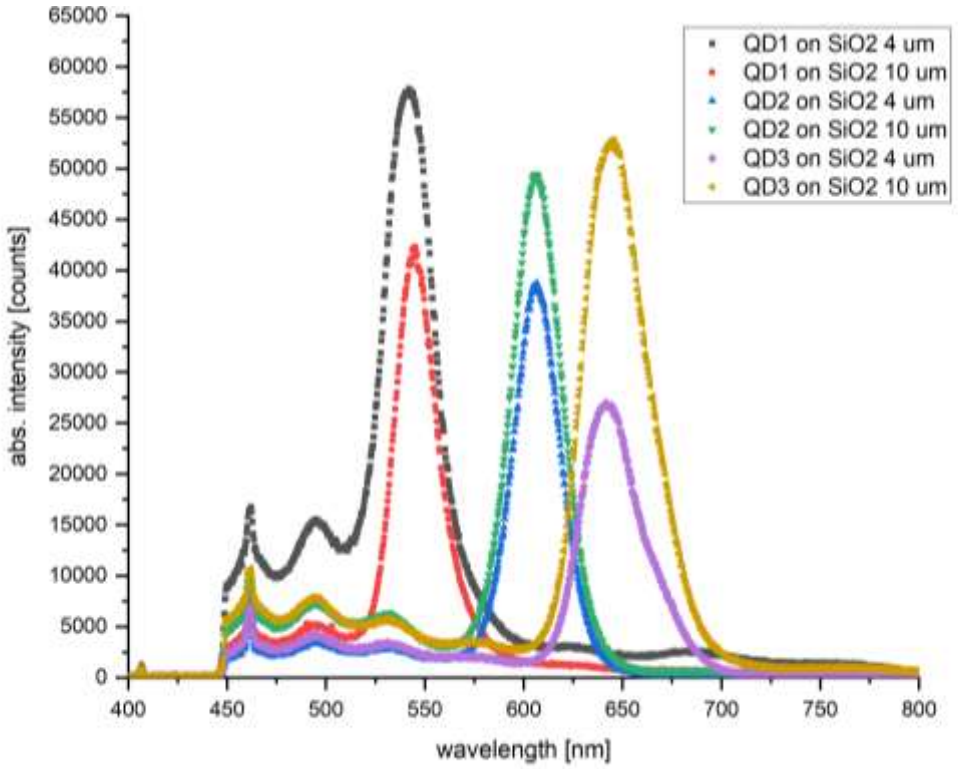

Figure 23. Exemplary emission spectra of all synthesis combinations (overlay). The black curve was the synthesis run with a higher QD concentration, which led to a broader and more intense peak. All measurements were conducted with the same spectral settings and an integration time of 200 ms.

The tendency of a higher signal while using similar amounts of QD in proportion to the surface areas was confirmed, and the optional formation of multiple layers when the needed QD amount was exceeded (black curve) was proven through these experiments. This implemented that the QD amounts and reaction conditions need to be properly adjusted to perform a monolayer coating. Uncertainties were introduced from the insufficient manufacturer data in terms of molar weight of QD, diameters of core and shell and other important parameters for the calculations. Because of the uncertainties, it was only possible to estimate the needed amounts, which decreased the precision of the

calculations. Another observed fact of these experiments was the enhancement of the impurity peaks in the range of 400-600 nm that were residing from sources, especially the solvents like ethanol and water. The enhancement of these peaks probably resided from a higher impurity within the powder from enclosed solvent molecules. Nevertheless, the observation that the impurities rose constantly with a higher concentration of QD indicated the possibility of interferences between QDs and impurities. The QD layers that resided from using higher QD amounts were not characterizable in detail, as two-dimensional images of the coatings were acquired with fluorescence microscopy. It was imaginable that no covalent bonding, but a physical bonding in terms of agglomeration and cluster formation between bonded and free QD was a probable reason to explain the layer formation beyond a monolayer or possible inhomogeneous coatings. The quality of the coating was further investigated by means of fluorescence microscopy, TEM-EDX, and SEM measurements for the microparticles and fluorescence microscopy for the single crystal wafers.

3.1.2 Coating of single crystal wafers

After adjusting the manufacturing process of the wafers in terms of QD activation and preparation, the single crystals were successfully coated. The hydrophilization with peroxymonosulfuric acid can be considered as successful as the reactions on the wafer surface were clearly visible through the formation of bubbles. The reduction of bubble formation also indicated the quantitative hydrophilization of the single crystal surfaces. The functionalization with amine groups using APTES was precisely described in literature and was also working properly for the used substrates, as the activated QD were successfully coated onto the substrates after hydrophilization and functionalization, as observed by fluorescence microscopy. It was also possible to acquire fluorescence-spectra of the QD-coated single crystals in comparison to uncoated single crystals, as shown below.

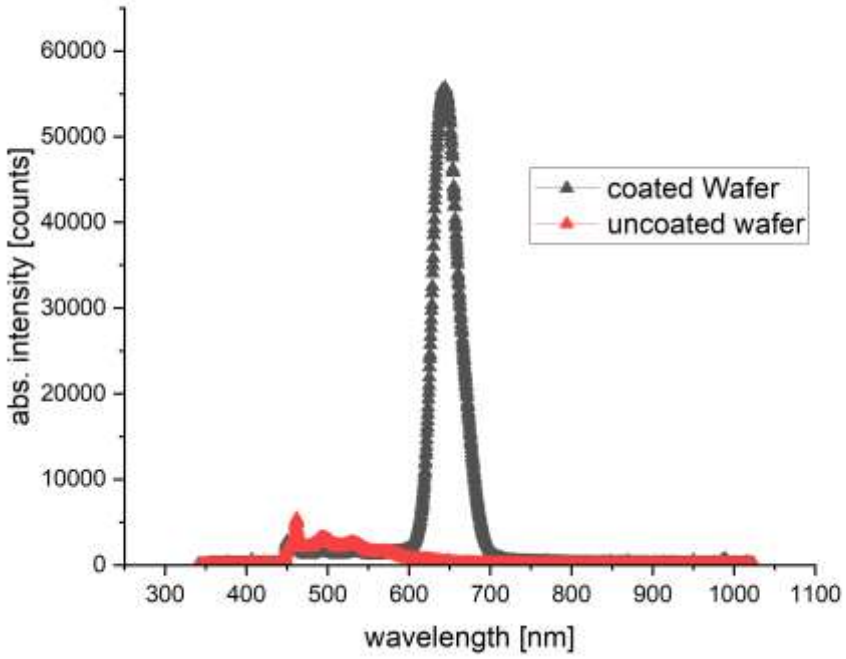

Figure 24. Comparison of fluorescence-spectra of coated and uncoated single crystal wafers in the same setup as for the measurements of the QD. The only signals from the uncoated wafers were residing from the used cuvette and residual moisture. The peaks clearly showed strong intensity at an integration time of 100 ms.

As the substrate had to be pre-functionalized, the coating process seemed to be more complicated than the process for the microparticles. As there was a possibility of non-quantitative hydrophilization or APTES-functionalization, the included reactions had to be more reliable in comparison to the microparticle coating process. As observed in the spectra and in the microscopy data, all the steps worked for the used substrate and QDs and could be reproduced in the future. It still was to consider that APTES

functionalization as a monolayer only worked with low concentrations off APTES, as the primary amines could react with in-situ formed silanes which would result in cluster formations with increasing coating thickness (change from 2D monolayer to 3D structure). These undesirable effects had to be suppressed with the right concentration of the APTES solution, which was successfully done with concentrations lower than 2% v/v in aqueous acetic acid, as literature suggested.[11]

3.2 Storage stability

In summary, different storage stability measurements were carried out to determine the optimal storage conditions, including the proof of stability of the coatings in well-defined conditions. For this, storage stability measurements at 20°C and 2°C with and without light exposure were conducted. As the results have shown, the dried powders did not need cooled and dark storage in comparison to the pristine QD. This was explained by the low stability and coagulation tendencies of colloidal QD solutions, which was not expected nor observed for the dried and coated powders.

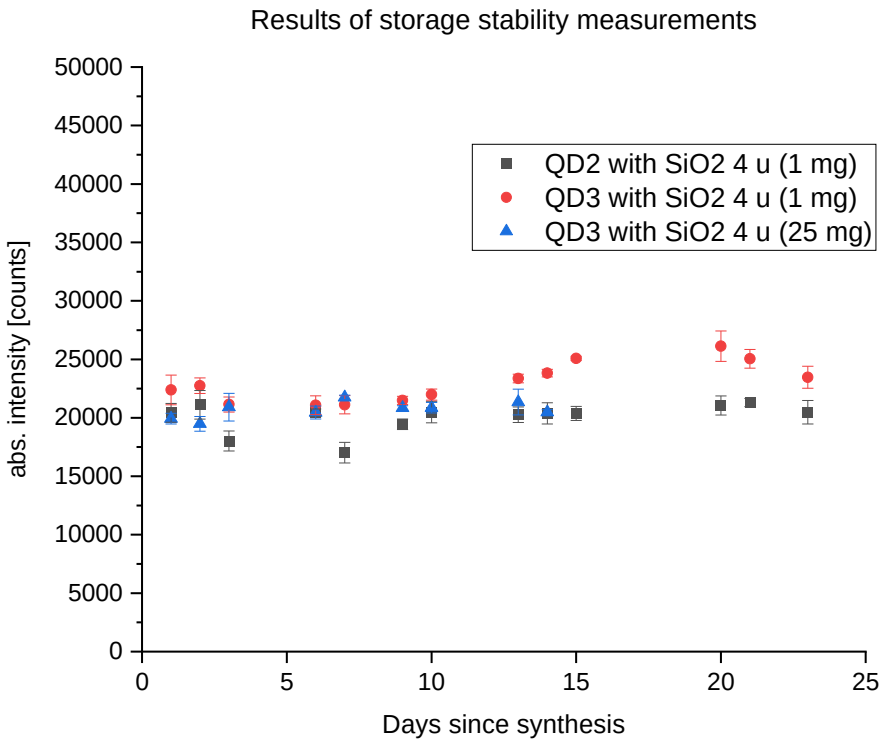

Figure 25. Results of storage stability measurements of the dried powders at room temperature, normal pressure and without nitrogen protection. There was still a fluctuation of signal detectable which was attributed to the slightly inhomogeneous coating of the powders and the exceptionally low sample sizes below 5 mg which were not sufficient to fill the used cuvette high enough to acquire a saturated signal. Every data point consists of 10 measurements with standard deviation shown in y-direction.

After the sample sizes were increased to 25 mg for the experiments in real plasma conditions in Eindhoven and after the synthesis procedure was adjusted as stated above, a more linear and constant fluorescence intensity was measurable. This was initially not observed for the small sample sizes in the area of micrograms that were synthesized, caused by interferences between empty cuvette volume and coated particles in the cuvette when excited by the laser. The standard deviation of ten measurements of the same powder decreased as well, which confirmed the higher homogeneity of the coating. The small sample sizes and the extent of coating homogeneity were one of the most important parameters for a constant intensity within the spectra, as the intensity varied strongly after shaking when using very small sample sizes below 1 mg. The powders were storable for at least one month, and still showed fluorescence emission after 2-3 months of storage, which confirmed the storage stability for the coated microparticles at room temperature. In the following, no storage stability measurements in different conditions were conducted anymore, as the storage at room temperature without a degradational influence of e.g. light or thermal energy on the powders was defined as target at the beginning of the experiments.

3.3 SEM and TEM

To validate the monodisperse size distribution and spherical shape of the acquired and uncoated microparticles, SEM imaging was used. The measurement parameters were summarized in the bottom column of the pictures.

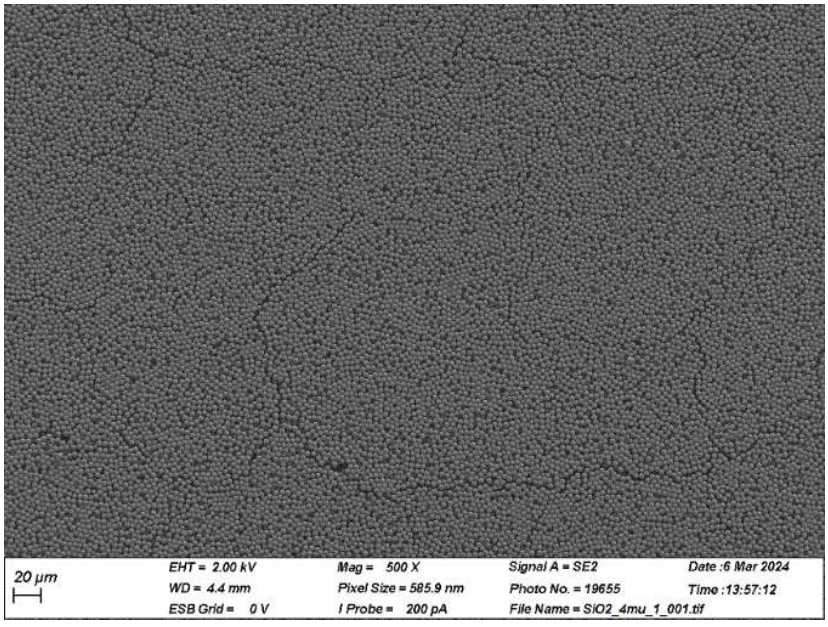

Figure 26. SEM-image of the smaller silica microparticles, acquired with a Zeiss SEM with secondary electron detection (SE). 500x magnification, 2 kV (electron source).

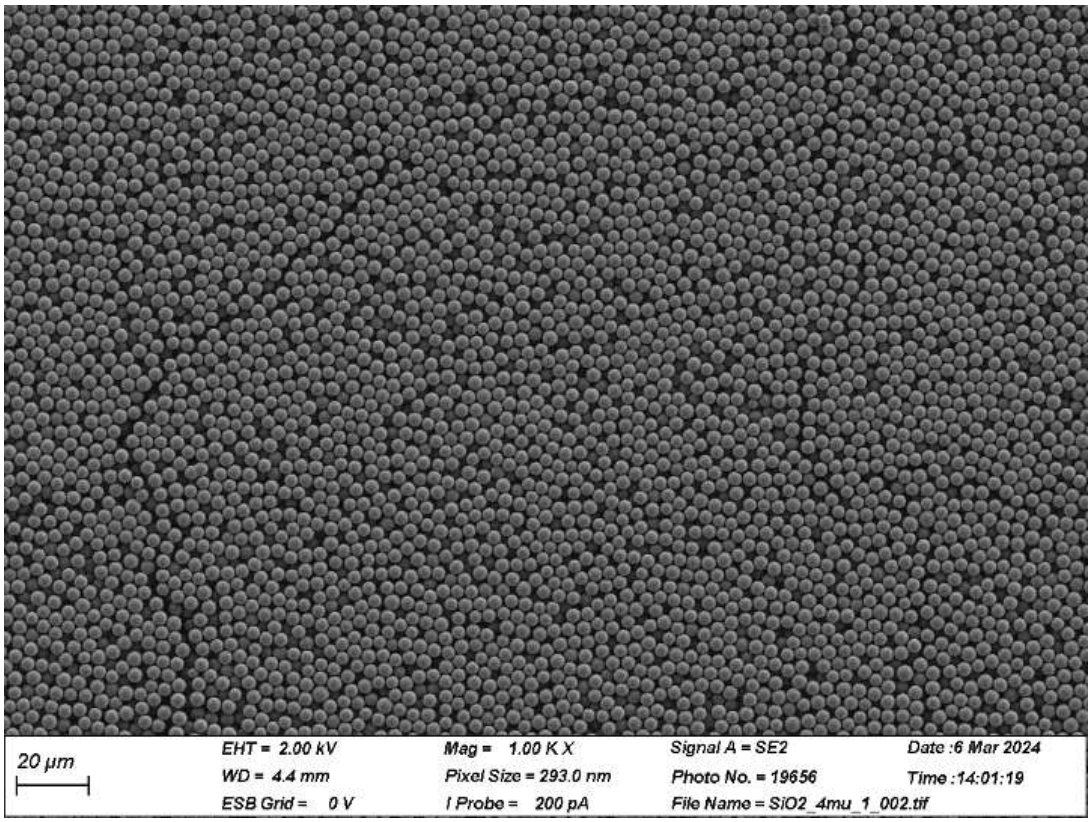

Figure 27. SEM-image of the smaller silica microparticles, acquired with a Zeiss SEM with secondary electron detection (SE). 1000x magnification, 2 kV (electron source).

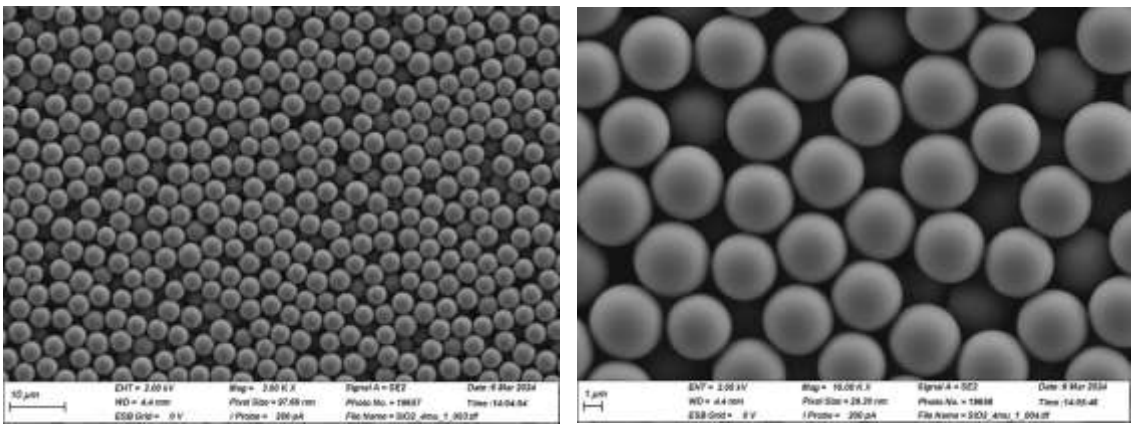

Figure 28. SEM-image of the smaller silica microparticles, acquired with a Zeiss SEM with secondary electron detection (SE). 3000x magnification (left) and 10000x magnification (right), 2 kV (electron source).

The highly monodisperse size distribution of the used microparticles was successfully confirmed through SEM. The microparticles appeared to be spherically shaped in a similar way, with some uncertainties in image interpretation. At the interface of the particles and background, some non-spherical shapes were observable, attributed to the resolution of SEM and to its optical aperture in combination with the spherical shape of the particles.

For the 10 µm SiO_2 microparticles, similar SEM measurements were ´conducted to confirm the monodisperse size distribution and spherical shape of both used reagents.

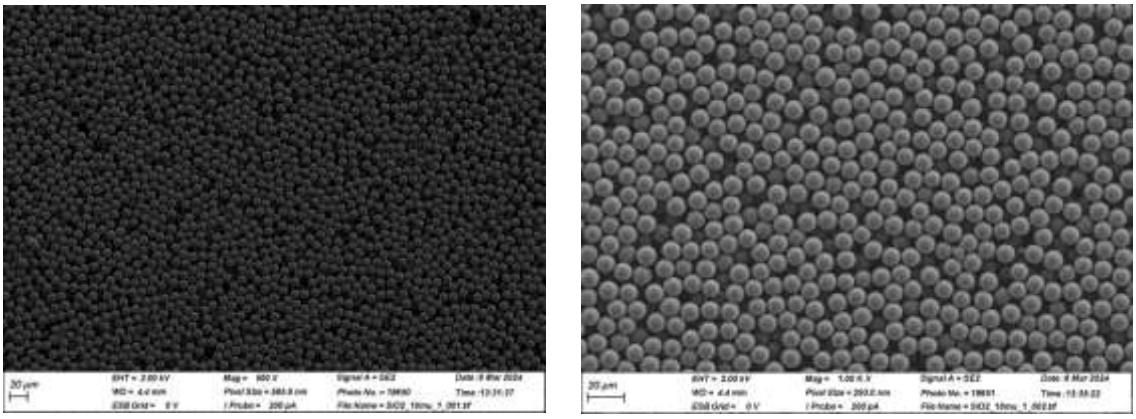

Figure 29. SEM-images of the 10 µm SiO_2 microparticles with 500x magnification (left) and 1000x magnification (right). 2 kV, secondary electron detector.

For the bigger microparticles, a highly monodisperse size distribution and a spherical shape of the used microparticles was also confirmed. The size range that was determined through SEM for both microparticles were comparable to the sizes stated by the manufacturer.

When further magnified, one was able to observe that the microspheres tend to stick and agglomerate, especially when dried, as seen in the following images.

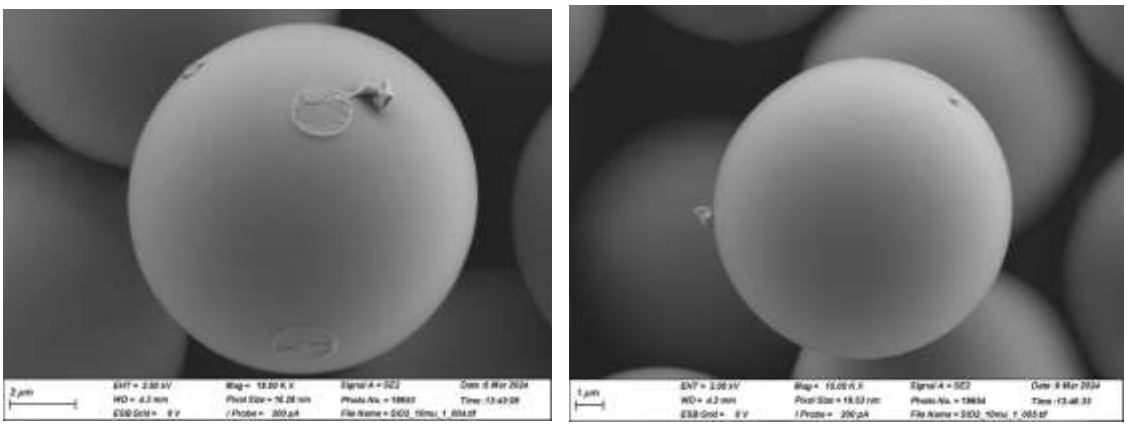

Figure 30. SEM-images of the 10 µm microparticles with 18000x magnification (left) and 15000x magnification (right): 2 kV, secondary electron detector.

As identified in the magnified images, the drying results in agglomerates which could be destroyed through mechanical forces or other influences. It had to be considered that the agglomeration tendency was a property of the coated powder. This led to agglomerates in the particle shaker for the plasma measurements, resulting in shaking problems that hindered the immersion of particles within the chamber. For this, a further adjustment of the procedure would be necessary if the project concept would show a need be

optimized further. The agglomeration issues observed in solution while performing the coating reaction had to be reduced through mechanical force (stirring), temperature (higher temperature resulted in higher mobility) and through the choice of the right solvent (in this case aqueous ethanol instead of water). After adjusting the procedure there were no agglomerations in solution observed, and there was no powder layer formation on the magnetic stirrer bar, which showed that the adjustments were enough to reduce the agglomeration problem, which led to reduced reactions on the surfaces before, amongst other reasons.

The coated microparticles were further investigated by means of SEM, where an altered surface structure was observed in contrast to the appearance of the uncoated microparticles.

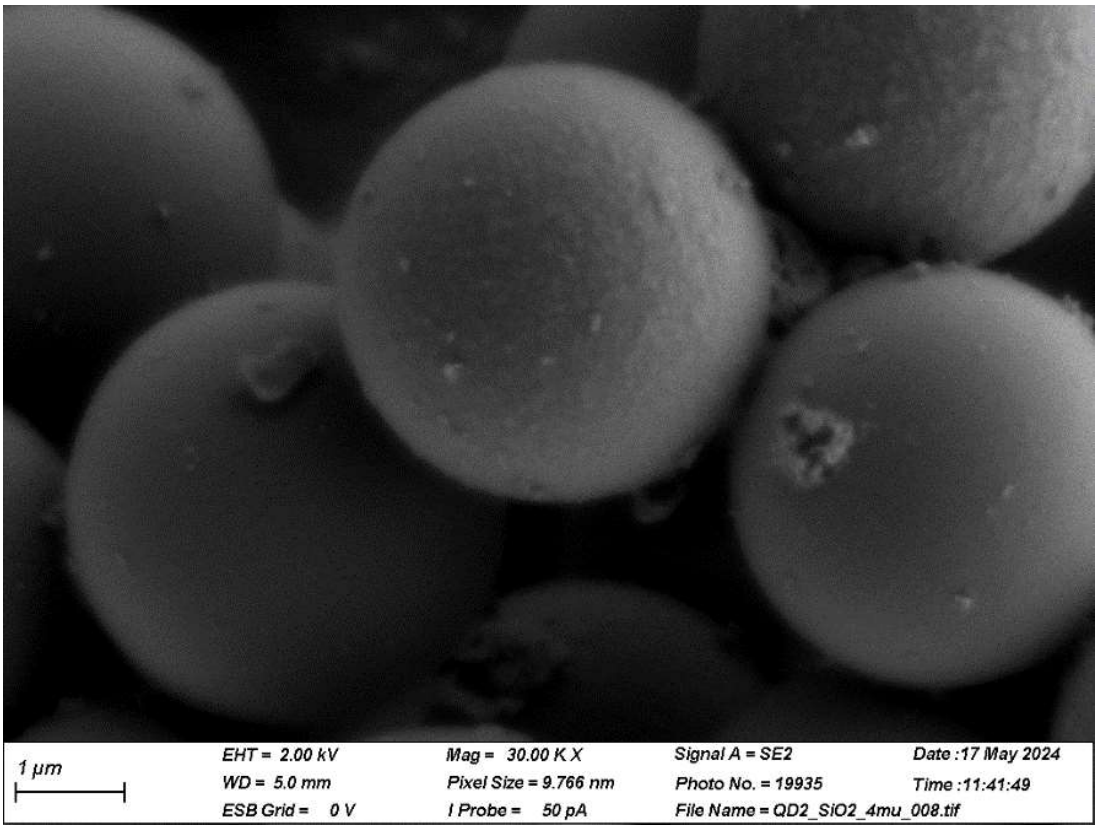

Figure 31. SEM images of an exemplary sample of coated microparticles. The surface structure was rougher in comparison to the uncoated particles. 2 kV, 30000x magnification, secondary electron detector

The altered structure was not detectable on any particle in similar ways. This suggested that the coating process was not taking place homogeneously on all microparticle surfaces, which had to be further investigated and understood to optimize the procedure.

The **TEM measurements** of the coated microparticles revealed further details about the produced coatings. As the diameters of the used microparticles exceeded the highest possible thickness for TEM samples, only the edges were observable. It was observed

that the microparticles acquired rough surface structures in contrast to the smooth surfaces observed with SEM, which confirmed that a coating had formed.

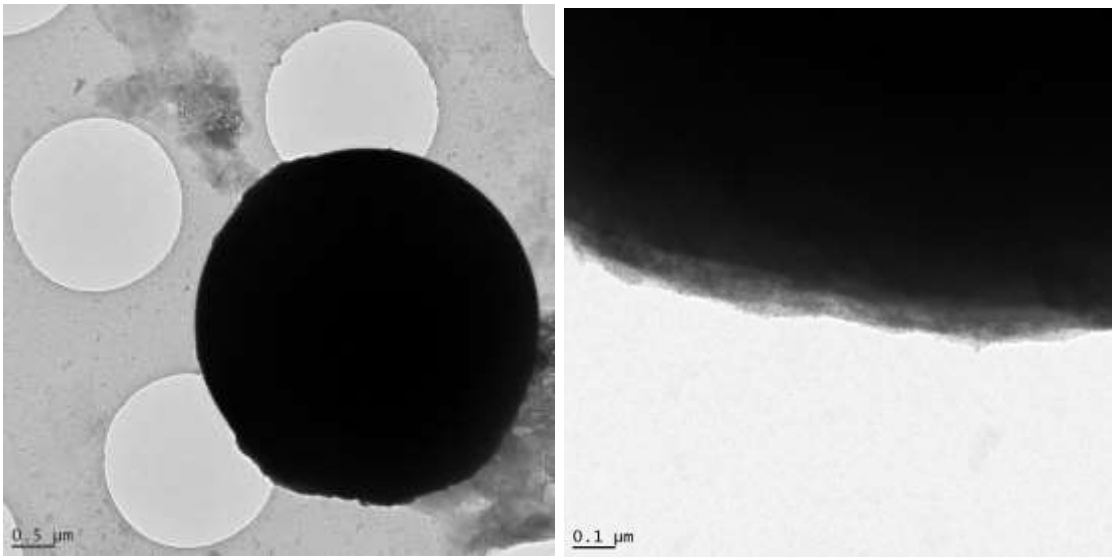

Figure 32. TEM-images of the coated 3,92 micrometre microparticles.

It was also possible to image pristine QDs and QD clusters with reveal of some information regarding the crystal structure of the used CdSe/ZnS-QDs which was confirmed to be cubic. The QD appeared to be homogenous (no core/shell-structure observable) which was attributed to the similar crystal structures of CdSe and ZnS with very small differences in the lattice constants.

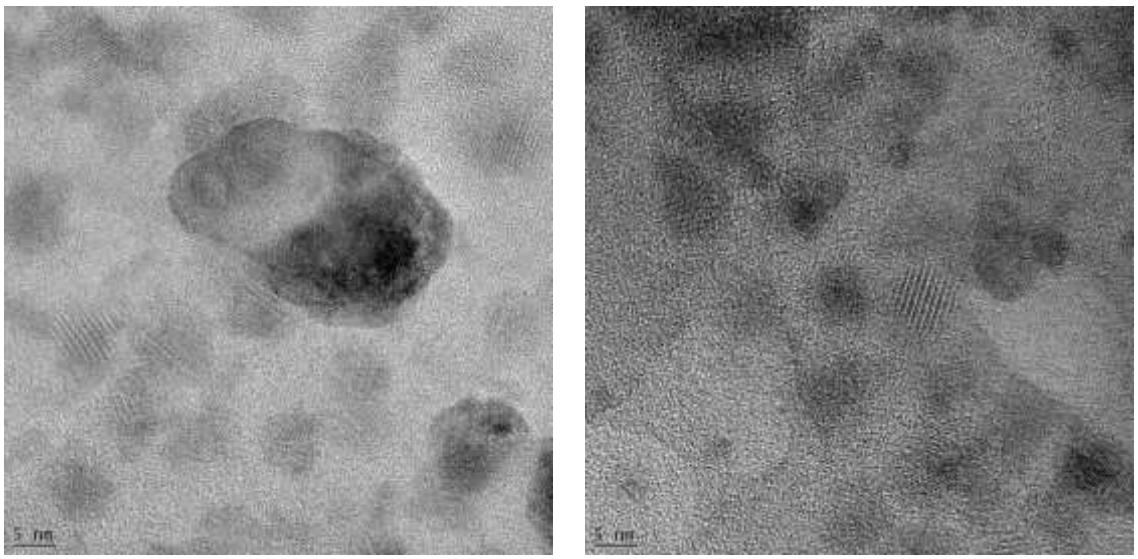

Figure 33. TEM-images of the bare QDs.

In combination with energy dispersive X-ray spectroscopy (EDX) it was possible to determine the atomic composition of the coating section circled in red as shown below.

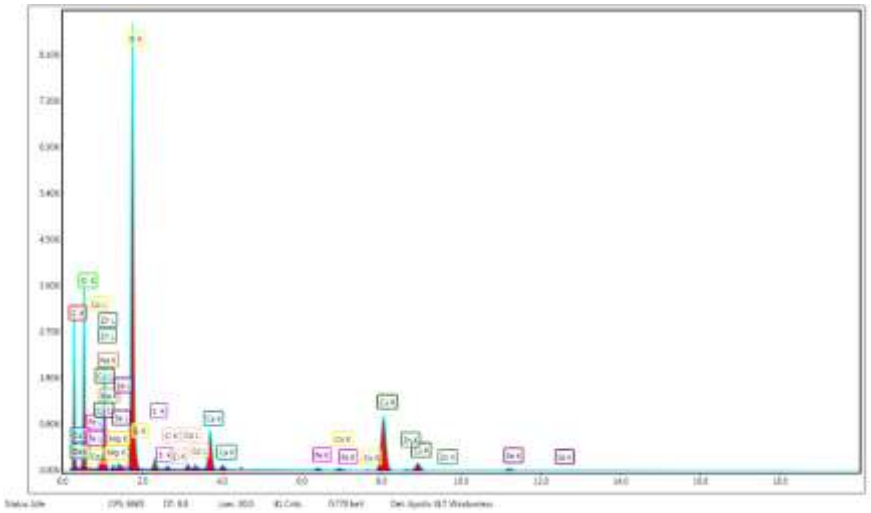

Figure 34. EDX-spectrum of the coating section circled in red as shown below.

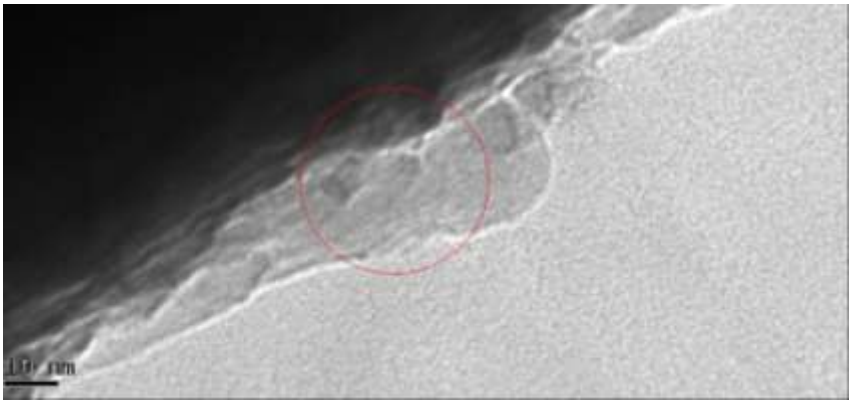

Figure 35. TEM-image of the coating area that was analysed by EDX.

The coating layer consisted of Cd and Se cores, amongst impurities like calcium salts as well as e.g. silicon and oxygen peaks caused by the microparticles. The shell material of the QDs (ZnS) was also detectable by EDX, which confirmed that the QDs were attached to the surface of the microparticles.

3.4 Fluorescence microscopy

For the determination of the coating quality and the QD density on the single crystal surfaces, fluorescence microscopy was used with single shots and a multiple scan of the whole single crystal area as shown in the following figures.

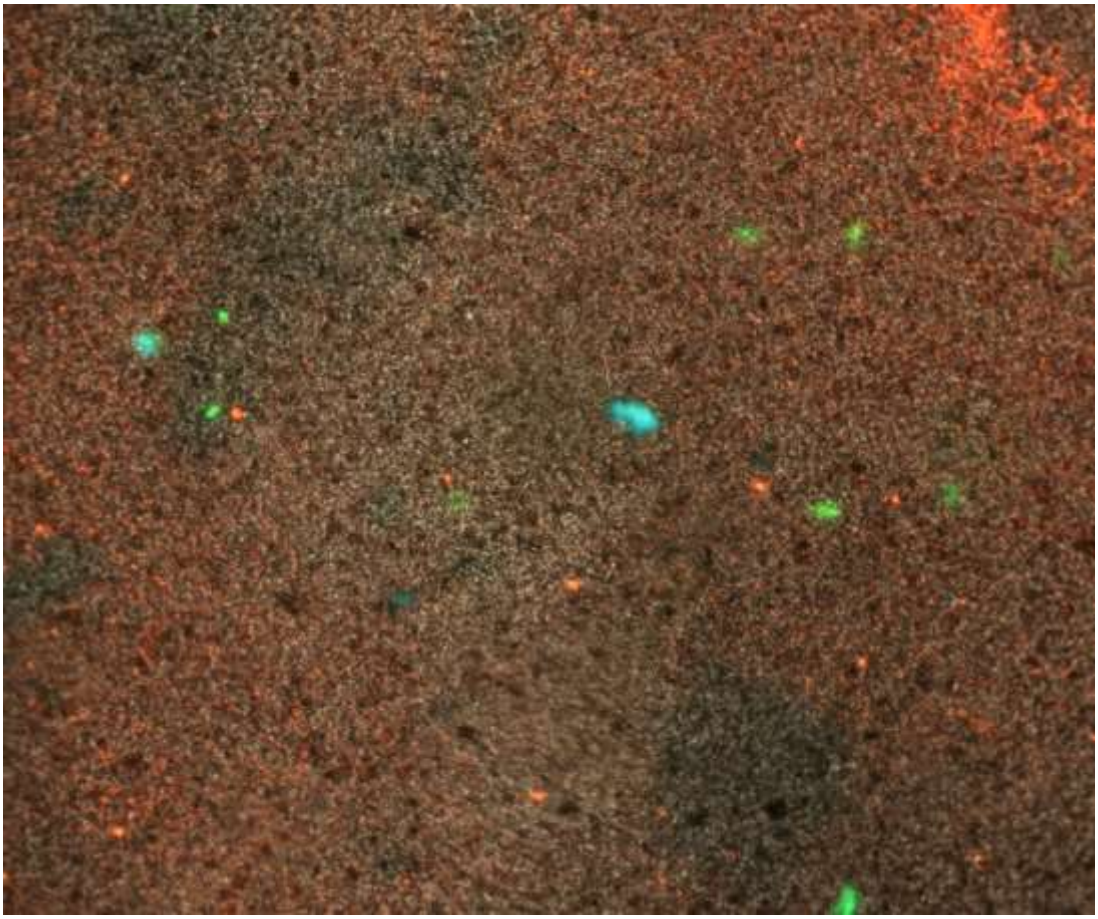

Figure 36. Full scan of a single crystal wafer (10x10x0,5 mm) coated with QD3 (red emission, 645 nm) with radiation effects of impurities (green, blue) and quantum dots (orange to red colour). The coating appeared to be inhomogeneous and showed a tendency to clustering (visible in the upper right corner).

In the figure above, the QD are shown as orange to red dots, the wafer was non-fluorescent and therefore appeared as grey to black. Some impurities were observed in the blue and green emission range which can reside from impurities that were introduced in the reaction, workup, storage or transport of the single crystal wafers. It was observed that the QD are not evenly distributed and formed local clusters (e.g. upper right corner of figure 30). This had to be considered when using the single crystals in realistic plasma conditions.

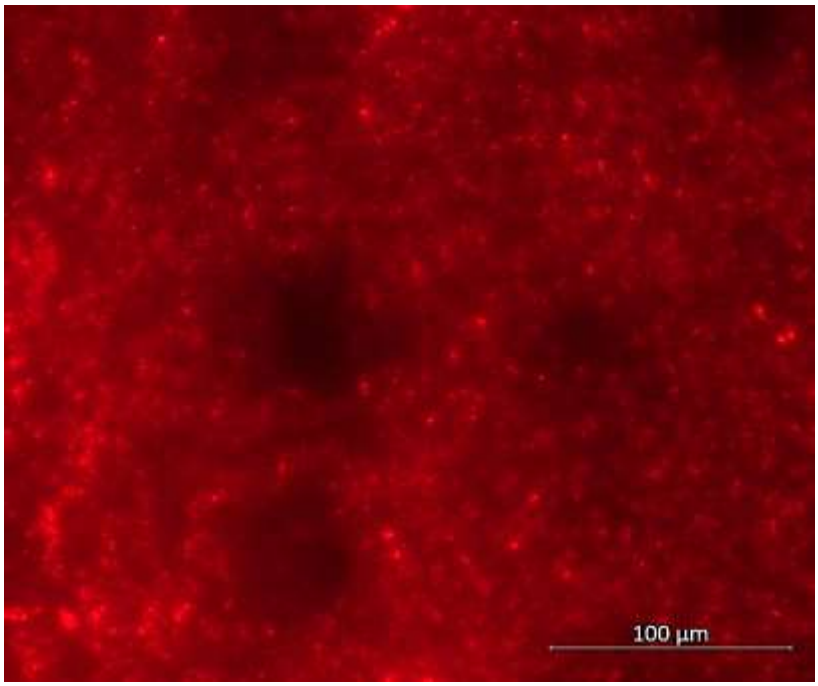

Figure 37. Full-scan fluorescence microscopy images of red emission area of QD_3-coated single crystal wafers.

The red area of fluorescence emission is shown in the figure above. Herein, clusters and agglomerates were visible as areas with saturated intensity. It was observed that some areas were slightly coated or even uncoated. This was explainable through higher local concentrations of QD on the surface while immersed in solution, as there was no stirring applied for constant homogenization.

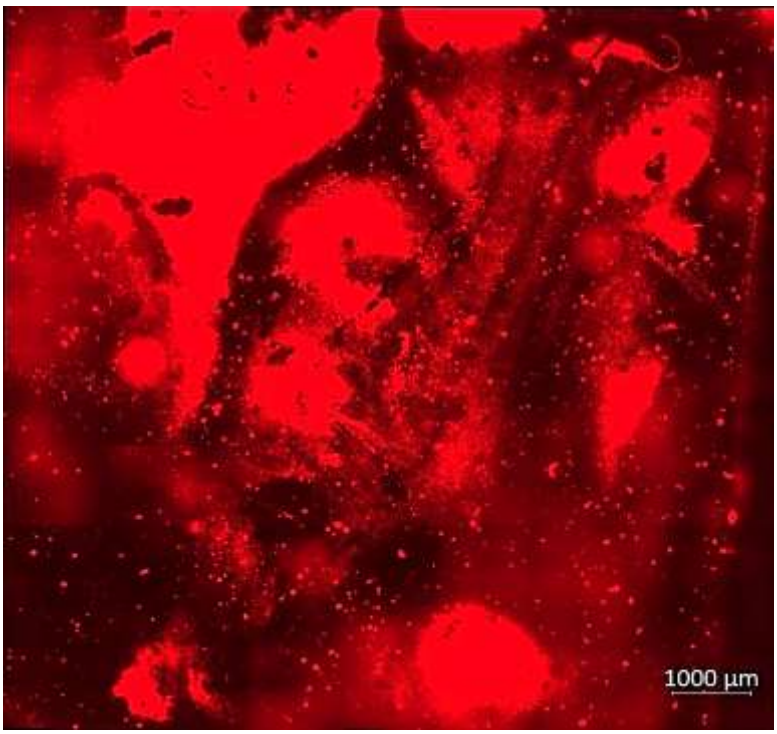

Figure 38. Red-attenuated full scan of a QD3-coated single crystal wafer with fluorescence microscopy after optimization of the coating procedure in terms of reaction times and used QD amounts. After increasing the QD amount to 300 µg from 200 µg.

In the two figures above, different QD amounts were used (200 µg of QD in figure 31, 300 µg of QD in figure 32), and it was observed that, for the coating of the whole wafer, an amount between 200-300 µg in combination with an optimized and controllable procedure was understood as the best strategy for optimization as the data of fluorescence microscopy suggested in the different measurement runs. When exceeding the QD concentration, strong clustering effects were observable that did most possibly not consist of a monolayer anymore, as seen in the saturated areas in figure 32. To optimize the coating homogeneity, the QD concentration and the constant homogenization of the reaction mixture was found to be particularly important to prevent clustering. The fluorescence microscopy images also proved that there was space for improvement in the coating procedure for single crystals in general.

3.5 Plasma tests

The experiments at the facilities of TU Eindhoven were conducted to determine the coating stability in plasma environments as well as for the possible measurement of Stark shift induced by the QCSE of the surface-coated QD on both the microparticles and the single crystal wafers. For the microparticles, plasma exposure had to be chosen in an amount that led to the levitation of the particles that were introduced to the plasma chamber by a shaker. This indicated that the particles were hypothetically more prone to degradation than the coated single crystals which were placed in a plate holder, and which experienced less plasma exposure (e.g. 23 seconds of measurements with 10 seconds of no plasma-exposure but with laser exposure, 3 seconds of plasma and laser exposure, and 10 more seconds of laser exposure). As the coating of the particles did not seem to be completely homogeneous in the powder, the fluorescence peak was complicated to determine. This issue was further increased by the tendency of the powders to be sticky and therefore forming clusters and agglomerates that hindered the powders to be shaken into the plasma environment, as the shaker just had a small hole (and not a mesh) where the particles were shaken. As the agglomerates were in the size of millimetres (observable with the eye), the measurement of the Stark shift was hindered, attributed to the agglomeration error in combination with inhomogeneous coatings. The behaviour of the powders could be hypothetically explained by the newly formed surface (the QD layer). The QD surfaces were coated with a polymer. Polymers are known to agglomerate due to the experienced stickiness that were also observed for the coated microparticles, even in a highly dried state. The adjustment of the hole size led to enough particles being shaken into the plasma, but also facilitated the immersion of agglomerates into the

plasma chamber which were too heavy to be levitated within the plasma and, therefore, gave no fluorescence signal.

In the experiments, the single crystal wafers showed detectable fluorescence emission in combination with a peak shoulder in a wavelength range of 550-620 nm, as shown in the figure below.

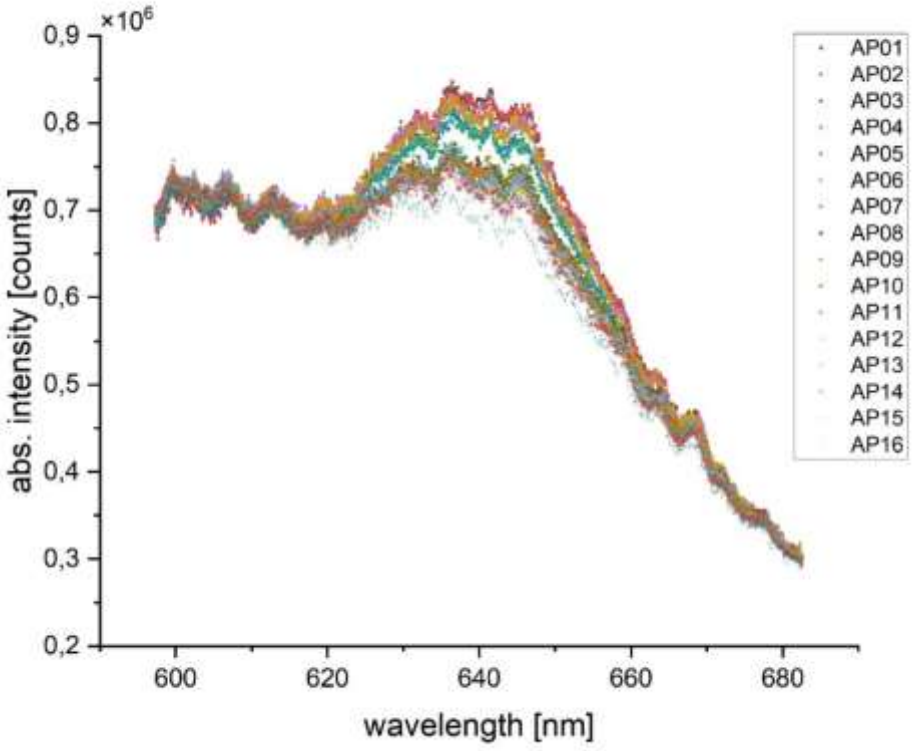

Figure 39. Fluorescence spectroscopy results of the measurement with a QD_3-coated single crystal wafer. The different curves were acquired subsequently with and without plasma exposure to determine the variation of peak intensity and the deviance in shoulder and peak form in dependence of conditions.

The shoulder effect was not observed before and could have resided from interferences between the QD layer and the silicon dioxide single crystal while excitation. Eventually, silicon dioxide single crystals are also able to interact with the excitation beam, could lead to refraction and exhibit own photoluminescent properties, which must be investigated further. The observed increase and decrease of the curves resided from measurements with and without plasma exposure. The plasma exposure is known to heat up inserted samples, and QD fluorescence intensity is known to decrease with rising temperature. The other QD_3-coated wafer that was tested exhibited the same behaviour with higher absolute intensity but similar shouldering effects in a similar wavelength range.

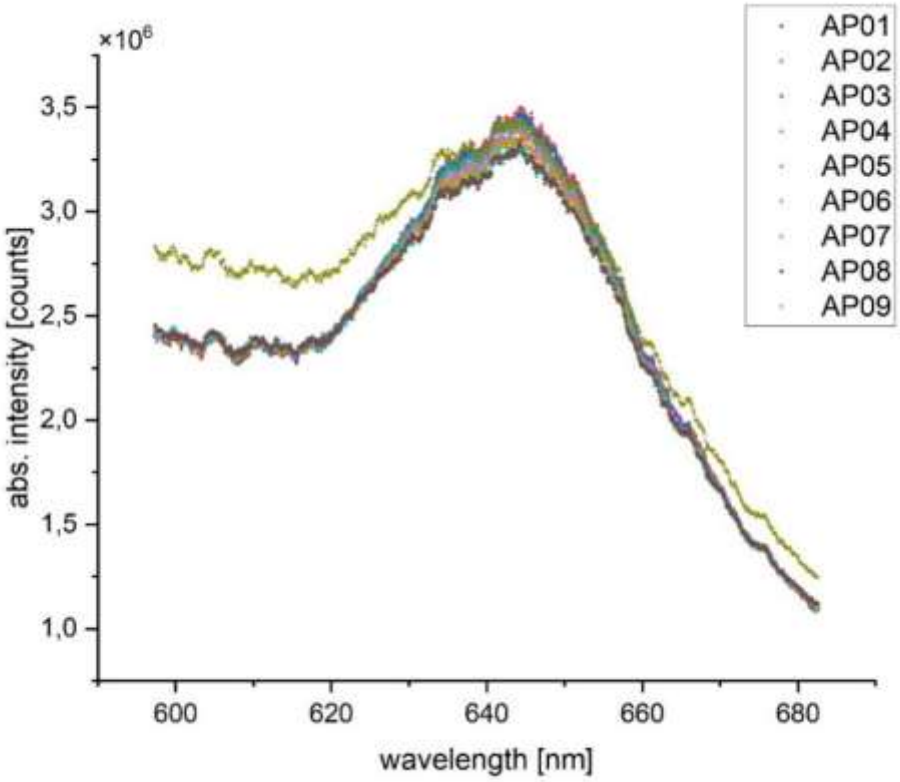

Figure 40. Fluorescence spectroscopy results of the measurement with a recently coated QD_3-coated single crystal wafer. The different curves were acquired subsequently with and without plasma exposure to determine the variation of peak intensity and the deviance in shoulder and peak form in dependence of conditions. The absolute intensity of the fluorescence was higher as for the previous wafer (fig. 41) that was stored for two months.

As the coating homogeneity varied depending on the spot of the plate that got excited by the laser, there was no clear information about degradation through plasma exposure or storage stability in general. The acquired results were used to determine a substrate or a new process that reduces the shoulder formation in the upcoming months.

4 Conclusion

After issues with the initial reaction system and reaction concepts, the feasibility of coating QD onto different surfaces through chemical bonding was confirmed successfully. After analysing the samples (powders and single crystal wafers) it was concluded that the homogeneity on the plates was not sufficient for the planned measurements, and that the coating process of the wafers still needs to be optimized soon.

After testing the single crystal wafers in plasma environments, a slight degradation of the surface-coated QDs was observed which resulted in the need of adjusting the procedure through e.g. an additional protective layer that can protect the surface-coated QD from degradation. The observed shouldering in the fluorescence spectra needs to be further understood and could probably be reduced or prevented by using a non-transparent substrate besides of SiO_2, e.g. silicon single crystals.

For the microparticles, a procedure was developed that was reproducible and that enabled to coat QD on microparticles of varied sizes in a wet chemical process involving ethanol and water as well as activation reagents and an extraction solvent for surface ligands on the QD, namely toluol. By activating the carboxyl groups on the QD surface in advance, an improved coating result was observed in the case of the microparticle and single crystal coating, which induced a more homogeneous colouring, and a more intense fluorescence peak compared to the previous syntheses. The storage stability of the coated microparticles and the coating stability and quality of the coated single-crystal wafers were successfully investigated using UV-VIS spectroscopy and microscopy techniques. The atomic composition of the coating layer was determined by TEM-EDX measurements, with proof of CdSe and ZnS within the coating layer.

The further development and application of this sensor technology as well as an increased understanding of the mentioned QCSE-based senor model of QD-coated particles and single crystal surfaces is planned, based on the observations within this thesis. An improved understanding of the charging effects on particle surfaces in low-temperature plasmas can be assumed in the future after the further optimization of the coating processes in the facilities of DLR in the upcoming months.

List of references

1. Girma, Wubshet & Fahmi, Zakki & Permadi, Adi & Abate, Mulu & Chang, Jia-Yaw. (2017). Synthetic strategies and biomedical applications of I-III-VI ternary quantum dots. J. Mater. Chem. B. 5. 10.1039/C7TB01156C.

2. Murray C.B.; Norris D. J.; and M.G. Bawendi, J. Am. Chem. Soc., 1993, 115, 8706.

3. Anupam Sahu, Dharmendra Kumar, Core-shell quantum dots: A review on classification, materials, application, and theoretical modeling, J. Alloys Compd., Volume 924, 2022, 166508

4. Hao, J.J., Zhoua, J., Zhang, C.Y.: A tri-n-octylphosphine-assisted successive ionic adsorption and reaction method to synthesize multilayered core-shell CdSe-ZnS quantum dots with extremely high quantum yield. Chem. Commun. 49, 6346-6348 (2013)

5. Tusher, M.M.H. Microbial synthesis of Cadmium selenide quantum dots (CdSe QDs), influencing factors and applications. *Opt Quant Electron* 55, 332 (2023).

6. Luminescence Properties of CdSe Quantum Dots: Role of Crystal Structure and Surface Composition. K. B. Subila, G. Kishore Kumar, S. M. Shivaprasad, and K. George Thomas. J. *Phys. Chem. Lett.* 2013, 4, 16, 2774–2779

7. PubChem-Eintrag zu Zinksulfid, zuletzt aufgerufen am 07.04.2024: https://pubchem.ncbi.nlm.nih.gov/compound/ZINC-sulfide

8. Miller, D. (1984). "Band-Edge Electroabsorption in Quantum Well Structures: The Quantum-Confined Stark Effect". Phys. Rev. Lett. 53 (22): 2173–2176.

9. *M Y Pustylnik* et al. *(2022).* J. Phys. D: Appl. Phys. *55 095202*

10. Shimura, F. (2017). Single-Crystal Silicon: Growth and Properties. In: Kasap, S., Capper, P. (eds) Springer Handbook of Electronic and Photonic Materials. Springer Handbooks. Springer, Cham.

11. Sypabekova, M.; Hagemann, A.; Rho, D.; Kim, S. Review: 3-Aminopropyltriethoxysilane (APTES) Deposition Methods on Oxide Surfaces in Solution and Vapor Phases for Biosensing Applications. *Biosensors* 2023, *13*, 36.

12. Hambly, Adam & Henderson, Rita & Baker, Andy & Stuetz, Richard & Khan, Stuart. (2012). Cross-connection detection in Australian dual reticulation systems by monitoring inherent fluorescent organic matter. Environ. Technol. Rev, 1. 10.1080/09593330.2012.696724.

13. Vogt, C., Wondergem, C.S., Weckhuysen, B.M. (2023). Ultraviolet-Visible (UV-Vis) Spectroscopy. In: Wachs, I.E., Bañares, M.A. (eds) Springer Handbook of Advanced Catalyst Characterization. Springer Handbooks. Springer, Cham.

14. Morfill, G. E., & Ivlev, A. V. (2009). *Complex plasmas: An interdisciplinary research field. Rev. Mod. Phys, 81(4), 1353–1404.*

15. G. Korotcenkow. Cd and Zn-based wide band gap II-VI semiconductors. Handbook of II-VI Semiconductor-based Sensors and Radiation detectors, p. 21-22.

16. O. de Melo. Introduction in II-VI semiconductors. Handbook of II-VI Semiconductor-based Sensors and Radiation detectors, p. 6-8.

17. Abbassi, Abderrahman & Zarhri, Zakaryaa & Azahaf, Ch & Ez-Zahraouy, Hamid & Benyoussef, Abdelilah. (2015). Boltzmann equations and ab initio calculations: comparative study of cubic and wurtzite CdSe. SpringerPlus. 4. 543. 10.1186/s40064-015-1321-z.

18. Boyce, Adrian & Barrie, Craig & Samson, Iain & Williams-Jones, Anthony. (2015). Boyce, A. J., Barrie, C. D., Samson, I. M., and Williams-Jones, A. E., 2015, Aspects of the geochemistry of zinc – a journey to sphalerite, in Archibald, S. M. and Piercey, S. J. (eds.), Current perspectives on zinc deposits: Dublin, Irish Association for Economic Geology, p. 17-35.

19. Lakowicz, J.R. (1999). Introduction to Fluorescence. In: Principles of Fluorescence Spectroscopy. Springer, Boston, MA. https://doi.org/10.1007/978-1-4757-3061-6_1

20. M.Y. Pustylnik, J. Beckers et. al, Phys. Plasmas 30, 120601 (2023)

21. P. Atkins, R. Friedman. (2005). Molecular Quantum Mechanics. Chemistry Faculty Publications.

22. W. Paili, P.Achuthan, K.Venkatesan. (1980). General Principles of Quantum Mechanics. Springer Publishing.

23. Onyia, Augustine & Ikeri, H.I. & Nwobodo, Anthonia. (2018). Theoretical study of the quantum confinement effects on quantum dots using particle in a box model. J. Ovonic R, 14. 49-54.

24. Chem. Commun., 2010,46, 5584-5586

25. *Appl. Phys. Lett.* 119, 254104 (2021)

26. Ivan B. Djordjevic. Physical Implementations of Quantum Information Processing. Quantum Information Processing, Quantum Computing, and Quantum Error Correction (Second Edition),(2021).

27. Prachi Chopade, Shweta Jagtap, Suresh Gosavi,5 - Material properties and potential applications of CdSe semiconductor nanocrystals, Nanoscale Compound Semiconductors and their Optoelectronics Applications, Woodhead Publishing (2022), pp. 105-153, ISBN 9780128240625, https://doi.org/10.1016/B978-0-12-824062-5.00013-0.

28. Press release: The Nobel Prize in Chemistry 2023 - NobelPrize.org

29. Fahelelbom, Khairi Mustafa Salem & Saleh, Abdullah & Al-Tabakha, Moawia & Ashames, Akram. (2022). Recent applications of quantitative analytical FTIR spectroscopy in pharmaceutical, biomedical, and clinical fields: A brief review. Rev. Anal. Chem, 41. 21-33. 10.1515/revac-2022-0030.

30. Akhtar, K., Khan, S.A., Khan, S.B., Asiri, A.M. (2018). Scanning Electron Microscopy: Principle and Applications in Nanomaterials Characterization. In: Sharma, S. (eds) Handbook of Materials Characterization. Springer, Cham. https://doi.org/10.1007/978-3-319-92955-2_4

31. The Scanning Electron Microscope | Engineering Atoms (cam.ac.uk), last access at 14.08.2024

32. Reimer, L. (2013). *Transmission Electron Microscopy: Physics of Image Formation and Microanalysis*. Springer

33. Ardimas. (2020). Report in the Optical Microscopy for Nanotechnology course Microscopy 2020.

34. Lichtman, J. W., & Conchello, J. A. (2005). Fluorescence microscopy. *Nat. Methods*, 2(12), 910-919.

35. Kushagra Agarwal *et al* (2023), *Material Research Express,* 10 062001

36. Medintz, I. L., Uyeda, H. T., Goldman, E. R., & Mattoussi, H. (2005). Quantum dot bioconjugates for imaging, labelling and sensing. *Nat. Materials, 4*(6), 435–446. DOI: 10.1038/nmat1390

37. Algar, W. R., Krull, U. J. (2008). Quantum dots as donors in fluorescence resonance energy transfer for the bioanalysis of nucleic acids, proteins, and other biological molecules. *Anal. Bioanal. Chem., 391*(5), 1609–1618. DOI: 10.1007/s00216-008-2114-5UV

Appendix

Fluorescence-spectroscopy

Pre-trials (reagent and blank characterization)

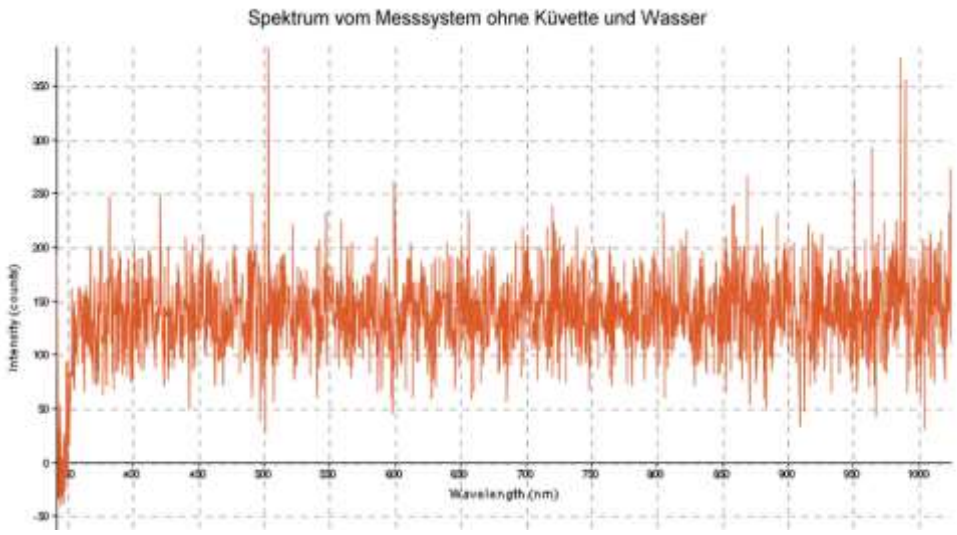

Figure 41. UV/VIS spectra of the blind peaks of the measurement system.

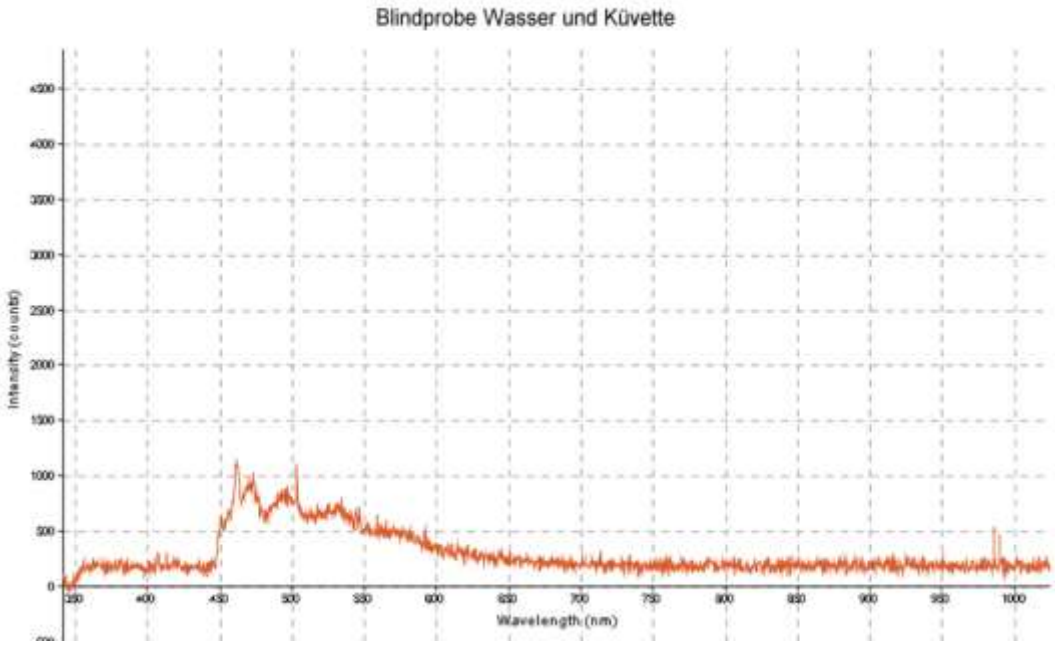

Figure 42. UV/VIS spectra of the blind peaks of the measurements system and water.

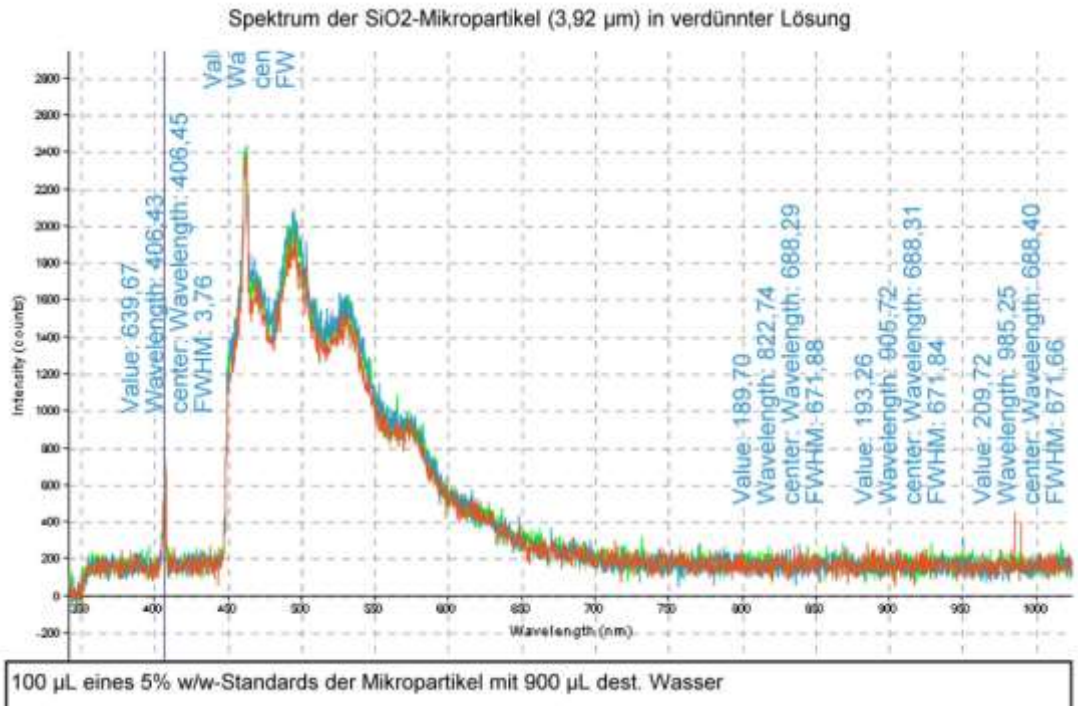

Figure 43. UV/VIS spectra of the smaller and uncoated silica microparticles (size = 4 micrometres).

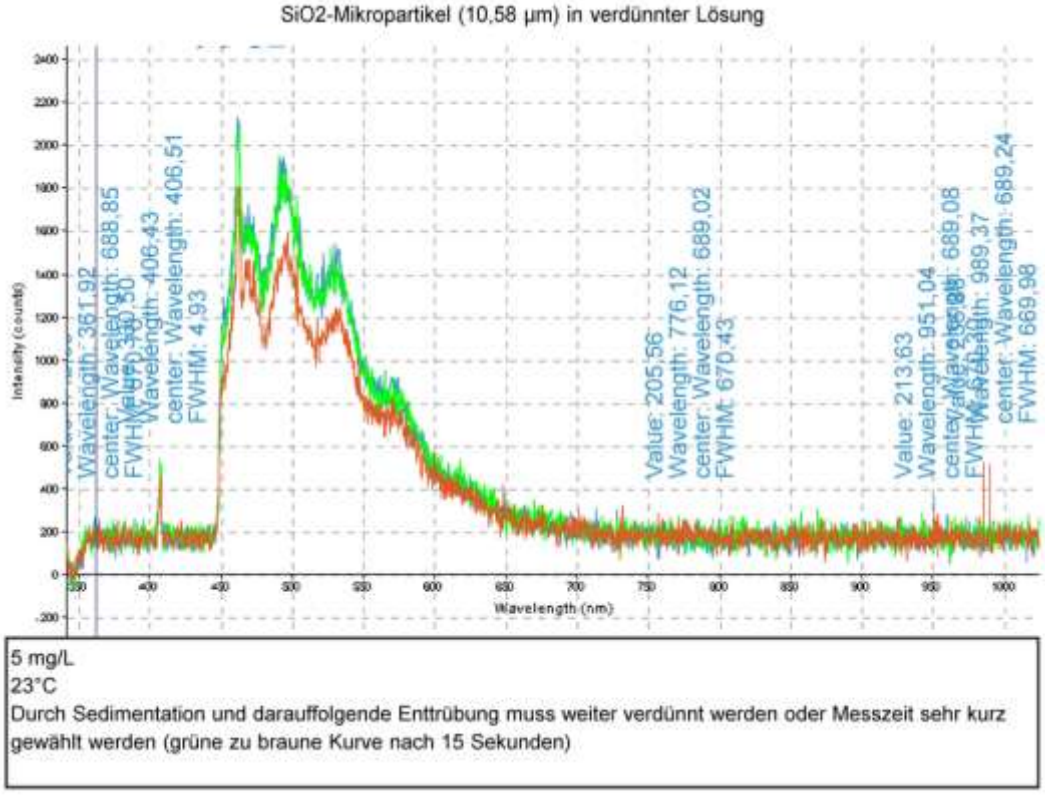

Figure 44. UV/VIS spectra of the larger and uncoated silica microparticles (size = 10 micrometres).

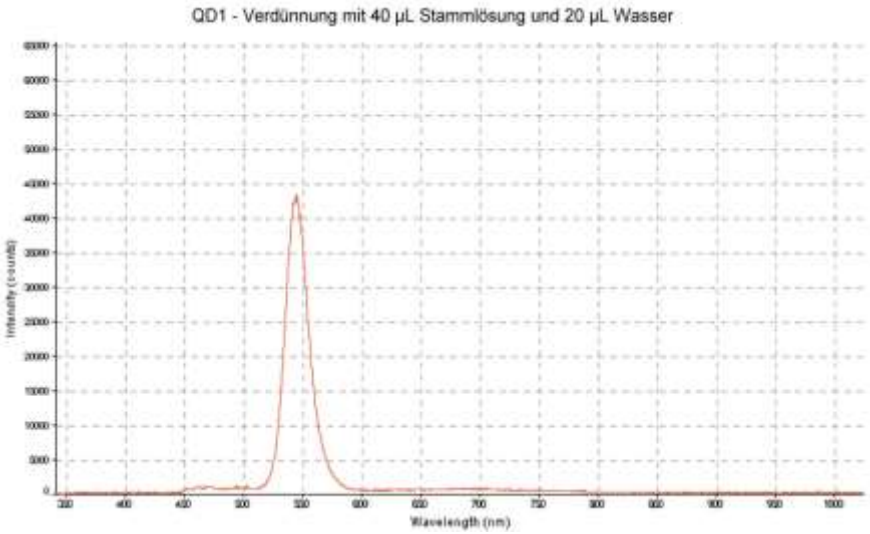

Figure 45. UV/VIS spectra of fluorescence peak from QD1 in diluted form.

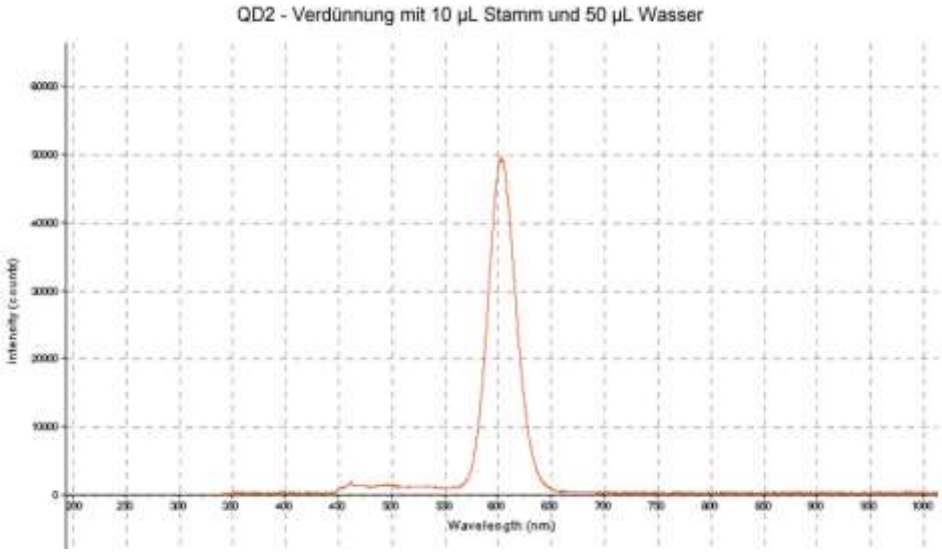

Figure 46. UV/VIS spectra of fluorescence peak from QD2 in diluted form.

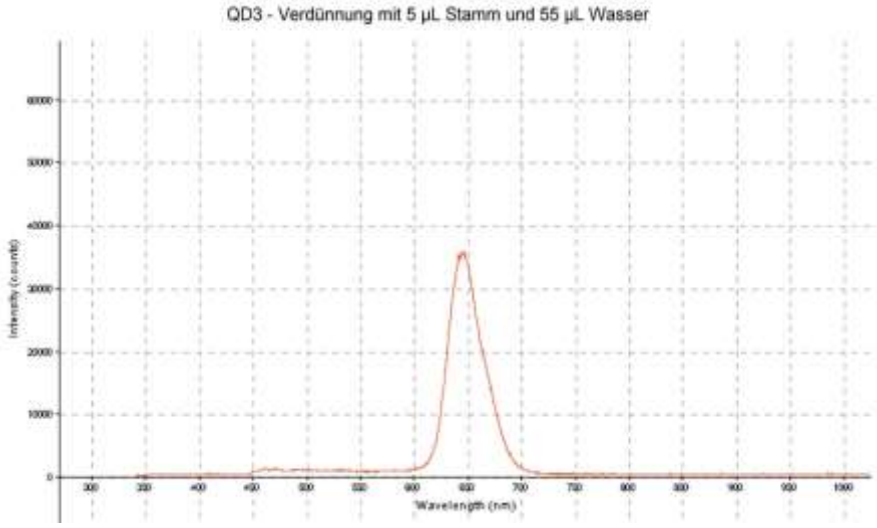

Figure 47. UV/VIS spectra of fluorescence peak from QD3 in diluted form.

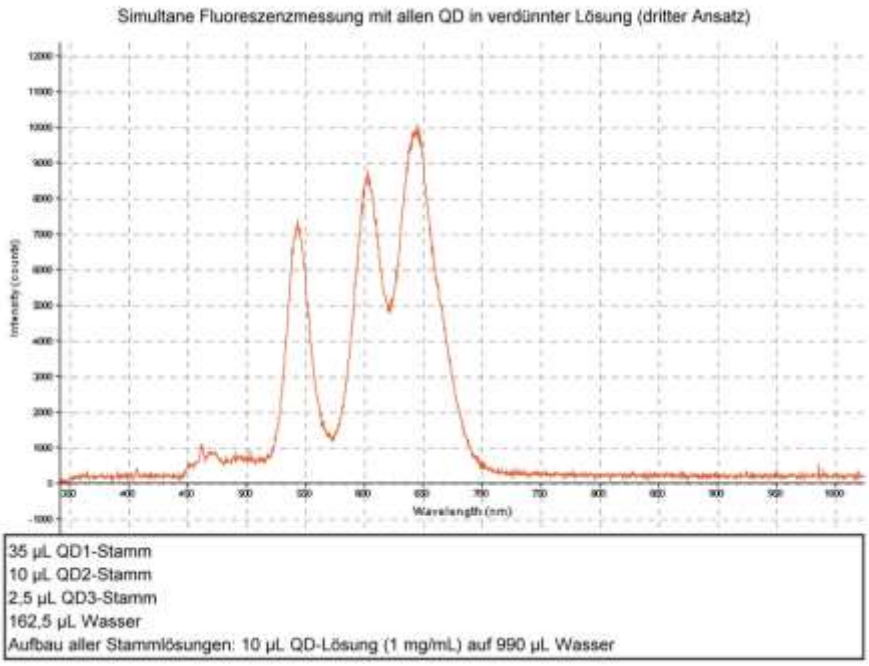

Figure 48. UV/VIS spectra of simultaneous fluorescence measurements of all three used QDs in diluted form.

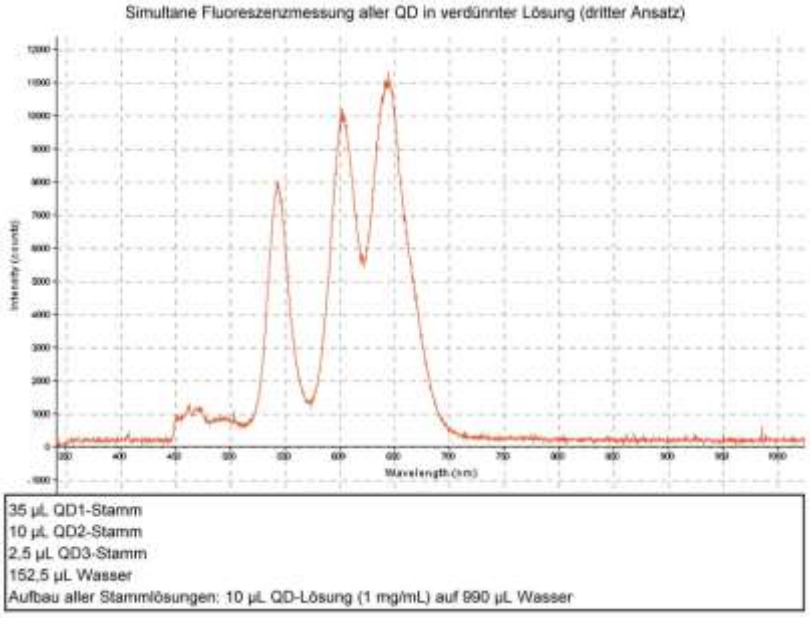

Figure 49. UV/VIS spectra of simultaneous fluorescence measurements of all three used QDs in diluted form.

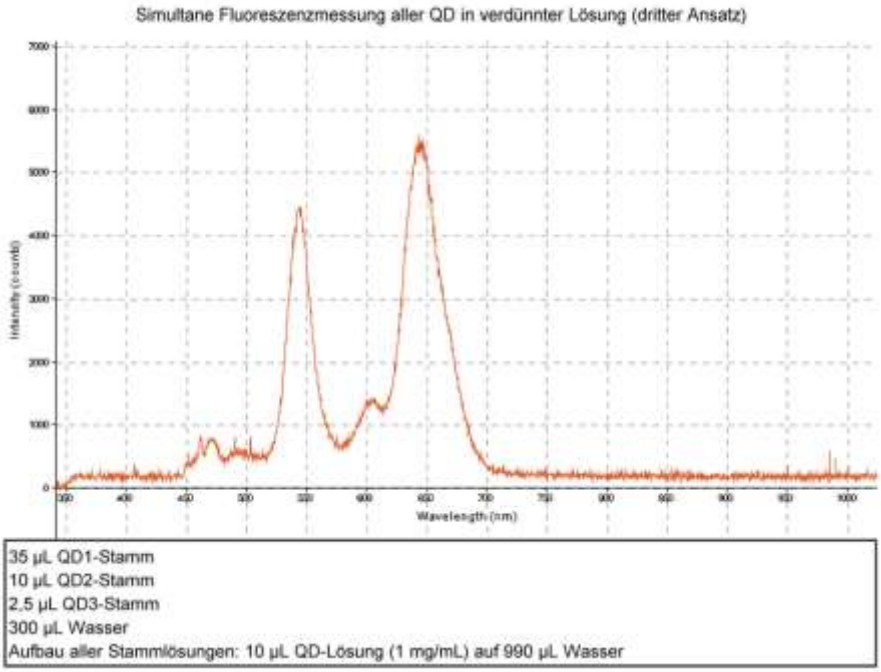

Figure 50. UV/VIS spectra of simultaneous fluorescence measurements of all three used QDs in diluted form.

Product characterization

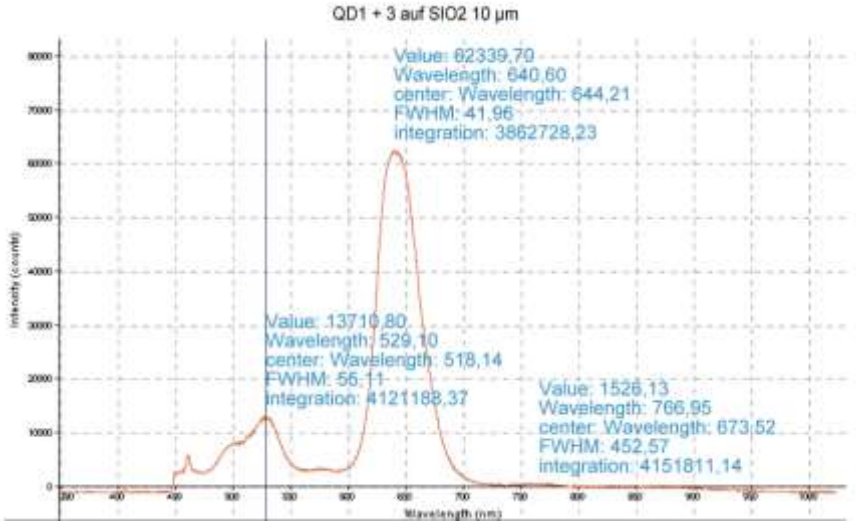

Figure 51. UV/VIS spectra of QD1+3-coated SiO_2 microparticles (size = 10 micrometres).

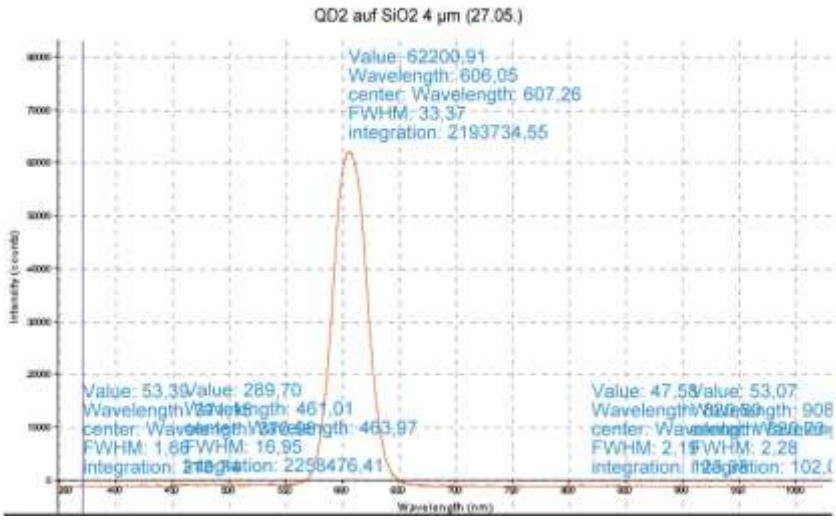

Figure 52. UV/VIS spectra of QD2-coated SiO_2 microparticles (size = 4 micrometres).

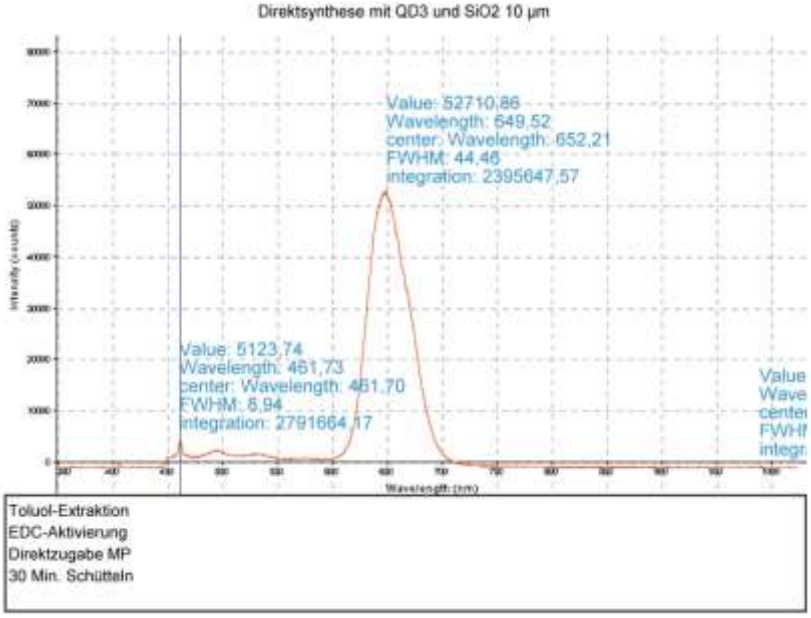

Figure 53. UV/VIS spectra of QD3-coated SiO_2 microparticles (size = 10 micrometres).

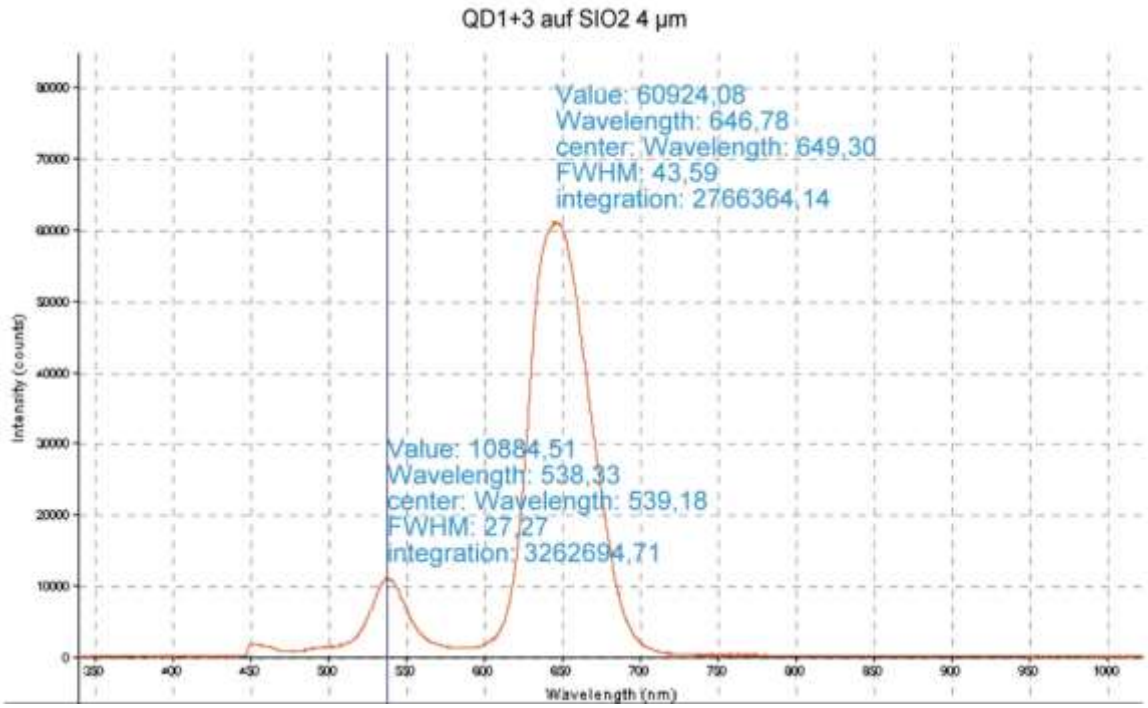

Figure 54. UV/VIS spectra of QD1+3 coated SiO_2 microparticles (size = 4 micrometres).

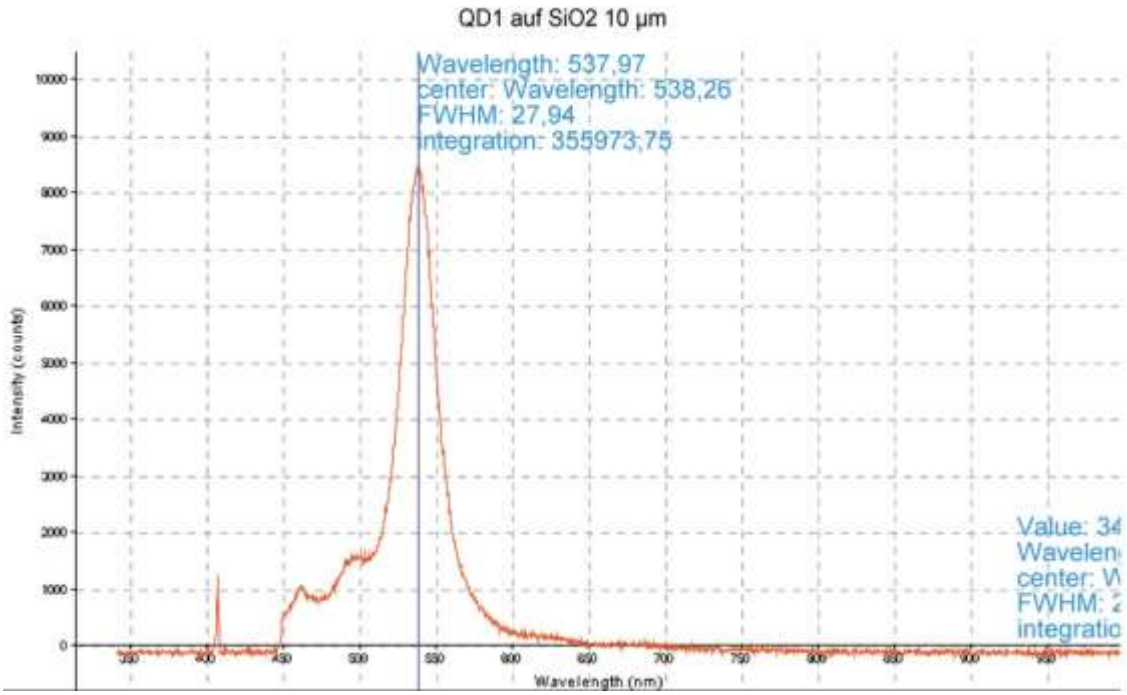

Figure 55. UV/VIS spectra of QD1-coated SiO_2 microparticles with size of 10 micrometres.

Fluorescence microscopy images

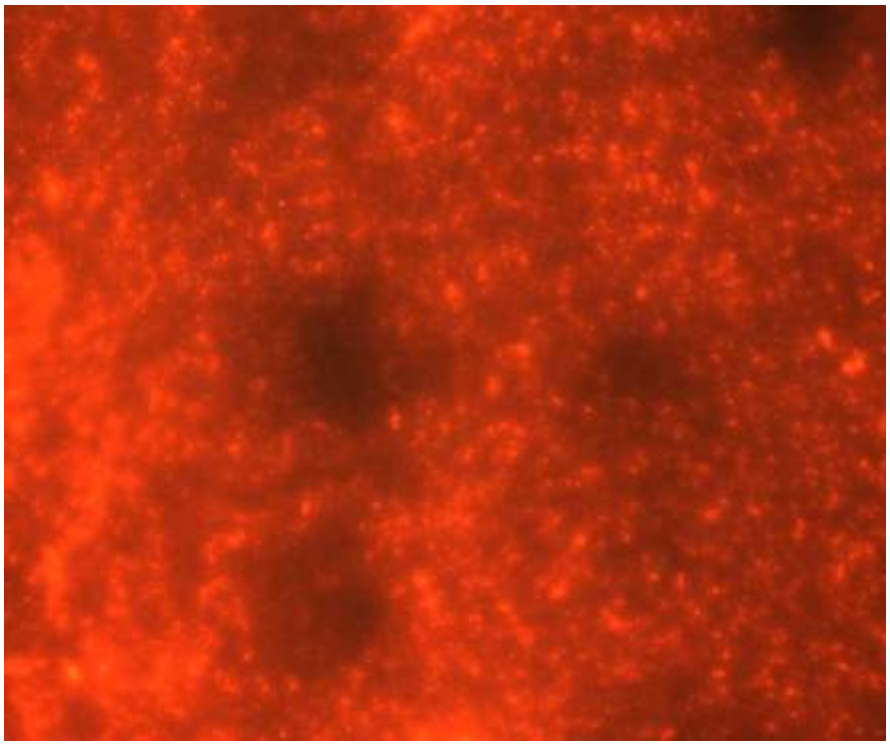

Figure 56. Fluorescence microscopy image of QD3-coated single crystal wafers with red emission range. Bright spots indicate clustering or high QD density, darker areas are less coated or uncoated.

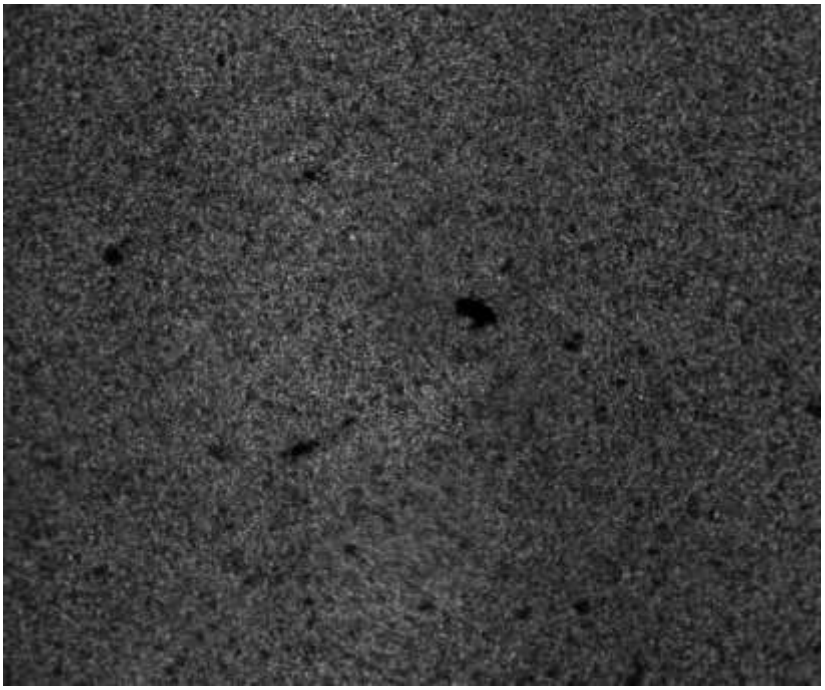

Figure 57. Fluorescence microscopy image of QD3-coated single crystal wafers. The brighter areas symbolize the QD, the darker areas indicate uncoated areas on the wafer.

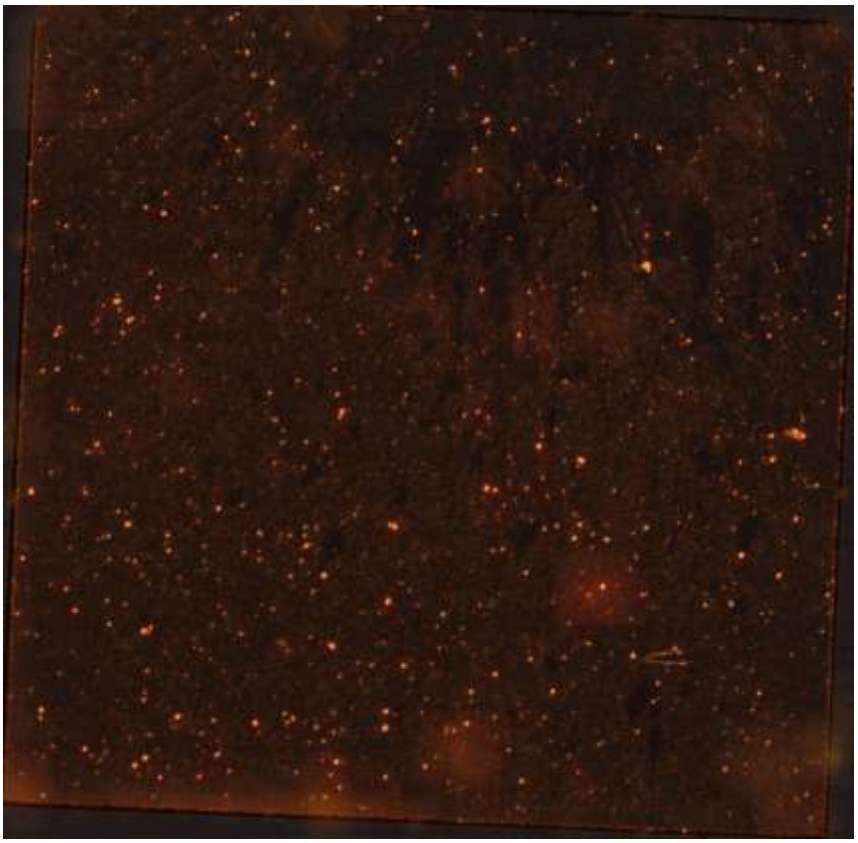

Figure 58. Full-scan of a QD3-coated single crystal wafer in size of 10x10x0,5 mm.

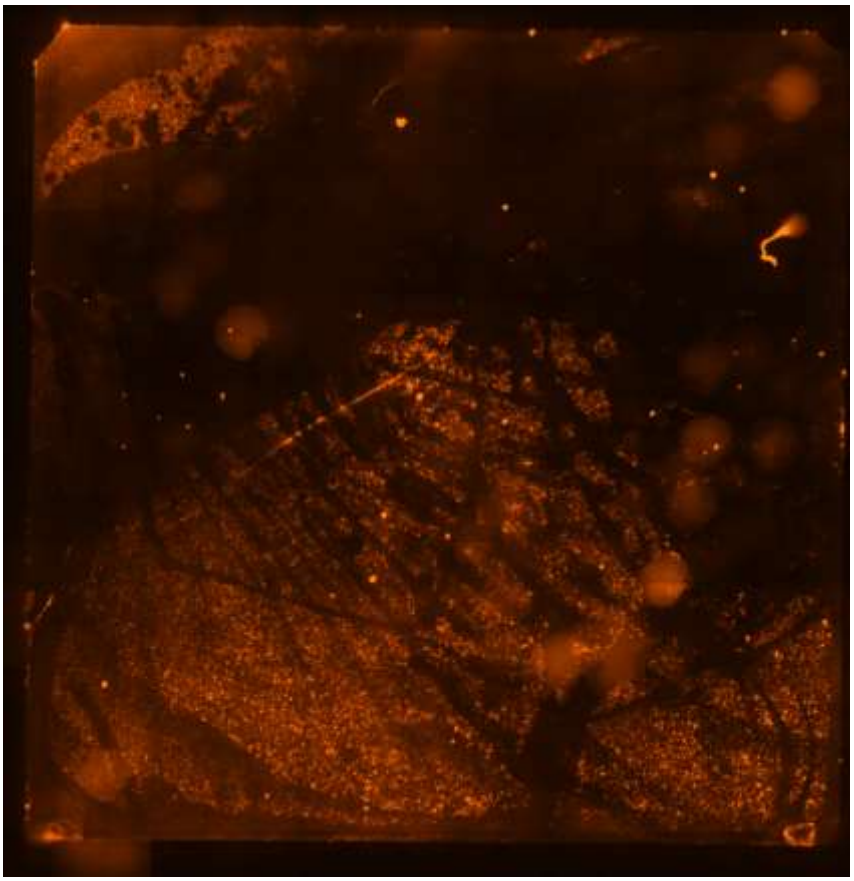

Figure 59. Full scan of a QD2-coated single crystal wafer in size of 10x10x0,5 mm.

Scanning electron microscope images

Reagents (SEM)

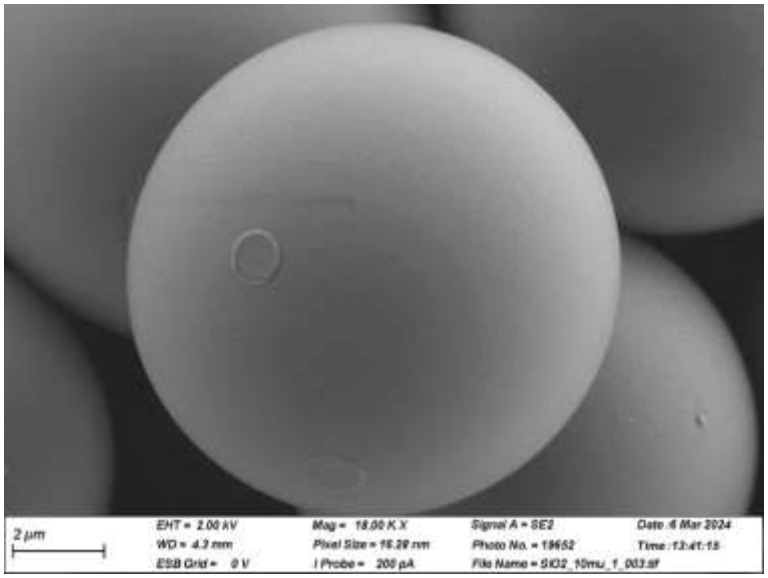

Figure 60. SEM image of uncoated microparticles. 18000x magnification, secondary electron detector.

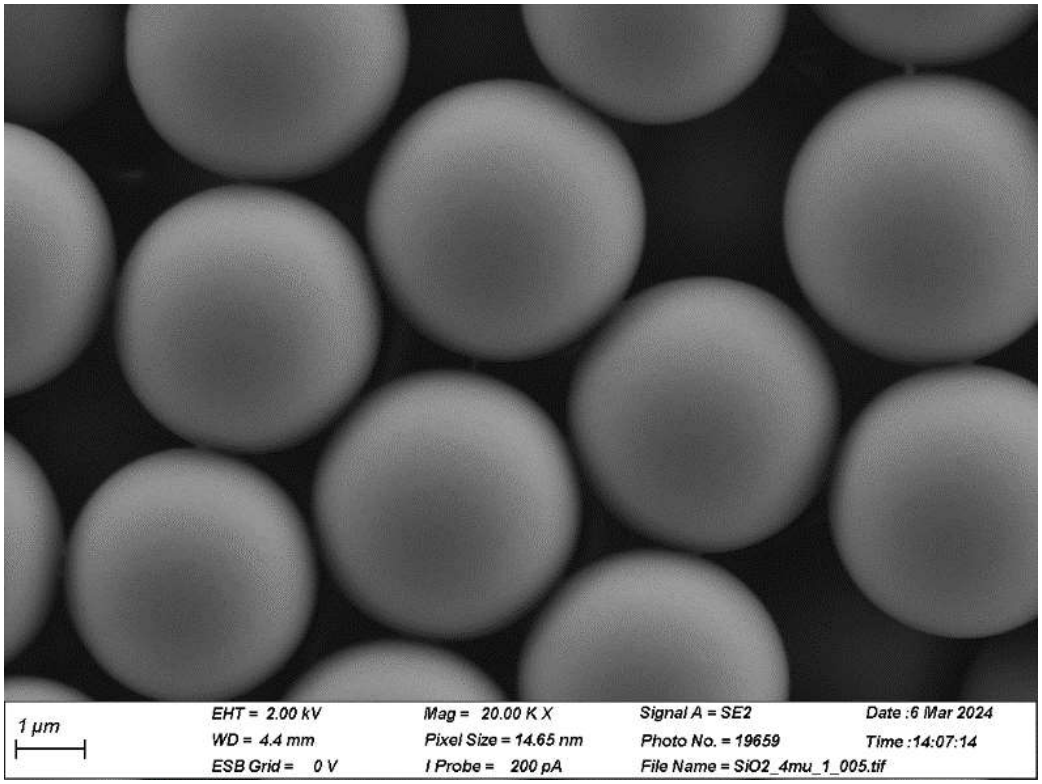

Figure 61. SEM image of uncoated microparticles. 20000x magnification, secondary electron detector.

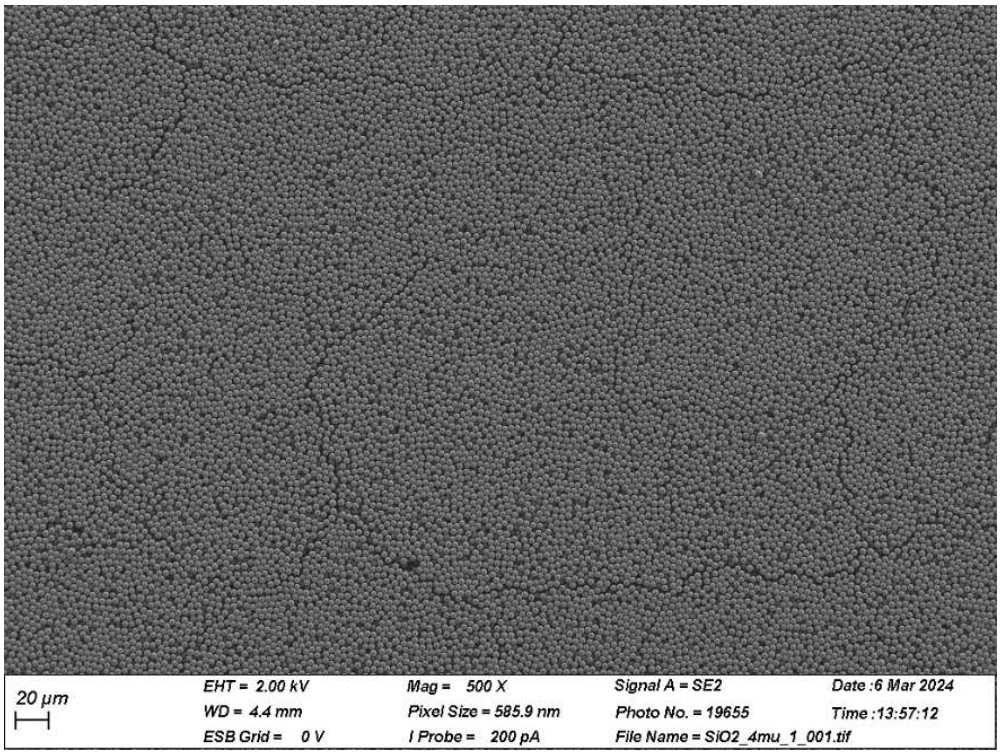

Figure 62. SEM image of uncoated microparticles. 500x magnification, secondary electron detector.

Products (SEM)

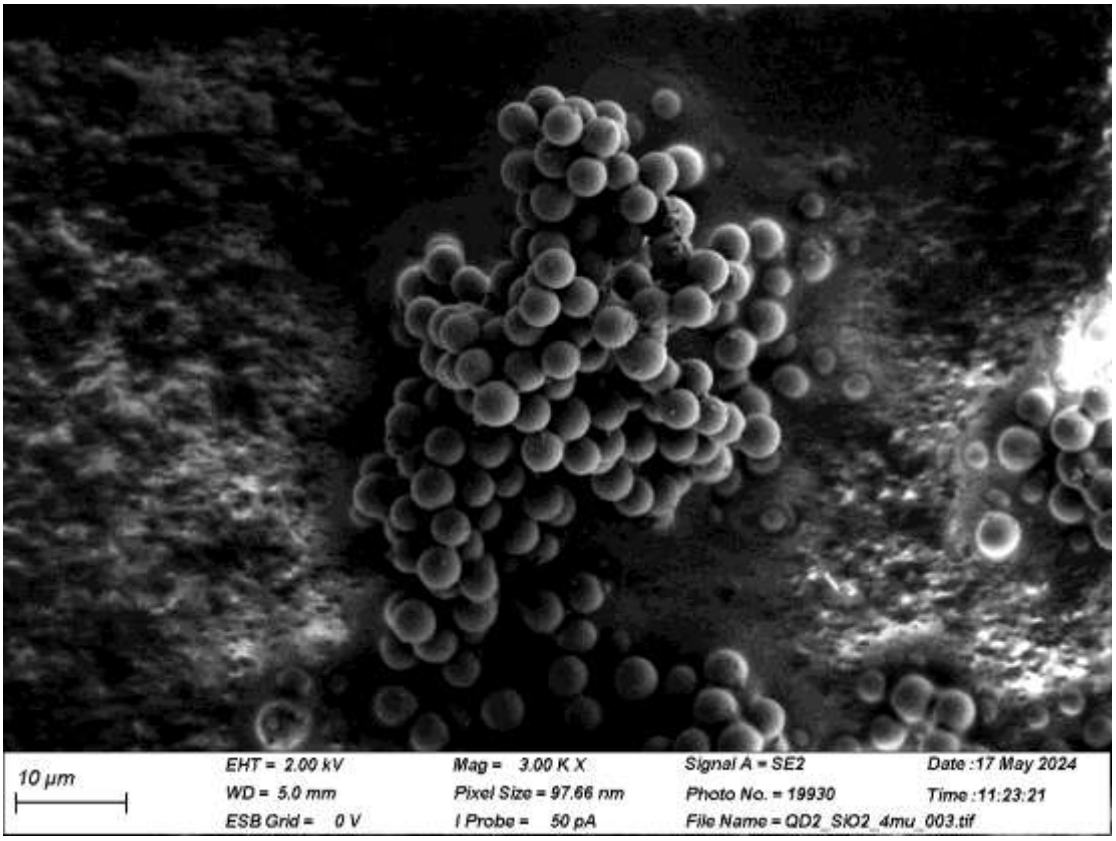

Figure 63. SEM image of coated microparticles. 3000x magnification, secondary electron detector.

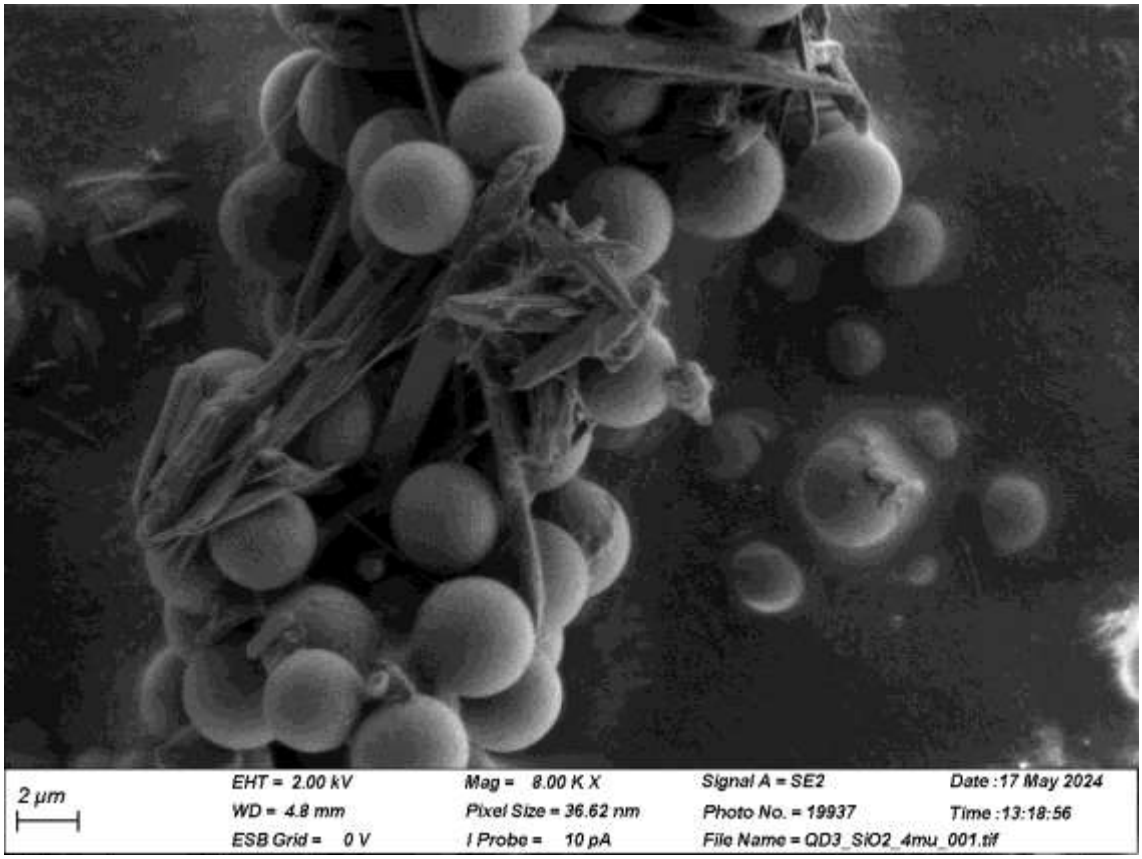

Figure 64. SEM image of coated microparticles. 8000x magnification, secondary electron detector.

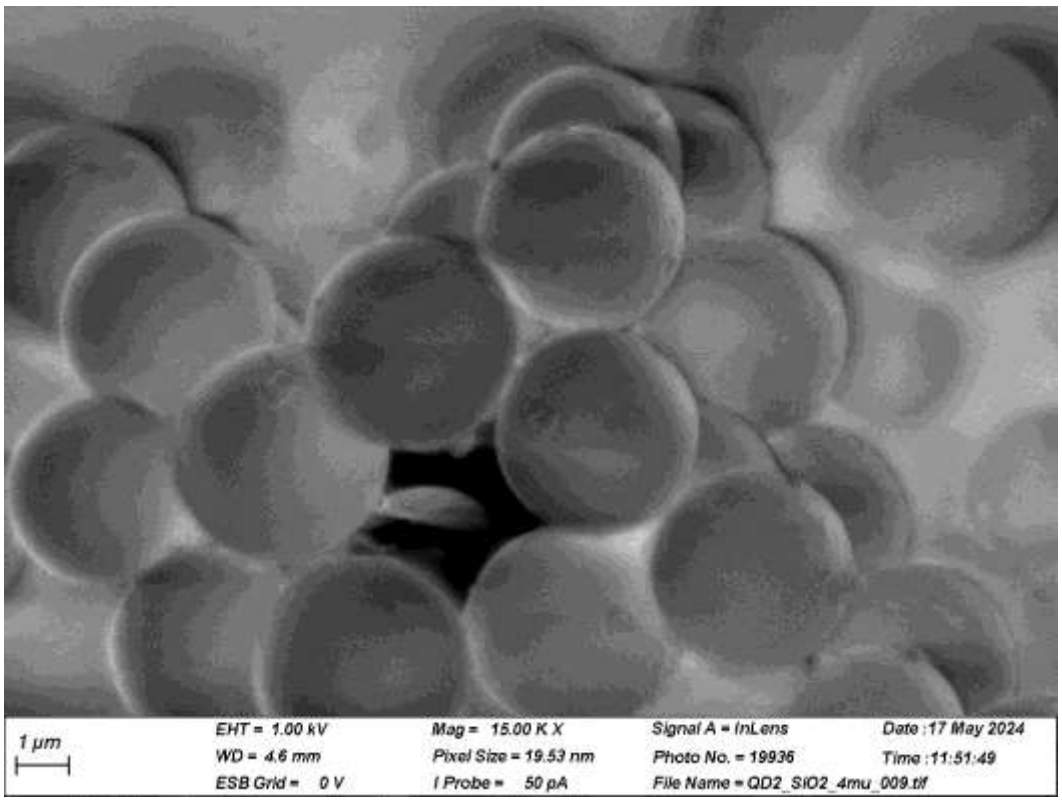

Figure 65. SEM image of coated microparticles. 15000x magnification, InLens-detector.

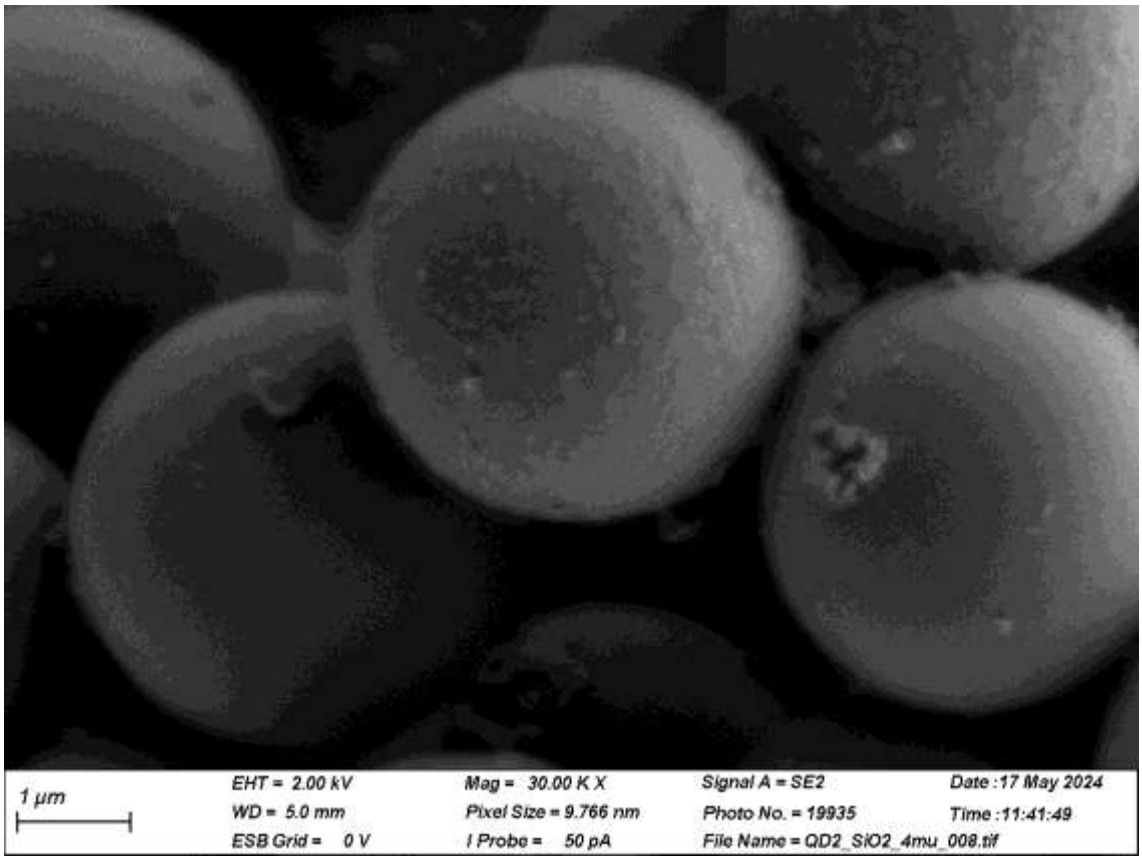

Figure 66 SEM image of coated microparticles. 30000x magnification, secondary electron detector.

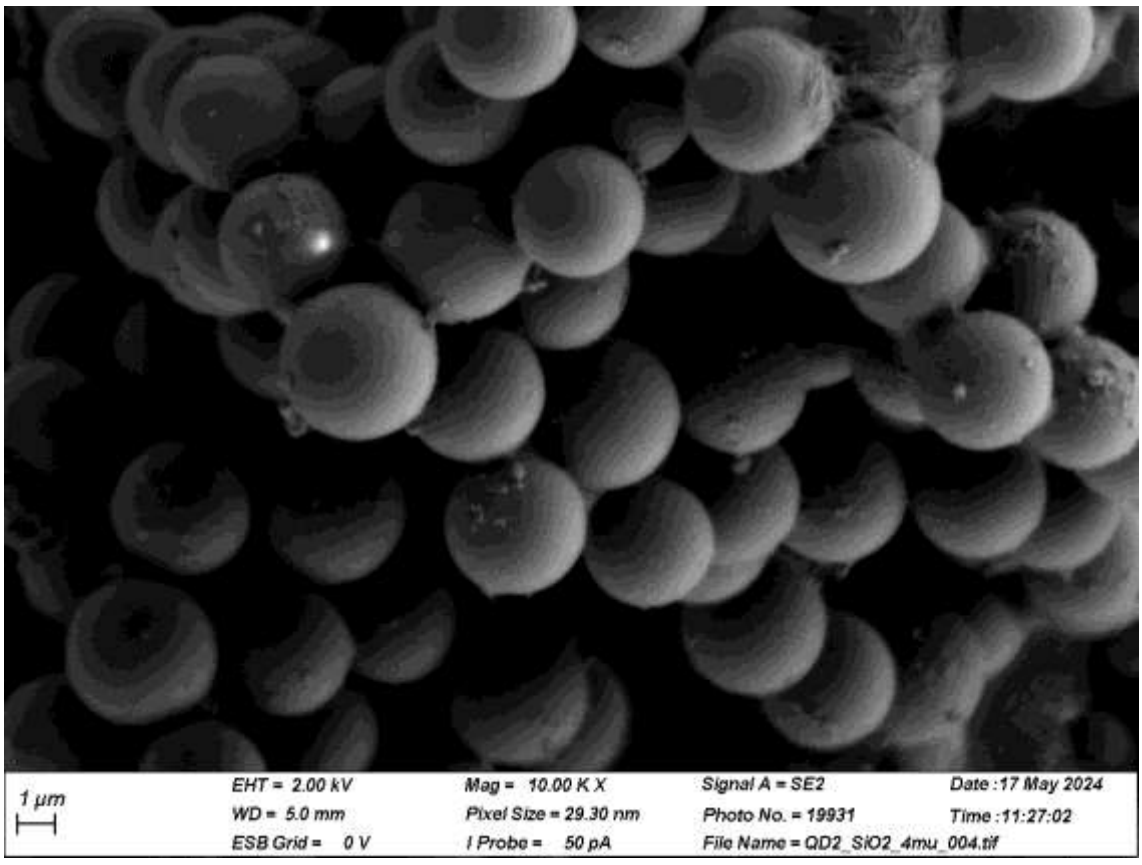

Figure 67. SEM image of coated microparticles. 10000x magnification, secondary electron detector.

Transmission electron microscope images

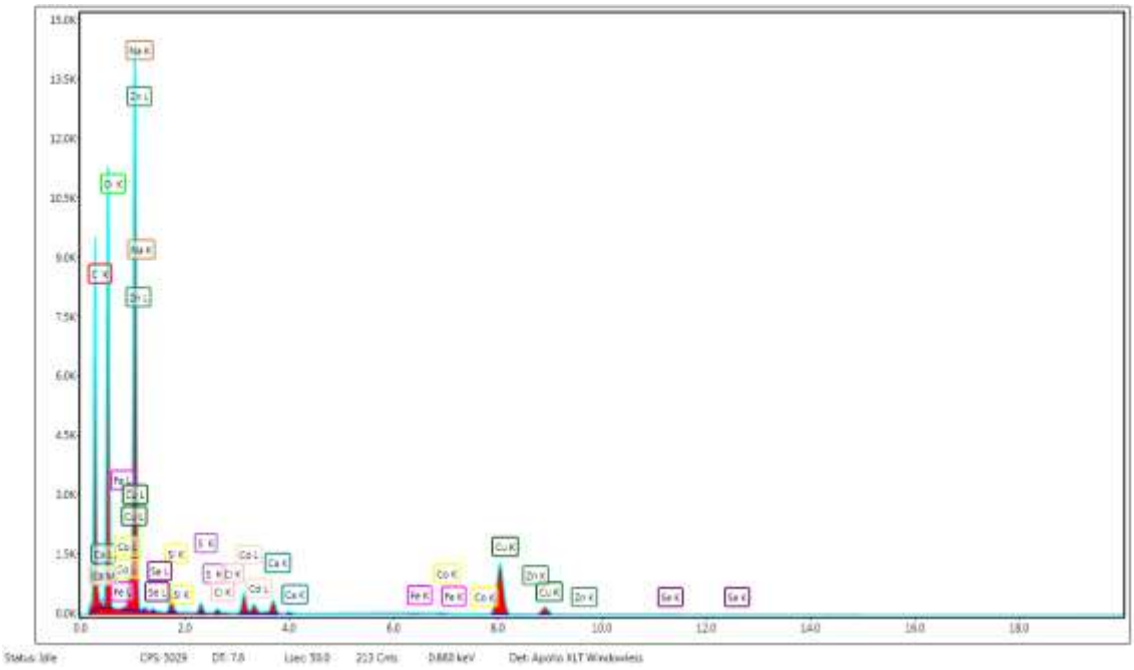

Figure 68. EDX data to the following TEM-image of a QD-coated microparticle.

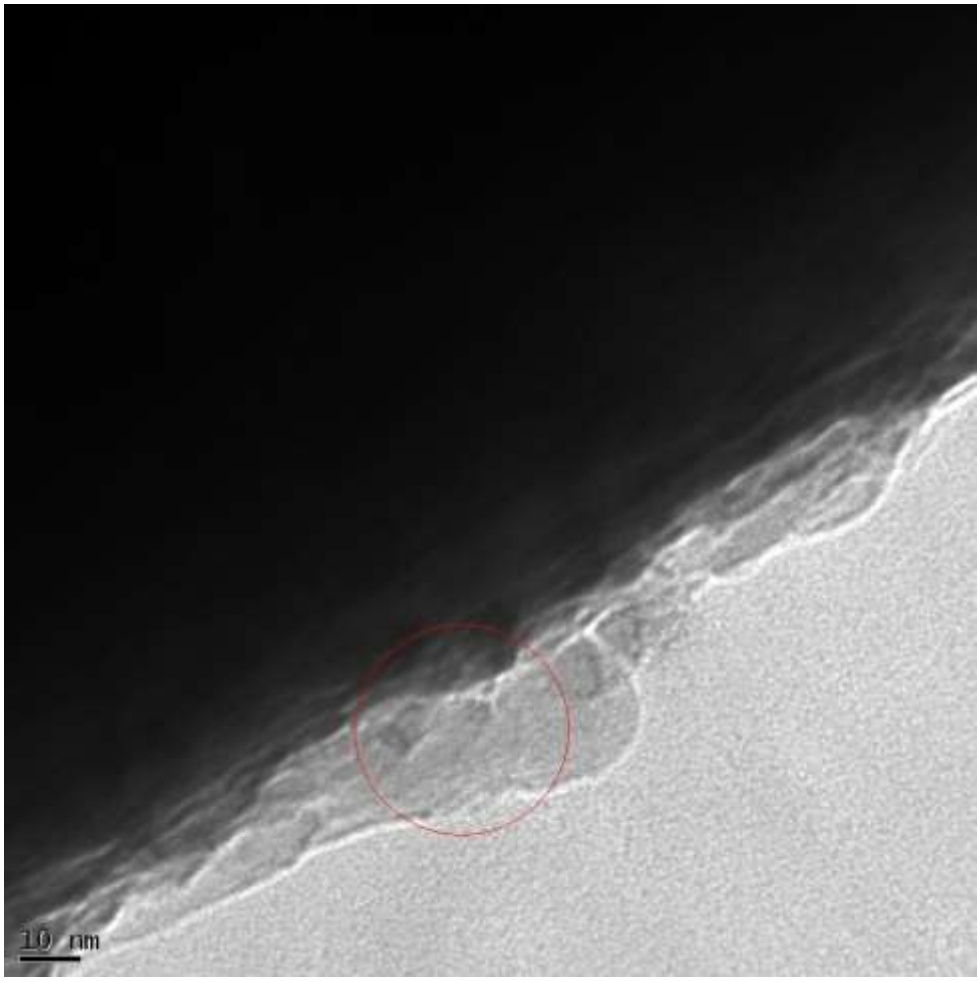

Figure 69. Corresponding TEM-image to the previous EDX data.

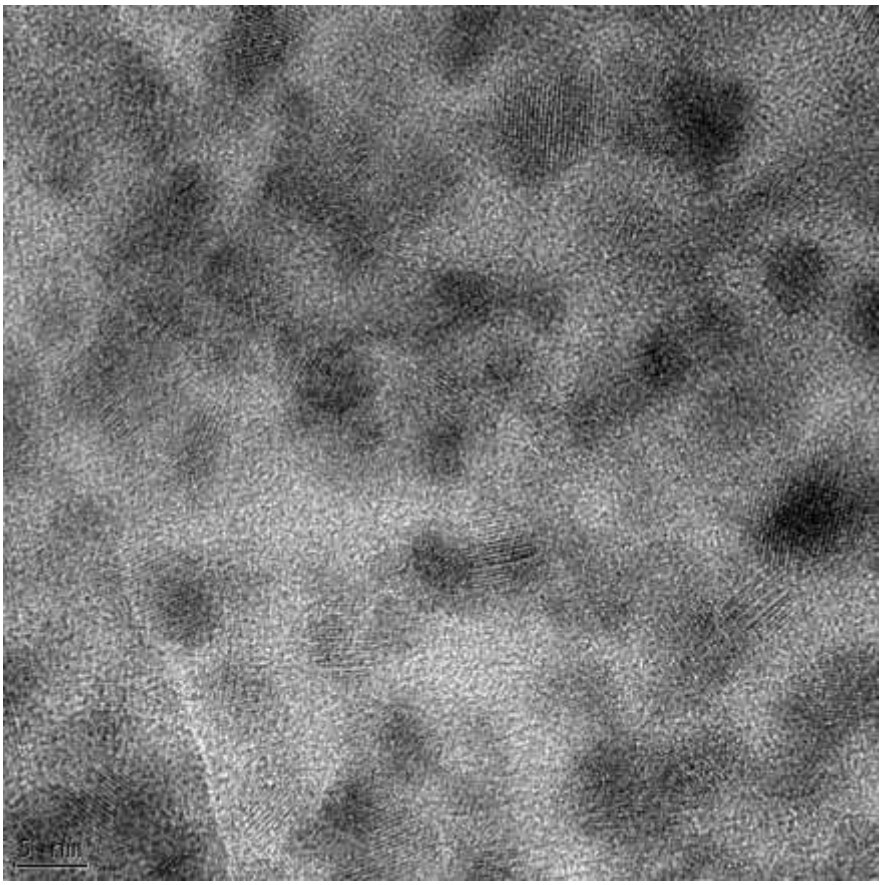

Figure 70. TEM-image of the pristine QDs

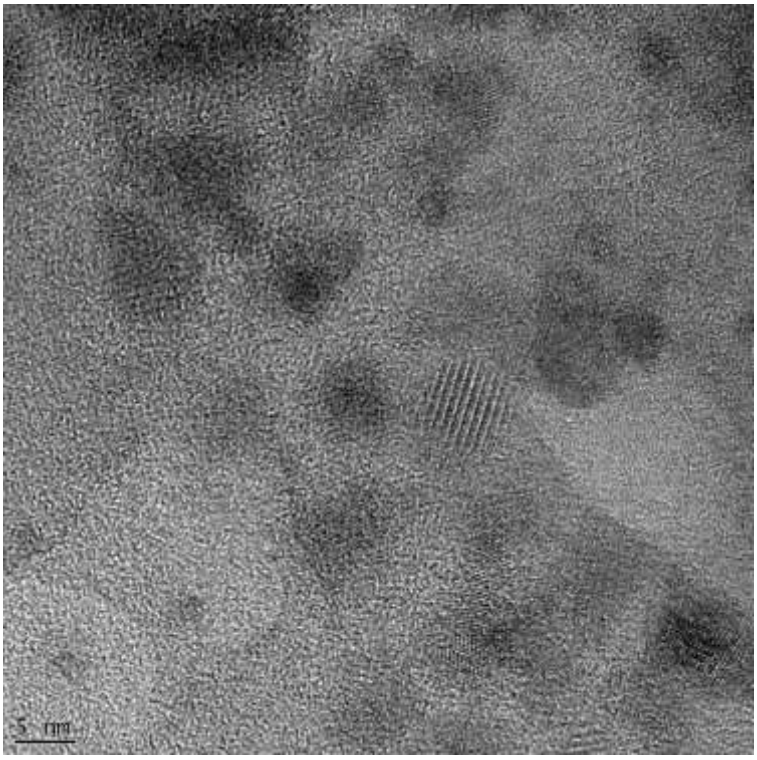

Figure 71. TEM-image of the pristine QDs.

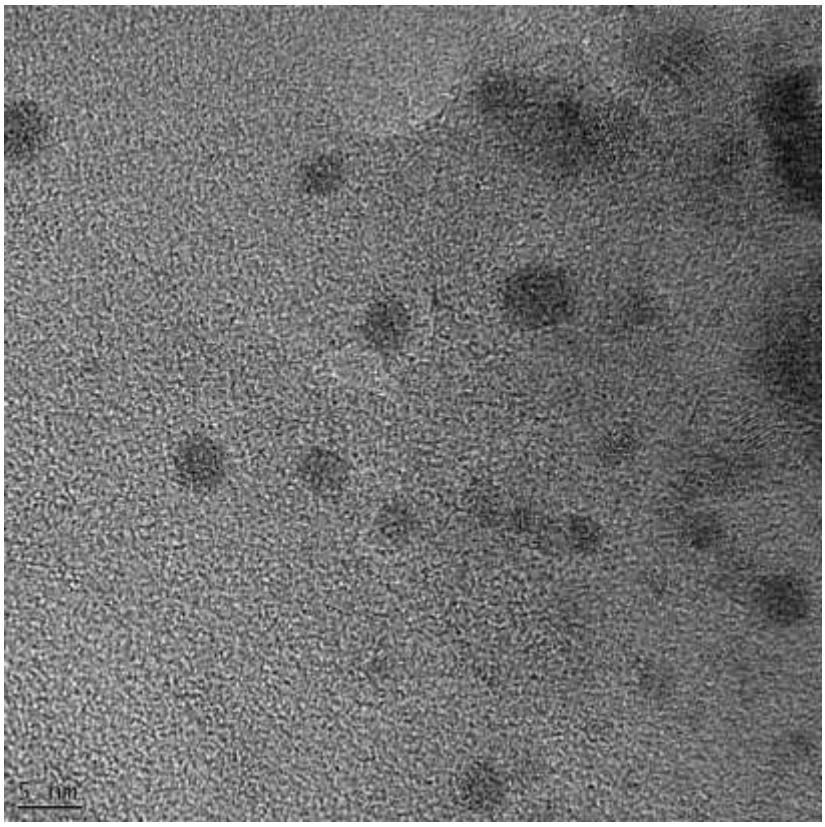

Figure 72.. TEM-image of the pristine QDs.

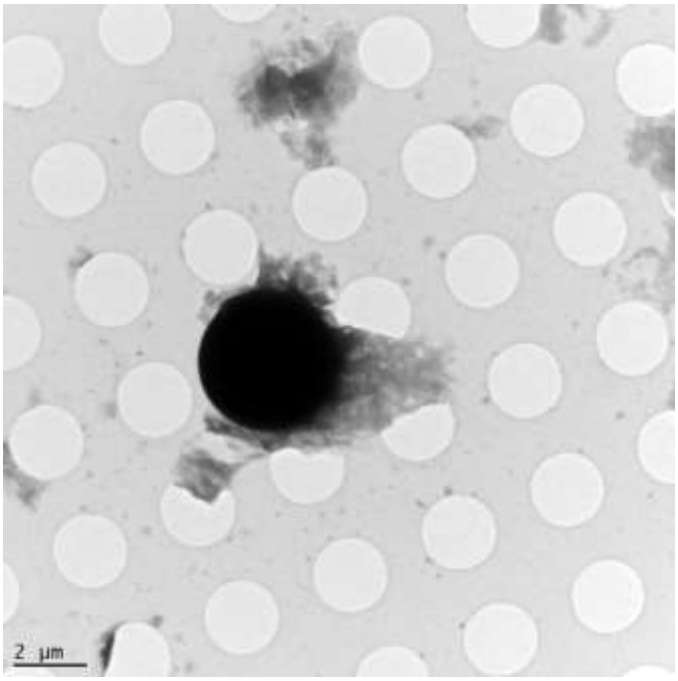

Figure 73. TEM-image of a coated microparticle with some impurities around the edges.

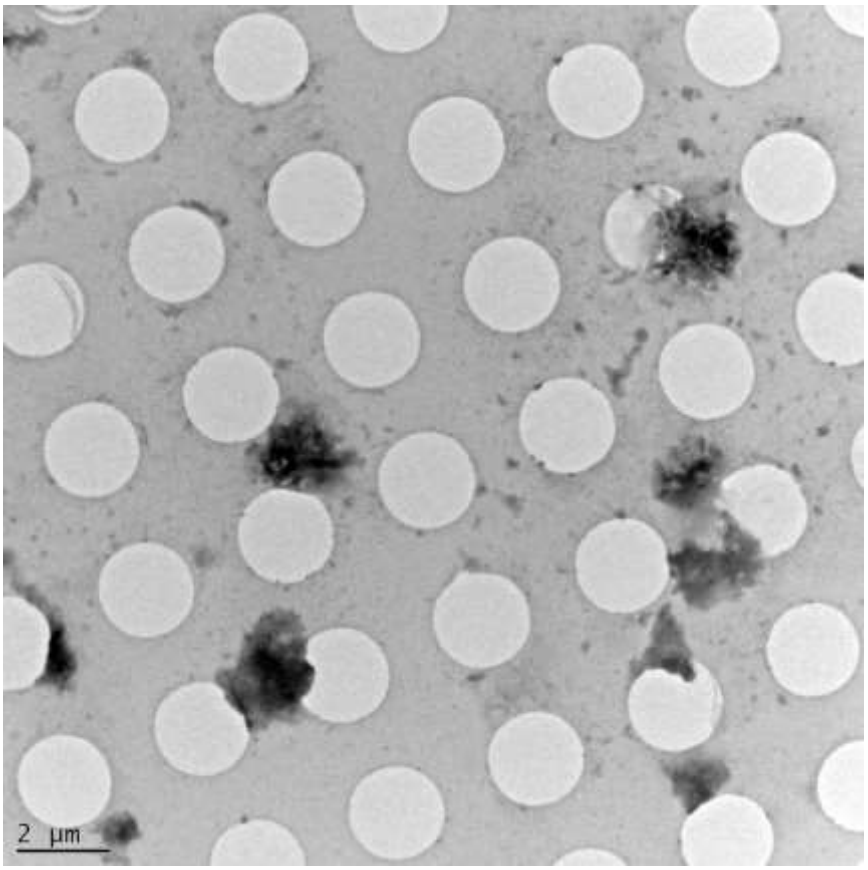

Figure 74. TEM-image of observed QD clusters.

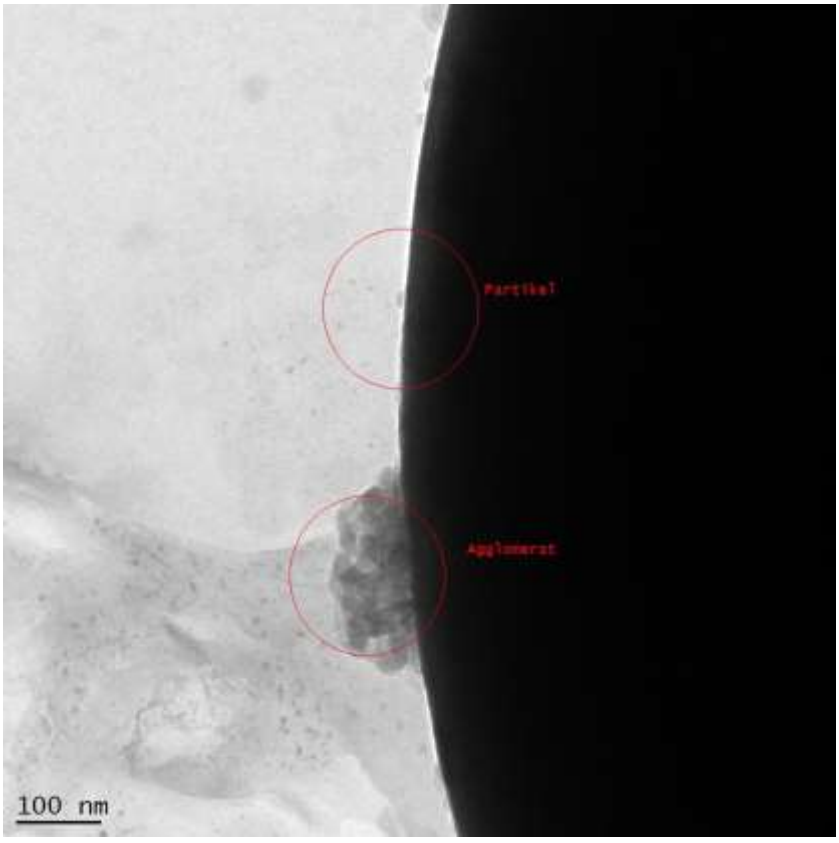

Figure 75. TEM-image of a comparison between adsorbed particles and agglomerate formation within the coating procedure.

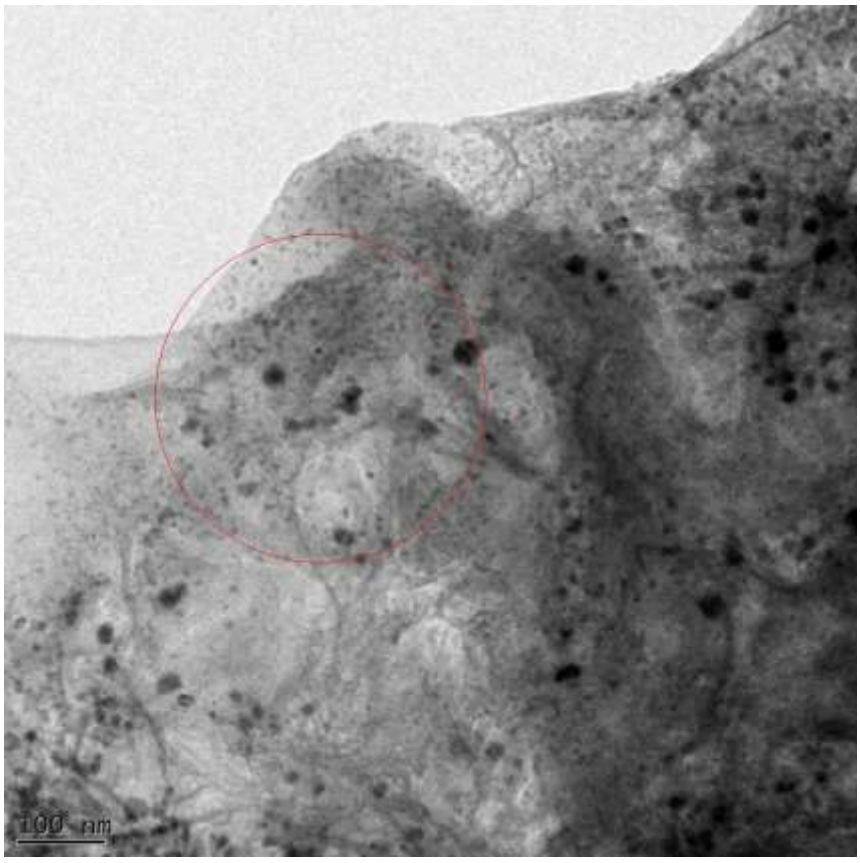

Figure 76. TEM-image of QD clusters embedded in a matrix, probably residing from salts and polymers of the surfaces.

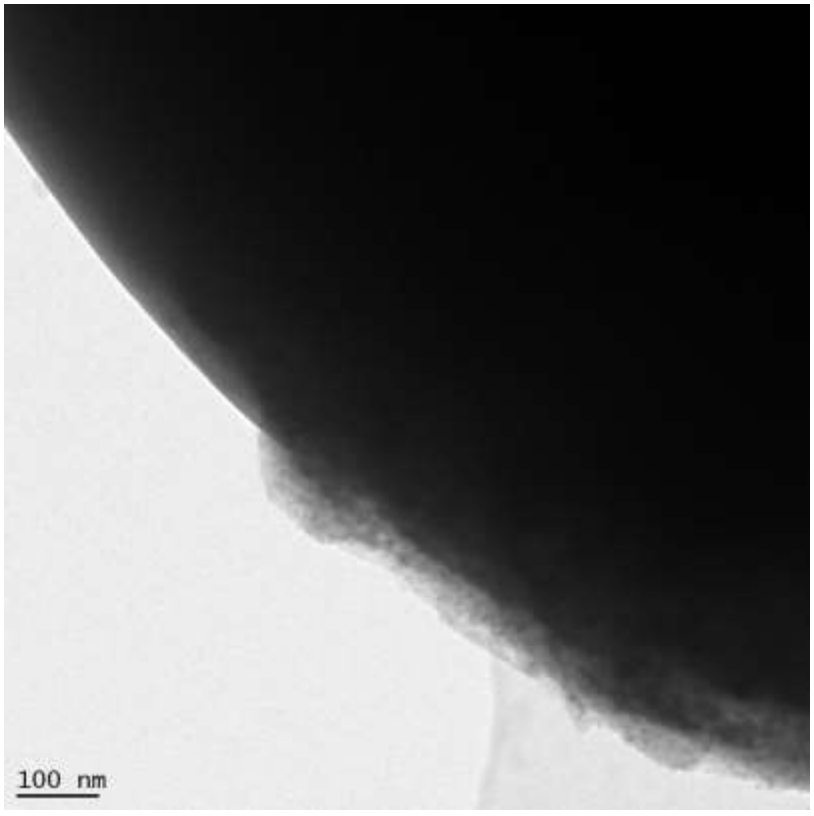

Figure 77. TEM-image of a coated microparticle with coated and uncoated surface.

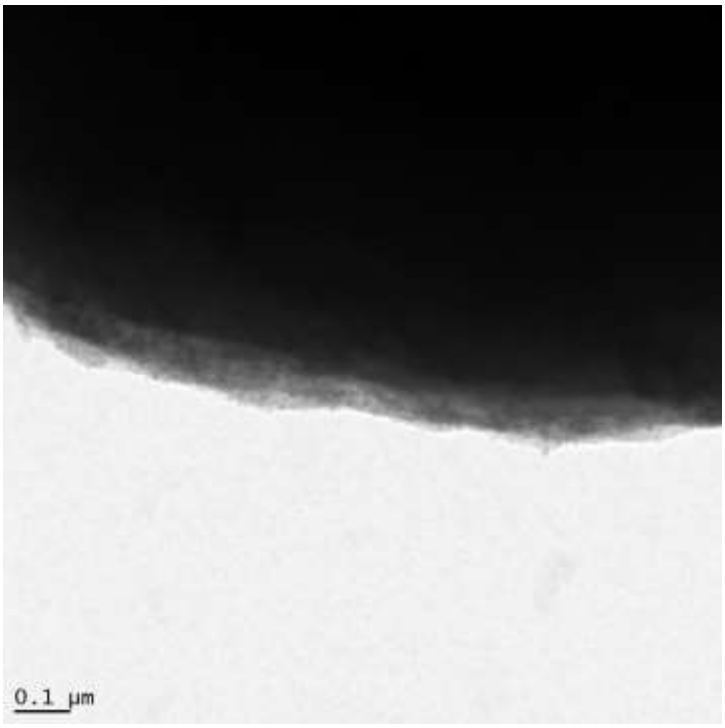

Figure 78. TEM-image of acoated microparticle.

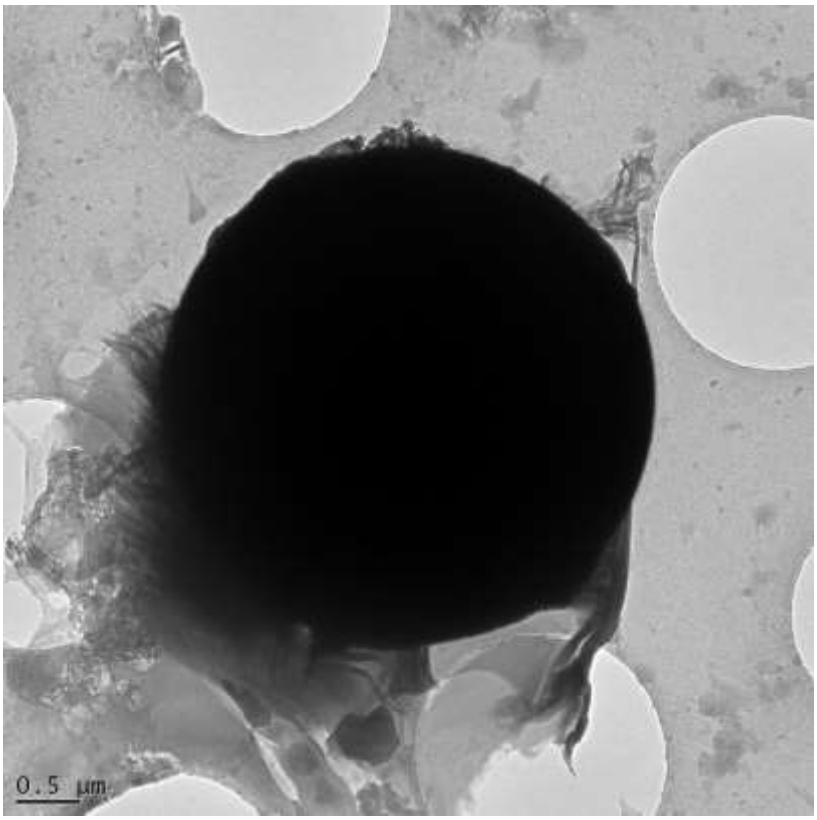

Figure 79. TEM-image of a coated microparticle and some impurities (further magnified).